



Susanne Junghans (03675853)

## **Contraction Region Estimate for State-Dependent-Riccati-Equation-Based Controllers and its Application to a Two-Wheeled Inverted Pendulum**

Term Paper

at the Technical University of Munich Department of Mechanical Engineering

Supervisor(s): Prof. Dr.-Ing. habil. Boris Lohmann  
Chair of Automatic Control

Advisor(s): Julio Pérez Cruz, M.Sc.

Submitted by: Susanne Junghans (03675853)

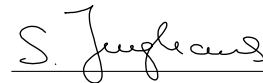
Submission date: 01 October 2020 in Garching bei München



## Erklärung

Ich versichere hiermit, dass ich die von mir eingereichte Arbeit selbstständig verfasst und keine anderen als die angegebenen Quellen und Hilfsmittel benutzt habe.

Garching bei München, den 01. Oktober 2020

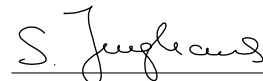
 (Susanne Junghans)

## Freiwillige ergänzende Erklärungen

Mit der zeitlich unbefristeten Aufbewahrung meiner Arbeit in der Lehrstuhlbibliothek erkläre ich mich einverstanden.

Ich stelle die Software, die ich im Rahmen dieser Arbeit entwickelt habe, dem Lehrstuhl für Regelungstechnik unter den Bedingungen der 3-Klausel-BSD-Lizenz zur Verfügung. Ich behalte dabei die sämtlichen Urheber- sowie Nutzungsrechte und werde als Autor namentlich genannt.

Garching bei München, den 01. Oktober 2020

 (Susanne Junghans)

Chair of Automatic Control (Prof. Dr.-Ing. habil. Boris Lohmann)  
Technical University of Munich  
Boltzmannstraße 15  
85748 Garching bei München  
Germany

Lehrstuhl für Regelungstechnik (Prof. Dr.-Ing. habil. Boris Lohmann)  
Technische Universität München  
Boltzmannstraße 15  
85748 Garching bei München  
Deutschland



## Abstract

Controller synthesis based on the so-called State-Dependent-Riccati-Equation (SDRE) offers a systematic technique for non-linear controller design also applicable to systems of higher order with inherently fast dynamics. In the context of this paper, the SDRE-method is employed to design a controller stabilizing a Two-Wheeled Inverted Pendulum (TWIP) robot in its upright position and resulting controller performance as well as input efficiency is investigated and subsequently compared to a LQR-controller based on the system's linearized dynamics.

Despite the numerous benefits of SDRE-based controller design, e.g. applicability to a wide range of non-linear systems, efficient online computation, and the capability to impose soft constraints on the input, an open issue remains in providing stability margins of the regulated system as generally the closed-loop dynamics are not accessible explicitly. Thus, in this paper additionally a novel technique to systematically analyse closed-loop dynamics only defined for specific system states is introduced. As Lyapunov's direct method – the most established technique within non-linear stability analysis – does not allow to infer global properties from local analysis, the proposed approach instead employs the more recently developed contraction theory. Contraction analysis permits the definition of attraction regions for closed-loop dynamics exclusively known pointwisely which suggests its application to SDRE-controlled systems.

## Kurzfassung

Die sogenannte *State-Dependent-Riccati-Equation* (deutsch: Zustandsabhängige-Riccati-Gleichung, kurz SDRE) bietet eine Möglichkeit zum systematischen Reglerentwurf für nichtlineare dynamische Systeme. Anders als eine Vielzahl der etablierten nichtlinearen Reglerentwurfsmethodiken ist der SDRE-basierte Reglerentwurf auch auf hochdimensionale und hochdynamische Systeme anwendbar. Deshalb wurde im Rahmen dieser Arbeit ein SDRE-basierter Regler entworfen, um ein zweirädriges inverses Pendel in seiner aufrechten Fahrhaltung zu stabilisieren. Der resultierende Regler wurde auf Regelleistung sowie -effizienz untersucht und mit einem LQR-Regler verglichen, der auf Basis der linearisierten Roboterdynamik entworfen wurde.

Trotz der zahlreichen Vorteile, die die SDRE-basierte Entwurfsmethodik bietet – wie beispielsweise die weitläufige Anwendbarkeit, effiziente Onlineberechnung sowie die Beschränkung der Systemeingänge durch *Soft Constraints* – besteht ein offenes Problem darin, den geschlossenen Regelkreis auf Stabilität zu untersuchen. Da die Lösung der SDRE für Systeme höherer Ordnung meist nicht analytisch sondern nur punktweise für bestimmte Systemzustände bestimmt werden kann, ist die Stabilitätsanalyse auf Basis der weitverbreiteten Direkten Methode nach Lyapunov nicht möglich, da diese die Definition globaler Stabilitätscharakteristika auf Grundlage lokaler Analyse nicht zulässt. Die im Laufe der 1990er Jahre entwickelte *Contraction Analysis* als „differentielle Erweiterung“ der Lyapunov Theorie erlaubt hingegen genau dies, was ihre Anwendung für SDRE-geregelte Systeme nahelegt. Aus diesem Grund wird im Rahmen der vorliegenden Arbeit auf Basis der *Contraction Analysis* zusätzlich ein Ansatz vorgestellt, um ein Einzugsgebiet der aufrechten Ruhelage des geregelten Systems zu ermitteln.

# Contents

<b>Abstract/Kurzfassung</b>	<b>v</b>
<b>1 Preface</b>	<b>1</b>
1.1 Introduction and Motivation . . . . .	1
1.2 Objectives . . . . .	2
1.3 The TWIP and Tools Employed . . . . .	3
<b>2 Dynamic Models of the Two-Wheeled Inverted Pendulum</b>	<b>5</b>
2.1 Generalized Coordinates and Notations within Different Models . . . . .	6
2.2 Comparison of Dynamic Models . . . . .	9
2.2.1 Yaw Motion of the TWIP . . . . .	10
2.2.2 Driving Velocity of the TWIP . . . . .	12
<b>3 Non-linear Systems and Stability</b>	<b>15</b>
3.1 Classification of Dynamical Systems . . . . .	15
3.2 Stability of Equilibria and Linear Stability Analysis . . . . .	17
3.3 Non-linear Stability Analysis – Lyapunov Theory . . . . .	18
3.3.1 Stability According to Lyapunov . . . . .	18
3.3.2 Lyapunov’s Direct Method . . . . .	20
3.3.3 Remarks on Lyapunov-based Stability Analysis . . . . .	22
3.4 Non-linear Stability Analysis – Contraction Theory . . . . .	23
3.4.1 Convergence to a Single Trajectory and Contracting Systems . . . . .	23
3.4.2 Generalization of Coordinates and Contraction Metrics . . . . .	25
3.4.3 Remarks on Contraction Analysis . . . . .	28
3.5 Controllability of Non-linear Systems . . . . .	29
3.6 Remarks on Non-linear System Analysis . . . . .	31
<b>4 SDRE-based Controller Synthesis</b>	<b>33</b>
4.1 The LQR-Problem and its Generalization to Non-linear Systems . . . . .	33

4.2	Significance of SDC-Parametrization in SDRE-based Controller Design . .	35
4.2.1	State-Dependent-Coefficient Form of Non-linear Systems . . . . .	35
4.2.2	Uniqueness and Optimality . . . . .	36
4.2.3	Controllability and Stabilizing Solutions . . . . .	36
4.2.4	Guideline on Defining a SDC-Representation . . . . .	37
4.3	Further Design Steps in SDRE-based Controller Synthesis . . . . .	38
4.3.1	Choosing Weighting Matrices, $\mathbf{Q}(\mathbf{x})$ and $\mathbf{R}(\mathbf{x})$ . . . . .	38
4.3.2	Solving the SDRE . . . . .	39
4.4	Remarks on SDRE-based Controller Synthesis . . . . .	39
<b>5</b>	<b>Application of SDRE-based Controller Synthesis to the TWIP</b>	<b>41</b>
5.1	SDC-Parametrization of the TWIP's Non-linear Dynamics . . . . .	41
5.1.1	Constructing a Continuously Differentiable System Matrix, $\mathbf{A}(\mathbf{x})$ .	42
5.1.2	Pointwise Controllability of SDC-Parametrizations . . . . .	45
5.2	Further Design Steps in SDRE Controller Synthesis . . . . .	48
5.2.1	Choosing Weighting Matrices, $\mathbf{Q}(\mathbf{x})$ and $\mathbf{R}(\mathbf{x})$ . . . . .	48
5.2.2	Solving the SDRE . . . . .	50
5.3	Significance of Design Flexibilities Within SDRE-based Controller Synthesis	50
5.3.1	Comparison of Different Feasible SDC-Parametrizations . . . . .	51
5.3.2	Comparison of State-Dependent and Constant Penalty Matrices .	54
5.4	Comparative Study of SDRE-based and LQR-based Controllers for the TWIP . . . . .	57
5.4.1	Controller Performance when Stabilizing Different Initial States . .	58
5.4.2	Controller Performance in the Presence of Disturbance . . . . .	60
5.4.3	Controller Performance on Model with Non-linear Friction . . . . .	64
5.5	Remarks on SDRE-based Controller Synthesis for the TWIP . . . . .	66
<b>6</b>	<b>Contraction-based Stability Analysis of SDRE-controlled Systems</b>	<b>69</b>
6.1	Stability Characteristics and Analysis for SDRE-controlled Systems . . .	69
6.2	Motivation of Fitting a Contraction Metric Based on Frozen SDRE-Solutions	70
6.3	Introduction and Comparison of a Fitting Method for Contraction Metrics	72
6.4	Obtained Metric and Remarks on Fitting Method . . . . .	76
<b>7</b>	<b>Conclusion and Perspective</b>	<b>79</b>
7.1	Summary and Conclusion . . . . .	79
7.2	Perspectives . . . . .	80
<b>A</b>	<b>Dynamic Models of the TWIP</b>	<b>81</b>



A.1	Parameters of the Employed TWIP . . . . .	81
A.2	Constants and Auxiliary Variables . . . . .	82
A.3	Non-linear State-Space Model . . . . .	82
A.4	SDC-Parametrizations of the Non-linear State-Space Model . . . . .	83
A.4.1	SDC-Parametrization Used for Controller Design . . . . .	83
A.4.2	Inherently Non-Controllable SDC-Parametrization . . . . .	84
A.4.3	Physically Meaningless SDC-Parametrization . . . . .	85
A.4.4	Kim2017 SDC-Parametrization . . . . .	85
A.5	Dynamics Linearized about Upright Equilibrium . . . . .	85
	<b>List of Theorems and Other Statements</b>	<b>87</b>
	<b>List of Algorithms</b>	<b>89</b>
	<b>List of Figures</b>	<b>92</b>
	<b>List of Tables</b>	<b>93</b>
	<b>References</b>	<b>98</b>



# Chapter 1

## Preface

### 1.1 Introduction and Motivation

With its dynamics being non-linear, subject to non-holonomic constraints, and additionally inherently non-stable the Two-Wheeled Inverted Pendulum (TWIP) makes for a captivating academic example and has received a lot of attention within the control community [30]. Especially with the emerge of robotics during the last couple of years, also more application-oriented investigations have been made, as the TWIP – despite its postural instability – has a number of advantages compared to other mobile robots: Wheeled robots with more than two wheels for instance lack the TWIP’s slimness and manoeuvrability, as only the two-wheeled configuration has the ability to turn on the spot. Whereas legged robots are even harder to control than the TWIP due to their more complicated underlying dynamic models with a remarkably higher number of degrees of freedom [6]. The 2001 introduced Segway marks the first widely-known commercialisation of a TWIP-based personal transporter and further companies have proceeded development of similar transportation solutions [44, 34].

Any TWIP-based mean of transport will always rely on active stabilization through feedback control and consequently a variety of controllers for TWIP-style robots has been developed. Despite the multitude of proposed designs, the majority remains based on a linearization of the TWIP’s dynamics around the upright equilibrium point. Those linear controllers have proved themselves at maintaining postural stability for small deflections from the equilibrium point, as the system’s behaviour is close to linear for small pitch angles [6]. However, with the TWIP entering into non-linear system behaviour – whether on purpose to execute a specific manoeuvre or caused by external disturbance – the stabilization capacities of linear controllers are swiftly exceeded [26]. Namely, large pitch distortions, fast yaw rotations, and abrupt driving accelerations made linear controllers fail in experiments [30]. Yet, those system states can not be neglected as they are probable to arise within a real-life traffic environment.

A controller fully taking into account the system’s non-linear behaviour promises the ability to stabilize the robot for a larger state-space region and consequently also non-linear controllers have been proposed of which an overview is given in [6]. However, many of those controllers have not been sufficiently experimentally validated yet [6]. While generally a range of systematic approaches for non-linear controller design has been introduced and proven good performance in a variety of applications, they often remain

highly restrictive in terms of applicability. Techniques like feedback linearization or adaptive control are restricted to non-linear systems that exhibit special system structures or properties [41] and approaches like sliding mode control or non-linear model predictive control rely on exceptionally high gains or computational expenses [16]. In consequence, many of these non-linear design techniques can only be applied to the TWIP if strong assumptions and simplifications as in [38] are employed. As neuronal-network-based approaches continue to become more popular, it is additionally worth mentioning that these kind of black-box methods have the disadvantage that no systematic stability analysis of the closed-loop system can be executed and they therefore always rely on brute-force simulations as a sole mean to validate closed-loop characteristics.

State-Dependent-Riccati-Equation (SDRE)-synthesis as popularized in the 1990s offers a method technically applicable to a broad range of non-linear systems and additionally comprising the capability to regulate required inputs [11]. Ever since its introduction, an open issue with SDRE-based design however remains in providing stability margins for the controlled system [16]. In general, the closed-loop dynamics of SDRE-controlled systems are not accessible explicitly, but only known locally for certain system states and Lyapunov-based stability analysis does not allow to directly draw global conclusions from local properties. The more recently developed contraction theory however marks a novel approach enabling the deduction of stability margins from local analysis which suggests its application to SDRE-controlled systems.

## 1.2 Objectives

Accordingly, this work proposes a non-linear approach consisting of SDRE-based controller-synthesis as well as an evaluation of the obtained closed-loop system's stability by employing contraction theory. The SDRE-method is further explained in sec. 4 and the fundamentals of contraction theory are summarized in sec. 3. In [26] a SDRE-based controller for the TWIP is introduced and its performance demonstrated to be superior compared to a linear quadratic regulator (LQR)-controller for dynamically critical system states. The obtained non-linear controller is validated experimentally by showcasing how it manages to stabilize the robot in critical spinning modes the linear controller fails to restabilize. However, in [26] no systematic stability analysis of the resulting closed-loop system is executed but controller performance is exclusively validated experimentally for specific scenarios.

This paper will therefore propose a slightly different parametrization of the TWIP's dynamics as a basis for SDRE-synthesis and evaluate it in terms of its controllability and numerical properties in sec. 5.1. In the subsequent sec. 5.2, the influence of state-dependent weighting matrices determining the performance index will be surveyed and how they can be employed to achieve input efficiency and desirable state convergence.

Finally, a method based on contraction theory will be introduced that allows stability analysis of the only pointwisely known closed-loop dynamics describing the SDRE-controlled system. The proposed approach outlines how results from SDRE-synthesis might be utilized for the construction of a contraction metric and subsequent definition of a region of exponential stability. In [7] a method employing contraction theory to analyse closed-loop dynamics obtained from SDRE-based controller design has been proposed before. However, the technique varies widely from the one introduced in the context of this work and concrete differences will be highlighted and argued in sec. 6.3.

### 1.3 The TWIP and Tools Employed

In the context of this paper, a TWIP is considered a robot with two coaxial wheels mounted on either side of an intermediate pendulum body with its centre of mass above the wheel axle [6]. A further distinction can be made between fat-body and slender-body TWIPs depending on the distribution of the robot's mass and the resulting moments of inertia (MOIs) with respect to (w.r.t.) its body axes [26]. Although the TWIP's slenderness does affect its postural stability, the mathematical formulae to describe its dynamics remain the same and therefore the models discussed in sec.2 apply to any TWIP. The robot subject to this paper was developed at the Chair of Automatic Control at Technical University of Munich and a photograph of it is provided in fig. 1.1.



Figure 1.1: The TWIP developed at the Chair of Automatic Control at Technical University of Munich. Although – as demonstrated on the right-hand side – it has the ability to also drive in a horizontal position, the aim of this work will be to stabilize it in its upright position as pictured on the left-hand side.

Being a slim and lightweight robot, it can be considered a slender-body TWIP and its exact parameters are given in the appendix (A.1). The robot is equipped with a triaxial acceleration sensor and triaxial gyroscope such that full state feedback can be provided for the state-space model introduced in sec.2. The wheels of the examined TWIP are each actuated individually through a two-stage gear connected to DC motors which are powered by an integrated lithium-polymer rechargeable battery. For detailed information on the TWIP's configuration refer to [1, 15].

Similar to preceding works at the Chair of Automatic Control, within this paper all coding for controller design and validating simulations was executed using MATLAB and its toolboxes. The polynomial fitting approach to find a contraction metric in sec.6 uses the YALMIP toolbox which originated as a semi-definite programming (SDP)-toolbox and nowadays offer the handling of a variety of optimization problems relevant to control theory. As an external interior-point solver, the free MOSEK solver was employed [33].



## Chapter 2

# Dynamic Models of the Two-Wheeled Inverted Pendulum

The three most established methodologies for dynamic modelling are Newton's, Lagrange's, and the more recently developed Kane's method [36, 25]. Both, Lagrange's and Kane's method, can be considered an extensions of the original Newtonian approach by introducing generalized coordinates, applying the principle of virtual work or power and providing individual ways to handle kinematic constraints [36]. As the procedure for deriving dynamic models via Lagrange's method is well-known and has been widely discussed in the literature and Kane's method – even though less established – is presented for instance in [22, 25, 36], a detailed derivation will be omitted in this paper. Instead, two established models from preceding publications will be reviewed and demonstrated how they slightly differ. This immediate comparison should provide further insight to the two models and ease the transfer of results based on one model to the other. In conclusion, it will be presented what exact formulation was chosen for the context of this paper and briefly showcased why this choice was made.

Several dynamic models of the TWIP have been introduced of which the most widely recognised have been the ones derived by Pathak et al. in [38] and Kim and Kwon in [25]. While Pathak combines the model derivation, introduction of a frictionless state-space model, and controller synthesis in one publication [38], Kim and Kwon first derive their model in a separate paper [25] taking friction terms into consideration and then introduce a frictionless state-space model and controller in another publication [26]. Pathak and Kim both derive their models via Lagrange's method, while Kim additionally reaffirms his model by applying Kane's method. Furthermore, in [25] a range of models that had previously been published are discussed and certain mistakes made within those models are highlighted. Accordingly, for this work only the resulting state-space models neglecting friction terms of [38] and [26] will be considered and they will be referred to as the Pathak-Model or Kim-Model respectively. Before the mathematical description within each model will be discussed in sec. 2.2, a short comparison of the used notations is given in sec. 2.1 to avoid any confusion due to differing variable names. The variable names in either of the publications by Kim and Kwon, [25] and [26], are identical.

## 2.1 Generalized Coordinates and Notations within Different Models

In the process of dynamic modelling, the TWIP can be considered a system of three rigid bodies: the pendulum body and the two wheels. To fully describe the motion of these three bodies, Kim introduces thirteen generalized coordinates. However, after applying all holonomic constraints and the non-holonomic constraints due to no-slip assumption, only three degrees of freedom remain [25]. Accordingly, the following set of states is sufficient for a full system description: the position of the pendulum's horizontal axle that the wheels are mounted to,  $x$ , the robot's pitch angle,  $\theta$ , and its yaw angle,  $\psi$ . Therefore, in [26] Kim introduces the state-space vector for describing the TWIP as:

$$\mathbf{x}_K = [x \quad \dot{x} \quad \theta \quad \dot{\theta} \quad \psi \quad \dot{\psi}]^T. \quad (2.1)$$

Pathak derives the same remaining degrees of freedom, but introduces his state-space model as:

$$\mathbf{x}_P = [x_0 \quad y_0 \quad \theta \quad \alpha \quad \dot{\alpha} \quad v \quad \dot{\theta}]^T \quad (2.2)$$

with the apparent difference being its higher system order. Pathak defines two position variables,  $x_0$  and  $y_0$ , as coordinates within an inertial reference frame, while Kim uses the single position variable,  $x$ , describing the travelled path length of the TWIP. However, Pathak's coordinates,  $x_0$  and  $y_0$ , can easily be reconstructed from the travelled path length for any time step,  $i$ , given the initial position of the robot and the full state history. One option to do so is provided in the following algorithm:

---

**Algorithm 2.1 :** Reconstructing Pathak's Position Coordinates,  $x_0$  and  $y_0$ , from Travelled Path Length,  $x$ , and Yaw Angle,  $\psi$ .

---

```

1  $x_0(1) = x_{0,\text{init}} + x(1) \cos(\psi(1));$ 
2  $y_0(1) = y_{0,\text{init}} + x(1) \sin(\psi(1));$ 
3 for  $i = 2 : 1 : \text{length}(x)$ 
4      $x_0(i) = x_0(i-1) + (x(i) - x(i-1)) \cos(\psi(i));$ 
5      $y_0(i) = y_0(i-1) + (x(i) - x(i-1)) \sin(\psi(i));$ 
6 end
```

---

As the robot's current position additionally has no influence on the system's dynamics, in the context of this paper the reduced state vector introduced by Kim will be adopted. Figure 2.1 illustrates the state variables used within this paper.

In order to avoid ambiguity and to ease comparison, another distinction to be pointed out is the different choice of symbols to describe state variables within the two models. Particular attention should be drawn to the fact that Pathak defines the yaw angle as  $\theta$  and the pitch angle as  $\alpha$ , while Kim – and the remaining of this paper – denote the yaw angle as  $\psi$  and the pitch angle as  $\theta$ . Table 2.1 gives an overview of the different state variables and in addition tab. 2.2 provides a comparison of the variables describing the pendulum parameters within either model. For further evaluations, all mathematical equations from the Kim- or Pathak-Paper are “transcribed” into the Used-Model variable set listed in the provided tables.



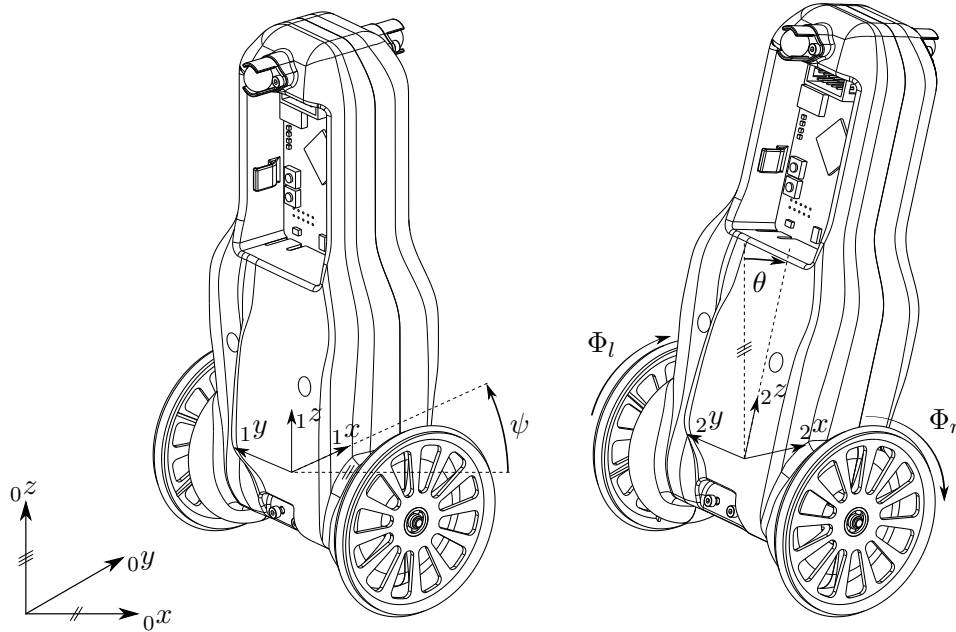


Figure 2.1: An overview of the state-space variables used in the context of this work. While the Pathak-Model involves position variables with respect to some inertial  ${}_0$ frame,  $x_0$  and  $y_0$ , the Kim-Model instead defines a single position variable describing the so far travelled path length,  $x$ . This was adopted due to the benefit of model reduction. The yaw angle,  $\psi$ , describes a rotation of the  ${}_0$ frame about its  ${}_0z$ -axis defining the robot's current driving direction. The pitch angle,  $\theta$ , represents the deviation of the TWIP from its upright equilibrium point defined through a rotation of the  ${}_1$ frame about its  ${}_1y$ -axis. Note that the wheels' rotational angles,  $\Phi_l$  and  $\Phi_r$ , are not contained in the set of generalized coordinates as they are eliminated during the modelling procedure when including the dynamic constraints as their concrete value is not of interest when trying to achieve postural stability.

Table 2.1: Comparison of state variables used within the Pathak- and Kim-Model. In the last column the variables chosen for the remaining of this work are provided which are identical to the ones introduced by Kim.

State	Pathak-Model	Kim-Model	Used-Model
Position	$x_0, y_0$	$x$	$x$
Driving velocity	$v$	$\dot{x}$	$\dot{x}$
Pitch angle	$\alpha$	$\theta$	$\theta$
Pitch rate	$\dot{\alpha}$	$\dot{\theta}$	$\dot{\theta}$
Yaw angle	$\theta$	$\psi$	$\psi$
Yaw rate	$\dot{\theta}$	$\dot{\psi}$	$\dot{\psi}$

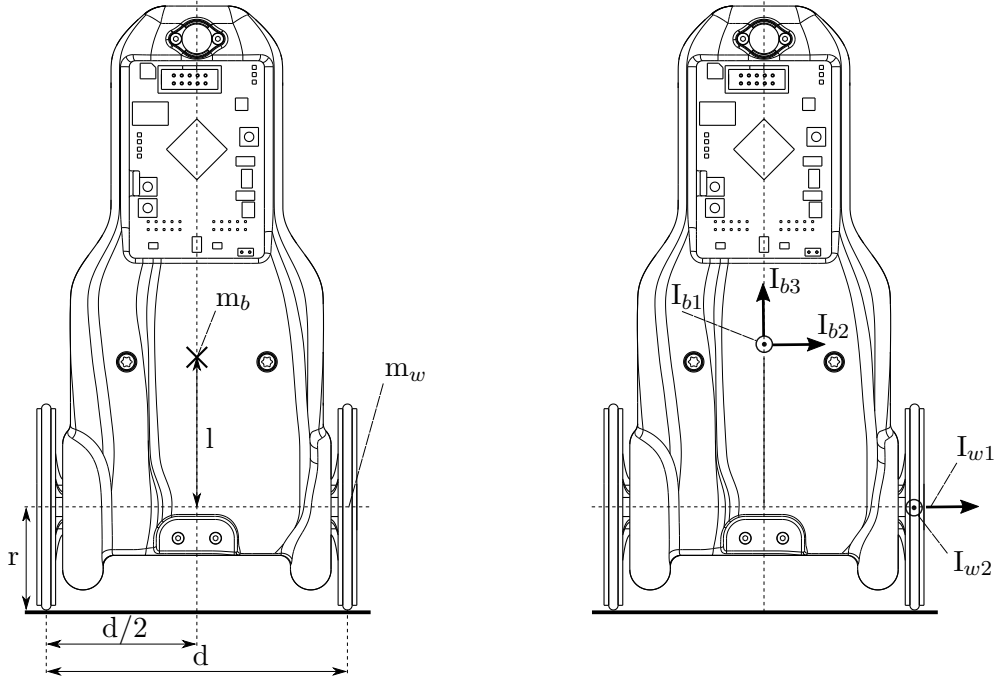


Figure 2.2: An overview of the TWIP's parameters denoted with the variables chosen within this paper as listed in tab. 2.2. All formulae discussed in the following will contain these parameters instead of the ones introduced by Pathak and Kim respectively to ease comparison of the two models.

Table 2.2: Comparison of variables used to describe the TWIP's parameters within the Pathak- and Kim-Model. The last column again provides the variables used for further discussion within this paper. The lower indices,  $b$  and  $w$ , indicate whether a parameter belongs to the pendulum's body or wheels.

Model Parameter	Pathak-Model	Kim-Model	Used-Model
Mass of the pendulum's body	$M_b$	$m_B$	$m_b$
Mass of either wheel	$M_w$	$m_W$	$m_w$
MOI of the body w.r.t. its driving axis	$I_{xx}$	$I_1$	$I_{b1}$
MOI of the body w.r.t. the TWIP's axle	$I_{yy}$	$I_2$	$I_{b2}$
MOI of the body w.r.t. its longitudinal axis	$I_{zz}$	$I_3$	$I_{b3}$
MOI of the wheels w.r.t. their axis	$I_{wa}$	$J$	$I_{w1}$
MOI of the wheels w.r.t. to their diameter	$I_{wd}$	$K$	$I_{w2}$
Height of the body's centre of mass	$c_z$	$l$	$l$
Radius of either wheel	$R$	$r$	$r$
Distance between the two wheels	$2b$	$d$	$d$

## 2.2 Comparison of Dynamic Models

In order to design a controller, Pathak in eq. (13-15) of [38] and Kim in eq. (2-3) of [26] introduce an input-affine non-linear state-space representation of the form:

$$\dot{\mathbf{x}} = \mathbf{f}(\mathbf{x}) + \mathbf{g}(\mathbf{x})\mathbf{u}, \quad (2.3)$$

where the input vector,  $\mathbf{u} = [\tau_l \ \tau_r]^T$ , contains the torques applied to the left and right wheel, respectively. For comparison, the two models were implemented and simulated for certain initial states and small constant inputs without any control law applied. As the TWIP can be considered to have “fallen over” for pitch deviations larger than approximately  $\pi/3$ , the simulations were stopped at this point. While the simulations resulted in similar dynamics regarding the pitch rate and driving velocity, a large deviation could be seen in the yaw dynamics. Consequently, the mathematical definitions within the models were further investigated to understand where this discrepancy arises from.

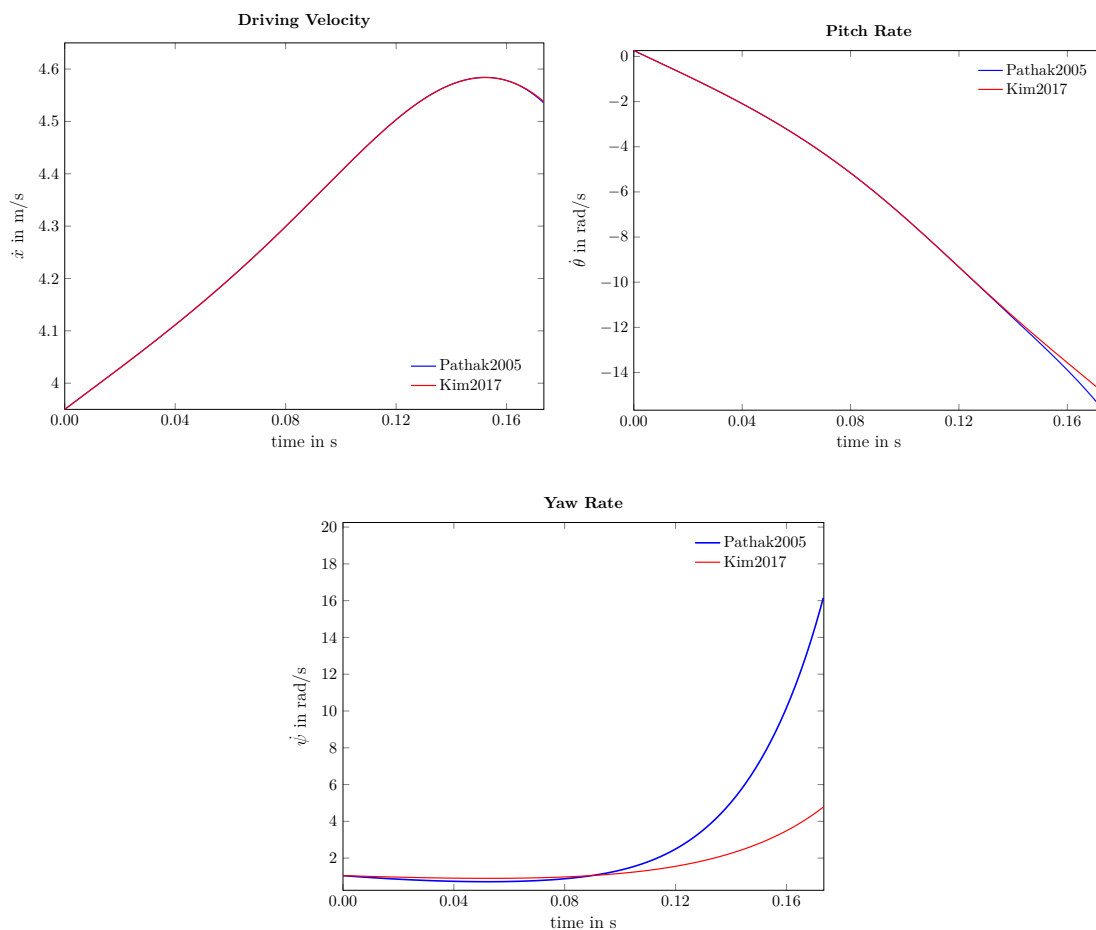


Figure 2.3: Comparison of the simulated dynamics of the Kim- and Pathak-Model. While the driving velocities seem to be identical, a drastic mismatch can be detected in the computed yaw rates.

### 2.2.1 Yaw Motion of the TWIP

The terms describing the TWIP's yaw motion within the two models were evaluated by first comparing the input influence defined by the corresponding entries in the input matrix,  $\mathbf{g}(\mathbf{x})$ . For the Kim-Model the input terms for the yaw motion are given in the appendix of [26]:

$$\ddot{\psi}_K = \dots - b_6(\mathbf{x})(\tau_l - \tau_r) = \dots - \frac{d}{r\eta_2(\theta)}(\tau_l - \tau_r). \quad (2.4)$$

However, when consulting the equations given in [25] the yaw motion due to the applied input is describes as:

$$\ddot{\psi}_K = \dots - \frac{d}{2r a_{33}(\theta)}(\tau_l - \tau_r). \quad (2.5)$$

As the division by 2 in eq. 2.5 is a geometric necessity due to the fact that  $d$  describes the full and not half-distance between the two wheels, this is assumed to be an error in eq. 2.4 – taken for now that the pitch-dependent terms,  $a_{33}(\theta)$  of [25] and  $\eta_2(\theta)$  of [26], are identical. Consequently, comparing  $a_{33}(\theta)$  and  $\eta_2(\theta)$  in detail displays that they are in fact equivalent except for the factorization of one term:

$$a_{33}(\theta) = I_{b3} + 2I_{w2} + \frac{d^2}{2}(m_w + J/r^2) + (I_{b1} + m_b l^2 - I_{b3}) \sin^2(\theta) \quad (2.6a)$$

$$\eta_2(\theta) = I_{b3} + 2I_{w2} + 2d^2(m_w + J/r^2) + (I_{b1} + m_b l^2 - I_{b3}) \sin^2(\theta). \quad (2.6b)$$

This is again considered to be a typo in the state-space model introduced in [26] as the corresponding terms of  $\frac{d^2}{2}$  can also be found in the course of the detailed derivation in [25] eq. (27). Now, if in the state-space model of [26] in eq. 2.5 the  $\eta_2(\theta)$ -term of [26] is corrected to be identical to  $a_{33}(\theta)$  of [25] and a division by two is added to the input matrix entry,  $b_6(\mathbf{x})$ , the resulting yaw motion can be compared to the one defined in the Pathak-Model:

$$\begin{aligned} \ddot{\psi}_{K,corr} &= \frac{\sin(\theta)}{a_{33}(\theta)}(-2(I_{b1} - I_{b3} + m_b l^2) \cos(\theta) \dot{\theta} \dot{\psi} - m_b l \dot{x} \dot{\psi}) \\ &\quad - \frac{d}{2r a_{33}(\theta)}(\tau_l - \tau_r) \end{aligned} \quad (2.7a)$$

$$\begin{aligned} \ddot{\psi}_P &= \frac{r^2 \sin(\theta)}{G_\alpha}(-2(I_{b1} - I_{b3} + m_b l^2) \cos(\theta) \dot{\theta} \dot{\psi} - m_b l \dot{x} \dot{\psi}) \\ &\quad - \frac{dr}{2G_\alpha}(\tau_l - \tau_r). \end{aligned} \quad (2.7b)$$

This comparison yields that the Pathak- and the corrected Kim-Model are identical if for the pitch-dependent factor,  $G_\alpha$ , introduced by Pathak  $\frac{G_\alpha}{r^2} = a_{33}(\theta)$  holds. Looking up the detailed definitions of the Pathak-factor, reveals that this is the case:

$$\begin{aligned} \frac{G_\alpha}{r^2} &= (m_b l^2 - I_{b3} + I_{b1}) (1 - \cos^2(\theta)) + I_{b3} + 2 I_{w2} + \frac{d^2}{2} m_w + \frac{d^2}{2 r^2} I_{w1} \\ &= (m_b l^2 - I_{b3} + I_{b1}) \sin^2(\theta) + I_{b3} + 2 I_{w2} + \frac{d^2}{2} (m_w + \frac{I_{w1}}{r^2}) = a_{33}(\theta). \end{aligned} \quad (2.8)$$

Repeating the simulation using the “corrected” Kim-Model underlines this outcome as the resulting yaw motions in fig. 2.4 are identical.

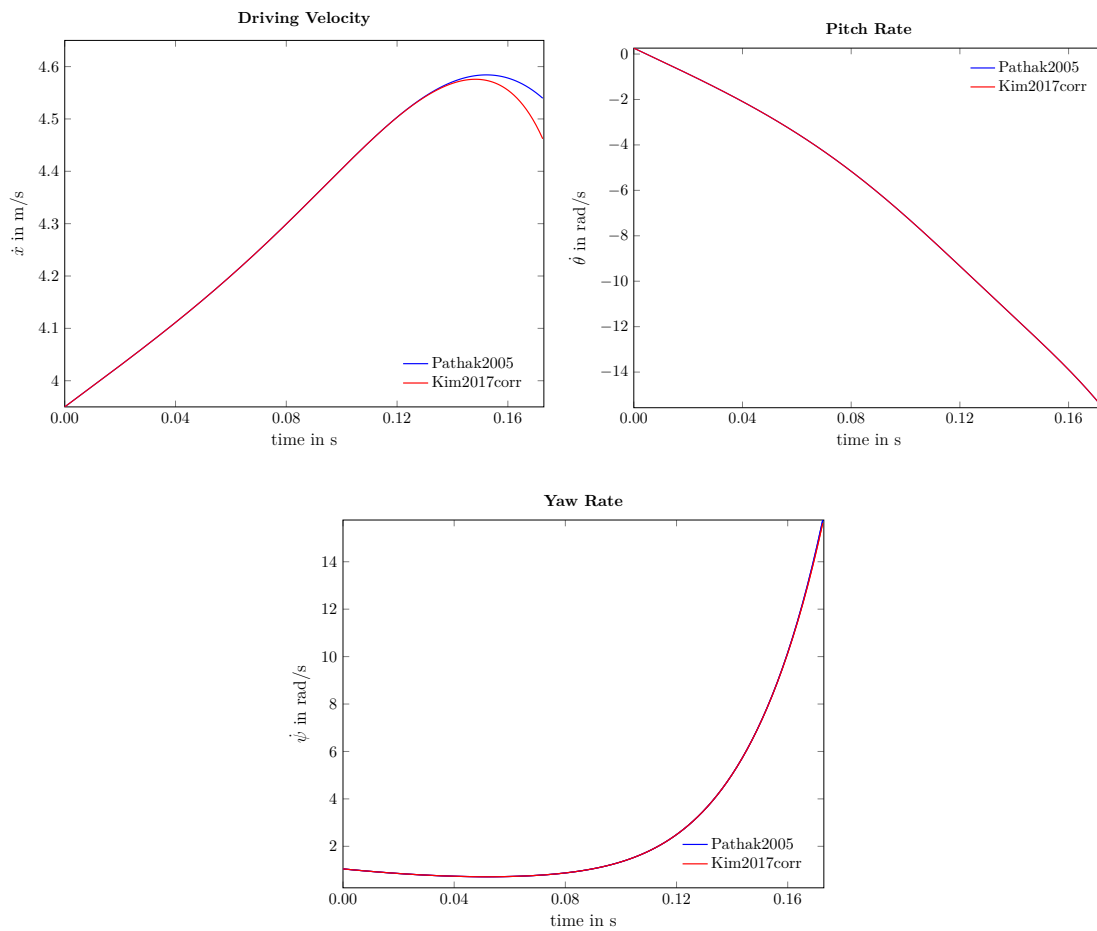


Figure 2.4: Comparison of the dynamics of the two models after the discussed corrections were executed on the Kim-Model.

In conclusion, the yaw dynamics derived in [38] and [25] are equivalent, however the state-space model introduced by Kim in [26] differs due to faulty factorizations. This is considered a typo within the Kim-Model of [26] and consequently the yaw dynamics of eq. 2.7 were implemented within this paper. While this correction explained the discrepancy in the yaw rates in the preceding simulations, fig. 2.4 also reveals that now the driving velocities are incompatible. In consequence, again the mathematical formulae were further investigated to explain this discrepancy.

### 2.2.2 Driving Velocity of the TWIP

Once again the two state-space models were at first evaluated in terms of how they compute the input influence on the system's forward acceleration:

$$\ddot{x}_K = \dots + \frac{1}{\eta_1(\theta)} \left[ (I_{b2} + m_b l^2)/r + m_b l \cos(\theta) \right] (\tau_l + \tau_r) \quad (2.9)$$

$$\ddot{x}_P = \dots - \frac{r^2}{D_\alpha} \left[ (I_{b2} + m_b l^2)/r + m_b l \cos(\theta) \right] (\tau_l + \tau_r), \quad (2.10)$$

which demonstrates that for the pitch-dependent factors,  $\eta_1(\theta)$  of [26] and  $D_\alpha$  of [38],  $\eta_1(\theta) = \frac{-D_\alpha}{r^2}$  has to hold for the input influence to be identical. Consulting the definition of  $D_\alpha$  in the appendix of [38]:

$$\begin{aligned} D_\alpha &= r^2 m_b^2 l^2 (\cos^2(\theta) - 1) - 2 r^2 m_w m_b l^2 - 2 r^2 I_{b2} m_w - I_{b2} m_b r^2 \\ &\quad - 2 I_{w1} m_b l^2 - 2 I_{b2} I_{w1} \\ &= -r^2 \left[ m_b^2 l^2 \sin^2(\theta) + m_b I_{b2} + 2 (m_w + I_{w1}/r^2)(I_{b2} + m_b l^2) \right] \\ &= -r^2 \eta_1(\theta) \end{aligned} \quad (2.11)$$

shows this correlation proves true. Accordingly, the difference has to lie within the inter-coupled state dynamics. Analysing the system state influence on the driving acceleration for both models:

$$\begin{aligned} \ddot{x}_K &= \frac{\sin(\theta)}{\eta_1(\theta)} \left[ -m_b^2 l^2 g \cos(\theta) + (I_{b2} + m_b l^2) m_b l \dot{\theta}^2 \right. \\ &\quad \left. + (I_{b2} + m_b l^2 + (I_{b3} - I_{b1} - m_b l^2) \cos^2(\theta)) m_b l \dot{\psi}^2 \right] + \dots \end{aligned} \quad (2.12)$$

$$\begin{aligned} \ddot{x}_P &= \frac{r^2 \sin(\theta)}{-D_\alpha} \left[ -m_b^2 l^2 g \cos(\theta) + (I_{b2} + m_b l^2) m_b l \dot{\theta}^2 \right. \\ &\quad \left. - \frac{D_\alpha}{r^2 \sin(\theta)} K_\alpha \dot{\psi}^2 \right] + \dots \end{aligned} \quad (2.13)$$

while recalling that  $\eta_1(\theta) = \frac{-D_\alpha}{r^2}$  it remains to investigate whether  $\eta_1(\theta) K_\alpha = [I_{b2} + m_b l^2 + (I_{b3} - I_{b1} - m_b l^2) \cos^2(\theta)] m_b l \sin(\theta)$  holds. Looking up the definition of  $K_\alpha$  given in the appendix of [38]:

$$K_\alpha = r^2 m_b l \left[ \left( -4I_{b2} - 3m_b l^2 + I_{b1} - I_{b3} \right) \sin(\theta) + \left( m_b l^2 + I_{b1} - I_{b3} \right) \sin(3\theta) \right] \quad (2.14)$$

and making use of the trigonometric identity,  $\sin(3\theta) = 3\sin(\theta) - 4\sin^3(\theta)$ , as well as further transformations yields:

$$\eta_1(\theta) K_\alpha = -4\eta_1(\theta) r^2 \left( I_{b2} + m_b l^2 + (I_{b3} - I_{b1} - m_b l^2) \cos^2(\theta) \right) m_b l \sin(\theta) \quad (2.15)$$

From eq. (2.15) it is apparent that the difference in the simulated velocities originates from the fact that the  $K_\alpha$ -factor defined by Pathak would have to be corrected through an additional division by  $4D_\alpha$  to result in the same dynamics as those defined by Kim, as:

$$\frac{K_\alpha}{-4\eta_1(\theta)r^2} = \frac{K_\alpha}{4D_\alpha} \quad (2.16)$$

holds. This is assumed to be a mistake within the Pathak-Paper as there is no apparent reason why the dynamic model received from the Euler-Lagrange-Equation in eq.(5) of [38] should result in a different factorization of the yaw rate terms than the one applied to the gravity and pitch rate terms.

After applying the correction of eq. (2.16) to the Pathak-Model, the simulations were executed once more and as the trajectories given in fig. 2.5 illustrate no differences could be detected any more. This leads to the assumption that the pitch dynamics defined within the two models were identical to begin with. Lastly, comparing the pitch dynamics in fact confirms this hypothesis:

$$\begin{aligned} \ddot{\theta}_K = & \frac{\sin(\theta)}{\eta_1(\theta)} \left[ (m_b + 2m_w + 2I_{w1}/r^2) m_b l g - m_b^2 l^2 \cos(\theta) \dot{\theta}^2 - \right. \\ & \left. (m_b^2 l^2 + (I_{b3} - I_{b1} - m_b l^2)(m_b + 2m_w + 2I_{w1}/r^2)) \cos(\theta) \dot{\psi}^2 \right] + \\ & \frac{-1}{\eta_1(\theta)} \left[ m_b + 2m_w + 2I_{w1}/r^2 + m_b l \cos(\theta)/r \right] (\tau_l + \tau_r) \end{aligned} \quad (2.17)$$

$$\begin{aligned} \ddot{\theta}_P = & \frac{-\sin(\theta) r^2}{D_\alpha} \left[ (m_b^2 l + 2m_w m_b l + 2m_b l I_{w1}/r^2) g - m_b^2 l^2 \cos(\theta) \dot{\theta}^2 - \right. \\ & (m_b I_{b3} + 2I_{b3} I_{w1}/r^2 - 2I_{b1} m_w - 2I_{b1} I_{w1}/r^2 - \\ & \left. - 2m_b l^2 m_w - 2m_b l^2 I_{w1}/r^2 - m_b I_{b1} + 2m_w I_{b3}) \cos(\theta) \dot{\psi}^2 \right] + \\ & \frac{r^2}{D_\alpha} \left[ m_b + 2m_w + 2I_{w1}/r^2 + m_b l \cos(\theta)/r \right] (\tau_l + \tau_r). \end{aligned} \quad (2.18)$$

In conclusion, the author considers the detailed derivation executed by Kim and Kwon in [25] to be correct and the deviation in the computation of the yaw rate within the deduced state-space model in [26] to be unintended. Pathak amounting to the same yaw dynamics reaffirms this assumption. Besides from these minor corrections, the state-space model introduced in [26] corresponds to the formulae derived in [25] and is taken as accurate.

The Pathak-Model deduced and introduced in [38] is identical to the one of [25] besides the minor deviation in the defined constant  $K_\alpha$ . Again, this is assumed to be correct within the Kim-Paper [25] as Pathak provides no explanation on why one term within the computation of the driving acceleration should be factored differently. An overview over the exact formulae that were consequently chosen to define the TWIP's dynamics for the remaining of this paper are provided in the appendix (A.3).

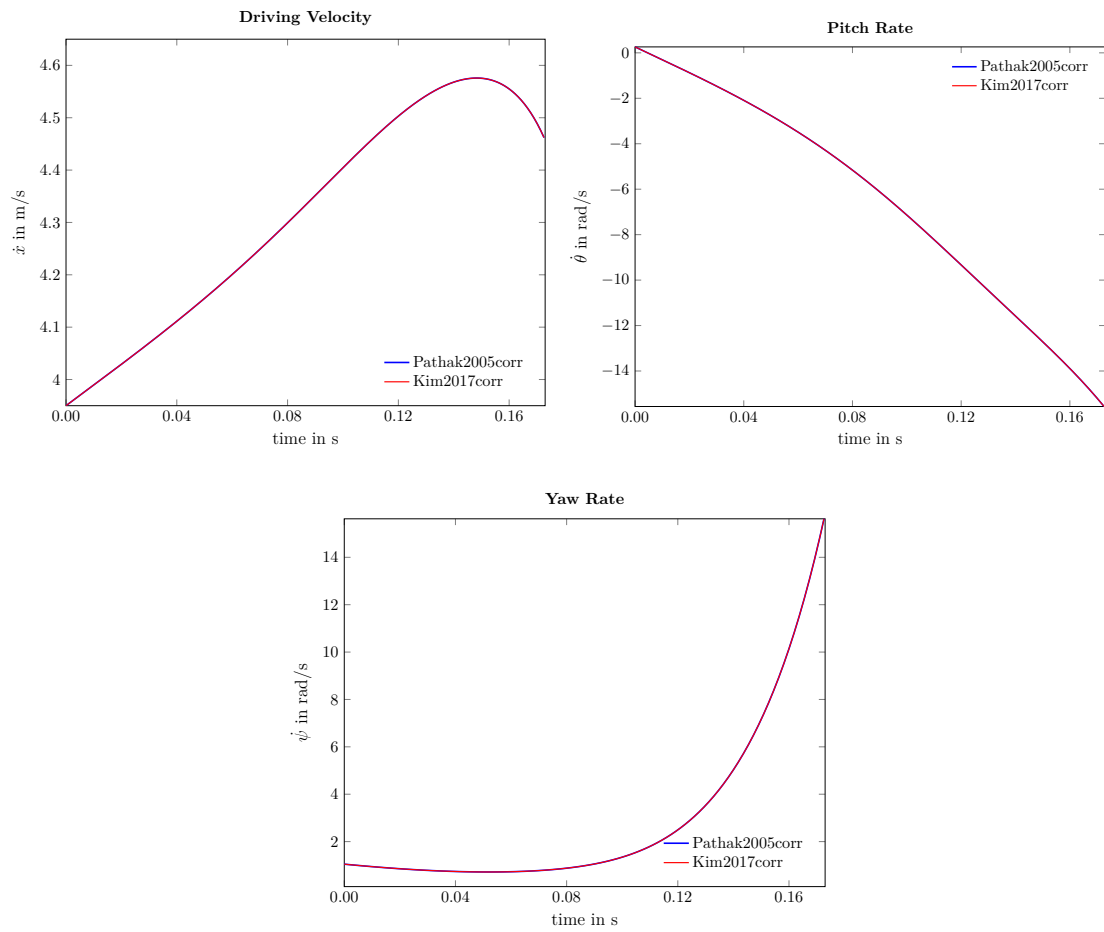


Figure 2.5: Comparison of the dynamics of the two models after the discussed corrections were applied to both models. The minor adaptation of the Pathak-coefficient resulted in the two models defining consistent dynamics.



## Chapter 3

# Non-linear Systems and Stability

Stability can be considered the most fundamental system property to achieve as a dynamically unstable system is most likely technically useless and in a worst case scenario even dangerous [42]. Technically, not an entire system itself but only its equilibrium points are evaluated in regards of stability – a simple pendulum with its upright and downward equilibrium points gives an intuitive idea of the difference between stable and unstable equilibria. Nonetheless, in the literature often an entire linear system is justifiably referred to as stable or unstable which motivates sec. 3.2 giving an overview on how stability analysis varies depending on whether a system’s dynamics are linear or not. Whereas for linear time-invariant (LTI)-systems there exist methodologically sound techniques for system analysis that can be applied using established linear algebra tools and under reasonable computational expenses, non-linear system analysis remains very restrictive [9] and can often result in non-feasible computational effort even for systems of relatively low order.

Still, non-linear system analysis has remarkably evolved and today the most widely known and applied approach to study stability in the context of non-linear control systems is the one developed by the Russian mathematician, Aleksandr Lyapunov [42]. The more recently introduced contraction theory by Lohmiller and Slotine relies on a slightly different notion of stability and is discussed in sec. 3.4. In the context of this paper, only contraction analysis will be applied, however as its formulation was based on the fundamentals laid by Lyapunov’s work, in sec. 3.3 a quick introduction to Lyapunov theory will be given first. Lastly, in sec. 3.5 controllability will be discussed as a system property closely related to stability. First of all, an overview of some characteristics of dynamical systems will be provided in sec. 3.1 to outline the TWIP’s dynamical characteristics and how these affects the analysis tools applicable.

### 3.1 Classification of Dynamical Systems

Generally, a dynamical system can be described through:

$$\dot{\mathbf{x}}(t) = \mathbf{f}(\mathbf{x}, t), \quad \mathbf{x}_0 = \mathbf{x}(t_0), \quad (3.1)$$

where  $\mathbf{x}_0$  defines its initial state at initial time  $t_0$ . The dimension of the vectors,  $\dot{\mathbf{x}}$  and  $\mathbf{f}$ , is referred to as the system order [42]. Assuming that the system vector,  $\mathbf{f}$ , and its first partial derivatives are continuous, a unique solutions,  $\mathbf{x}(t)$ , always exists [49]. Often, this solution is called a system trajectory, state trajectory or simply trajectory.

A special class of such dynamical systems are linear systems defined by:

$$\dot{\mathbf{x}}(t) = \mathbf{A}(t)\mathbf{x}(t), \quad \mathbf{x}_0 = \mathbf{x}(t_0), \quad (3.2)$$

where the quadratic system matrix,  $\mathbf{A}(t)$ , completely defines the system's dynamics. Note that both definitions in eq. (3.1) and eq. (3.2) are equally valid to either represent an unforced system or one subject to feedback control [42] as for:

$$\dot{\mathbf{x}}(t) = \mathbf{f}(\mathbf{x}, \mathbf{u}, t) \quad \text{subject to: } \mathbf{u}(t) = \mathbf{g}(\mathbf{x}, t) \quad (3.3)$$

the closed-loop dynamics can always be transcribed to:

$$\dot{\mathbf{x}}(t) = \mathbf{f}(\mathbf{x}, \mathbf{g}(\mathbf{x}, t), t) = \tilde{\mathbf{f}}(\mathbf{x}, t). \quad (3.4)$$

And analogously in the linear case:

$$\dot{\mathbf{x}}(t) = \mathbf{A}(t)\mathbf{x}(t) + \mathbf{B}(t)\mathbf{u}(t) \quad \text{subject to: } \mathbf{u}(t) = -\mathbf{K}(t)\mathbf{x}(t) \quad (3.5)$$

can be reformulated to:

$$\dot{\mathbf{x}}(t) = \mathbf{A}(t)\mathbf{x}(t) - \mathbf{B}(t)\mathbf{K}(t)\mathbf{x}(t) = \tilde{\mathbf{A}}(t)\mathbf{x}(t). \quad (3.6)$$

Consequently, all analysis tools based on state-space representations as defined in eq. (3.1) and eq. (3.2) can likewise be applied to investigate unforced or closed-loop system dynamics.

The TWIP's dynamics as introduced in sec. 2 define a so-called autonomous system, i.e. a system with dynamics that do not depend on time,  $t$ , explicitly:

$$\dot{\mathbf{x}}(t) = \mathbf{f}(\mathbf{x}), \quad \mathbf{x}_0 = \mathbf{x}(0), \quad (3.7)$$

whereas system dynamics as defined in eq. (3.1) are called non-autonomous. In the linear case, autonomous systems with a system matrix,  $\mathbf{A}$ , independent of time:

$$\dot{\mathbf{x}}(t) = \mathbf{A}\mathbf{x}, \quad \mathbf{x}_0 = \mathbf{x}(0), \quad (3.8)$$

are most commonly referred to as linear time-invariant (LTI)-systems and non-autonomous systems as defined in eq. (3.2) as linear time-varying (LTV)-systems. In the non-linear case however, Slotine suggests employing the terms "autonomous" and "non-autonomous" [42] which will be adopted within this paper.

The fundamental difference between autonomous and non-autonomous systems, is that trajectories of autonomous systems are independent of the initial time,  $t_0$ , while this generally does not apply to non-autonomous systems [42]. Naturally, this simplifies system analysis and accordingly the methods as introduced in the following will be restricted to autonomous systems. However the extension of Lyapunov theory to non-autonomous systems is straight-forward, requires only minor adaptations, and detailed definitions can be found in standard literature [42, 47, 49]. Contraction theory in its definition is indifferent to whether a system is autonomous or not and consequently the concepts introduced in sec. 3.4 apply to either. For easier readability, the time dependency of state variables will no longer be noted from here on.

## 3.2 Stability of Equilibria and Linear Stability Analysis

Although stability can be discussed in various contexts within control theory, most commonly the stability of a system's equilibrium is investigated [24]. An equilibrium state or point,  $\mathbf{x}_{\text{eq}}$ , is defined as configuration satisfying:

$$\mathbf{f}(\mathbf{x}_{\text{eq}}) = \mathbf{0} \quad (3.9)$$

for all times,  $t$ , and consequently describes a constant solution to eq. (3.1), where the system trajectory corresponds of a single point in state-space. In simple terms, a stable equilibrium point can be distinguished from an unstable one by the property that a trajectory starting close to it remains close to it for all times [24]. While a pendulum will naturally not remain in a position close to its unstable upright equilibrium, without external forces applied it will rest in its stable downward equilibrium forever after.

Non-linear systems – like the pendulum example – can have an arbitrary number of equilibrium points, whereas LTI-systems with a non-singular system matrix,  $\mathbf{A}$ , naturally only possess the trivial equilibrium point,  $\mathbf{x}_{\text{eq}} = \mathbf{0}$  [42]. Thus, for LTI-systems no further clarification regarding which equilibrium point is discussed needs to be provided, and often an entire system is classified as stable or unstable depending on the stability of its sole equilibrium,  $\mathbf{x}_{\text{eq}} = \mathbf{0}$ <sup>1</sup>.

Due to this property, for LTI-systems stability can synonymously be defined in the meaning that any initial condition,  $\mathbf{x}_0$ , excites an over all times,  $t$ , bounded system response [8]. Any LTI-system contains the solution,  $\mathbf{x} = \mathbf{x}_0 e^{\mathbf{A}t}$ , and for this solution trajectory to remain bounded invariably, each entry of  $e^{\mathbf{A}t}$  must stay bounded. This only holds if all eigenvalues of  $\mathbf{A}$  have strictly negative real-parts [8] which provides a necessary and sufficient condition for system stability in the LTI-case. This eigenvalue method only consists of a single numerical matrix evaluation as the system matrix,  $\mathbf{A}$ , neither depends on time nor state. Consequently, with the help of a numerical computing toolbox this technique is applicable even to systems of high order.

When on the other hand discussing an autonomous non-linear systems, remarkably different considerations have to be made. First of all, a non-linear system can possess an arbitrary number of isolated equilibria [42], such that clear reference needs to be provided which equilibrium point is examined. Additionally, eigenvalue analysis is a linear algebra tool and can not be applied to non-linear vector fields. Being familiar with linear control theory though, an intuitive idea would be to simply approximate the system's non-linear dynamics by computing the first-order Taylor-series expansion about some technically relevant equilibrium point:

$$\dot{\mathbf{x}} \approx \left. \frac{\partial \mathbf{f}}{\partial \mathbf{x}} \right|_{\mathbf{x}=\mathbf{x}_{\text{eq}}} (\mathbf{x} - \mathbf{x}_{\text{eq}}) = \bar{\mathbf{A}}(\mathbf{x} - \mathbf{x}_{\text{eq}}) \quad (3.10)$$

where  $\left. \frac{\partial \mathbf{f}}{\partial \mathbf{x}} \right|_{\mathbf{x}=\mathbf{x}_{\text{eq}}}$  denotes the system's Jacobian evaluated at the linearization point,  $\mathbf{x}_{\text{eq}}$ , consisting of the first-order partial derivatives of the non-linear system dynamics.

---

<sup>1</sup>LTI-systems with a singular system matrix,  $\mathbf{A}$ , possess infinite many equilibria, which are defined by the null-space of the system-matrix,  $\mathbf{A}$ . As these kind of systems will however not be relevant for the remaining of this work, they will not be further discussed.

In fact, this is exactly what Lyapunov’s linearization method suggests with the only restriction that first the equilibrium point of interest needs to be shifted to the origin as all of Lyapunov theory is exclusively defined for  $\mathbf{x}_{\text{eq}} = \mathbf{0}$ .

Now, analogously to analysis of LTI-systems the eigenvalues of  $\bar{\mathbf{A}}$  can be evaluated. If all of them possess strictly negative real-parts, the equilibrium point of the non-linear system is locally stable. If however at least one eigenvalue lies on the imaginary axis, no conclusions about the equilibrium point of the original non-linear system can be drawn. In fact, examples of simple non-linear systems as provided in [42] can be given that are globally asymptotically stable<sup>2</sup> while their linearization has a zero eigenvalue. Ultimately, Lyapunov’s linearization method provides a technique easily employed by anyone familiar with linear system theory but very limited in its use to classify the actual non-linear system of interest [47].

Additionally, this approach always relies on the key assumption of a small operating range around this fixed equilibrium state [42]. For larger deviations, the linear model of eq. (3.10) can no longer be assumed valid and consequently controllers based on linear design techniques are expected to perform poorly or even become unstable – and have been observed to do so [42]. In order to analyse non-linear dynamics within a considerable operating range, one can not rely on plain linearization-based methods but instead has to employ non-linear approaches as described in the following.

### 3.3 Non-linear Stability Analysis – Lyapunov Theory

In his doctoral thesis, Lyapunov presented two methods for stability analysis – the already discussed indirect or linearization method and the so-called direct method. As the name already implies, the indirect method only allows to draw very limited conclusions about local system behaviour. The direct method however, marked an utterly novel approach that enables analysis of the non-linear system dynamics by constructing and evaluating an “energy-like” scalar function,  $V(\mathbf{x})$  [42]. Before Lyapunov’s direct method is introduced in sec. 3.3.2, first a mathematically precise definition of stability according to Lyapunov is provided as so far the term “stability” was only defined quite loosely in verbal form. Note that Lyapunov’s definitions of stability as provided in the following always are stated with respect to the equilibrium point,  $\mathbf{x}_{\text{eq}} = \mathbf{0}$ , which however results in no loss of generality as this can always be achieved through an appropriate transformation of the state-space variables. The following definitions are adapted from [42].

#### 3.3.1 Stability According to Lyapunov

In his thesis, Lyapunov defines the stability of a system’s equilibrium point located in the origin accordingly:

**Definition 3.1** (Stability According to Lyapunov). The equilibrium point,  $\mathbf{x}_{\text{eq}} = \mathbf{0}$ , is said to be stable if for any  $r_\varepsilon$  there exists an  $r_\delta$  such that if  $\|\mathbf{x}_0\| < r_\delta$ , then  $\|\mathbf{x}\| < r_\varepsilon$  for all  $t \geq 0$ . Otherwise,  $\mathbf{x}_{\text{eq}} = \mathbf{0}$  is said to be unstable. ▲

---

<sup>2</sup>To be defined in the next section.

Figuratively speaking, there exists a sphere of radius,  $r_\delta$ , around the origin such that if a trajectory starts within this sphere, it forever remains in another sphere of radius,  $r_\epsilon$ , which obviously implies that in this case the system will not diverge. However, Lyapunov stability alone only guarantees for all trajectories starting within the  $r_\delta$ -sphere to stay within some region nearby the origin, not that they ever reach it. This motivates the definition of asymptotic stability as there often lies technical relevancy in a system to actually converge to the origin [42].

**Definition 3.2** (Asymptotic Stability According to Lyapunov). The equilibrium point,  $\mathbf{x}_{\text{eq}} = \mathbf{0}$ , is said to be asymptotically stable if it is stable and additionally there exists some  $r_\delta$  such that if  $\|\mathbf{x}_0\| < r_\delta$ , then  $\mathbf{x} \rightarrow \mathbf{0}$  as  $t \rightarrow \infty$ . ▲

Again employing the sphere-allegory, there exists some  $r_\delta$ -sphere around the origin such that all trajectories starting from this region will not just stay nearby the origin but continuously tend towards it. In conclusion, asymptotic stability guarantees for a technical system to always eventually return to its equilibrium state if not deviated too far from it. However, no bounds can be provided on how long it takes for the system to restore its equilibrium state. Lastly, the necessity of a technical system converging within finite time can be met through the definition of exponential stability.

**Definition 3.3** (Exponential Stability According to Lyapunov). The equilibrium point,  $\mathbf{x}_{\text{eq}} = \mathbf{0}$ , is said to be exponentially stable if it is stable and if additionally there exist two strictly positive numbers,  $\beta_\alpha$  and  $\beta_\lambda$ , such that there exists some  $r_\delta$  such that if  $\|\mathbf{x}_0\| < r_\delta$ , then  $\|\mathbf{x}\| \leq \beta_\alpha \|\mathbf{x}_0\| e^{-\beta_\lambda t}$  for all  $t \geq 0$ . ▲

If these inequalities hold, all trajectories of the system starting within some  $r_\delta$ -sphere converge to the origin at an exponential rate. Here,  $\beta_\lambda$  is often referred to as the convergence rate. Figure 3.1 illustrates the different notions of stability using the example of a scalar system and fig. 3.2 shows exemplary state-space trajectories for a two-dimensional system.

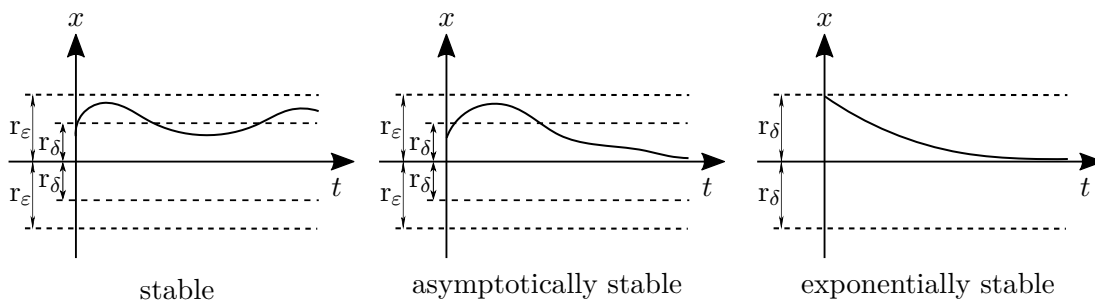


Figure 3.1: Lyapunov’s different notions of stability for a scalar system state plotted over time. The plots were adapted from fig. 4.4 of [49].

All of the notions of stability provided only hold for trajectories starting within a certain region close enough to the origin. Thus, they only describe local behaviour of the system valid for a particular set of initial states. Finally, the notion of global stability will allow classification of an entire dynamical system for all possible initial states.

**Definition 3.4** (Global Stability According to Lyapunov). If asymptotic or exponential stability of an equilibrium point holds for any initial state,  $\mathbf{x}_0$ , the equilibrium point is referred to as globally asymptotically or exponentially stable. ▲

If a system's equilibrium point is found to be globally stable, this obviously implies that it's the only equilibrium point within the system. For LTI-systems to be asymptotically stable, all eigenvalues have to lie strictly in the left-half complex plane. The exponential function solution,  $\mathbf{x} = \mathbf{x}_0 e^{\mathbf{A}t}$ , of any LTI-system, also illustrates that for LTI-systems asymptotic stability is synonymous with exponential and global stability [42].

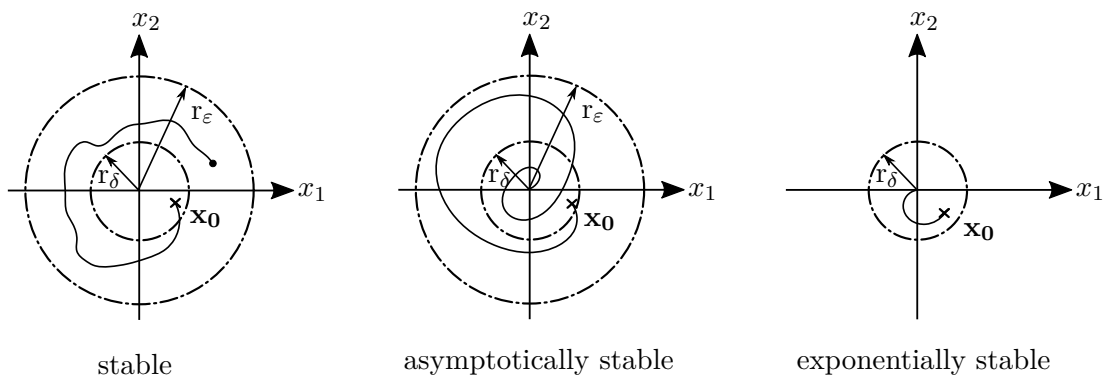


Figure 3.2: Lyapunov's different notions of stability for a two-dimensional system. The first plot describes a stable system as the trajectory starting close to the origin, remains close. The second plot defines asymptotic stability as the trajectory not only stays within the  $r_\epsilon$ -region for all times but eventually reaches the origin. The third plot describes exponential stability where the trajectory takes a "direct" path to the origin. The plots were adapted from fig. 4.3 of [49].

### 3.3.2 Lyapunov's Direct Method

In contrast to his linearization method, with his direct method Lyapunov introduced an approach completely independent of any approximation of the system's dynamics. Essentially, Lyapunov's direct method can be considered a mathematical relaxation of a fundamental physical observation: if a system's energy is continuously dissipated, it will eventually come to rest at some equilibrium point [42]. This is an observation that can be made regardless of the system's dynamics being linear or not. Accordingly, Lyapunov generalized the idea of conservative mechanical systems to make it applicable to any differential equation [47] and suggested to examine stability through scalar energy-like functions, so-called Lyapunov-functions,  $V(\mathbf{x})$ .

#### Stability through Lyapunov's Direct Method

In his according theorems, Lyapunov stated that stability of the equilibrium point,  $\mathbf{x}_{\text{eq}} = \mathbf{0}$ , can be concluded, if within a  $r_\delta$ -sphere around this equilibrium point a scalar function,  $V(\mathbf{x})$ , with continuous first partial derivatives can be found such that:

- $V(\mathbf{x})$  is positive-definite, meaning that  $V(\mathbf{x}) \geq 0$  for all  $\mathbf{x}$  and  $V(\mathbf{x}) = 0$  only holds for  $\mathbf{x}_{\text{eq}} = \mathbf{0}$

- $\dot{V}(\mathbf{x}) = \frac{\partial V}{\partial \mathbf{x}} \dot{\mathbf{x}}$  is negative-semi-definite, meaning that  $\dot{V}(\mathbf{x}) \leq 0$  for all  $\mathbf{x}$ .

Fulfilling these conditions,  $V(\mathbf{x})$  is called a Lyapunov-function of the system and often a scalar function,  $V(\mathbf{x})$ , that is positive-definite but  $\dot{V}(\mathbf{x})$  remains to be proven to be negative-semi-definite is referred to as Lyapunov-function-candidate.

### Asymptotic Stability through Lyapunov’s Direct Method

Further conditions on a Lyapunov-function,  $V(\mathbf{x})$ , can be specified to also prove asymptotic stability:

- if additionally  $\dot{V}(\mathbf{x})$  is negative-definite or in other words  $\dot{V}(\mathbf{x}) = 0$  only holds for  $\mathbf{x}_{\text{eq}} = \mathbf{0}$ , this local stability is asymptotic.

If the considered  $r_\delta$ -sphere is expanded to the entire state-space and

- if additionally  $V(\mathbf{x})$  is radially unbounded, meaning that  $V(\mathbf{x}) \rightarrow \infty$  as  $\|\mathbf{x}\| \rightarrow \infty$ , this asymptotic stability is global.

While the physical interpretation of dissipating energy is straight-forward, to underline the possible choice of not just the system’s total energy but any positive-definite scalar function,  $V(\mathbf{x})$ , a geometric interpretation as provided in fig. 3.3 can be handy to consult. For a two-dimensional system, the properties postulated for the Lyapunov-function,  $V(\mathbf{x})$ , to guarantee global asymptotic stability result in it describing a cup-shaped surface with its unique minimum located in the origin,  $\mathbf{x}_{\text{eq}} = \mathbf{0}$ . In order to assure asymptotic stability, the time derivative of the Lyapunov-function,  $\dot{V}(\mathbf{x})$ , defined by the scalar product of the Lyapunov-function’s gradient,  $\frac{\partial V}{\partial \mathbf{x}}$ , and the system’s velocity vector,  $\dot{\mathbf{x}}$ , must take negative values for all system states such that the angle between these two vectors is constantly greater than  $\frac{\pi}{2}$ . This yields a tangible image for all trajectories converging to the origin when projected on this cup-plane. Thinking this visualization further, these trajectories will still tend towards the origin, when retransformed to  $\mathbb{R}^2$ , as the “bending-up” of the trajectories to the cup-shaped surface does not affect their convergence. For higher-dimensional systems – as with many mathematical theories – comprehensive visualizations are hard to fathom but instead general mathematical proofs have to be trusted.

### Exponential Stability through Lyapunov’s Direct Method

Although, Lyapunov’s direct method is mostly applied to determine asymptotic stability, it can also be used to prove exponential stability by finding a Lyapunov-function,  $V(\mathbf{x})$ , for that within a  $r_\delta$ -sphere about the origin

- the inequalities,  $\beta_1 \|\mathbf{x}\|^k \leq V(\mathbf{x}) \leq \beta_2 \|\mathbf{x}\|^k$  and  $\dot{V}(\mathbf{x}) \leq -\beta_3 \|\mathbf{x}\|^k$ , hold where  $k, \beta_1, \beta_2, \beta_3$  all are positive constants.

The dynamical system it then proven to be exponentially stable and again if this inequalities are fulfilled in the entire state-space and not just within a certain  $r_\delta$ -sphere

about the origin, global exponential stability can be shown [47]. The inequality constraints on the Lyapunov-function,  $V(\mathbf{x})$ , and its time derivative,  $\dot{V}(\mathbf{x})$ , already demanded positive-definiteness and negative-definiteness respectively, and consequently assure stability. This condition for a Lyapunov-function to assure exponential stability is no longer to be motivated geometrically but by the fact that if the stated inequalities hold, this allows to conclude for that system's dynamics to have solutions that are exponentially bounded. For further explanations and insightful examples, the author refers to the extensive literature on the field, e.g. [42, 47, 24].

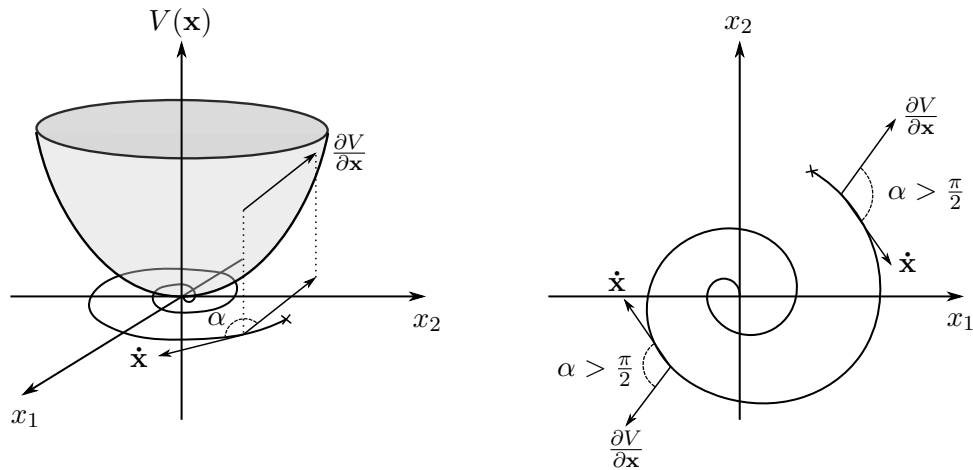


Figure 3.3: Geometrical interpretation of asymptotic stability through Lyapunov's direct method. The Lyapunov-function,  $V(\mathbf{x})$  defines a cup-shaped surface over the two-dimensional state-space. The scalar product of its gradient,  $\frac{\partial V}{\partial \mathbf{x}}$ , and the system's velocity vector,  $\dot{\mathbf{x}}$ , is strictly negative and therefore the angle between these two vectors is always greater than  $\frac{\pi}{2}$ . Consequently, all trajectories on it continuously tend towards the origin.

### 3.3.3 Remarks on Lyapunov-based Stability Analysis

In conclusion, when given a certain Lyapunov-function-candidate one can systematically determine whether through this scalar function the equilibrium's point (asymptotic or exponential) stability can be verified or not. However, if the prerequisites on its time derivative are not met with this particular choice, no conclusions can be drawn at all as the conditions given in the context of Lyapunov's direct method have sufficient not necessary character [42]. Interestingly enough, the converses of Lyapunov's stability theorems do hold, meaning that if an equilibrium point is stable, there exist a corresponding Lyapunov-function to prove so [47]. Still, the task remains to find one of those specific functions and while often a sound understanding of the dynamics of the system evaluated can ease the choice of a Lyapunov-function-candidate leading to success, in many instances also very random adaptations without any particular physical interpretation have to be made to end up with a suitable Lyapunov-function. In general, there exists no universal technique that guarantees the successful construction of a Lyapunov-function for arbitrary non-linear systems.



## 3.4 Non-linear Stability Analysis – Contraction Theory

While Lyapunov postulated his stability theory in 1892 already, it did not receive much attention in the Western academic world until the 1960s [47]. However, since Kalman brought Lyapunov theory to the field of automatic control, it remains the most elementary tool in non-linear system analysis and has been the basis of a wide range of design techniques. In the late 1990s, Lohmiller and Slotine developed an alternate approach to non-linear stability analysis referred to as contraction theory which even though still lesser-known has since been applied successfully in a number of non-linear applications. While contraction theory can also be applied in filter- or controller-synthesis, in the context of this paper it will only be used as an analysis tool. Hence, in the following a quick introduction to the concepts of contraction theory is given with a focus on its use for system classification.

### 3.4.1 Convergence to a Single Trajectory and Contracting Systems

While Lyapunov’s approach on defining and classifying stability can be interpreted as a generalization inspired by Lagrangian mechanics for rigid bodies, contraction analysis on the other hand can be considered to be motivated by fluid mechanics. Accordingly, in his thesis Lohmiller introduces a slightly different concept of stability [32] – based on the notion that a stable systems over time “forgets” its initial condition and any occurring disturbances. Motivated by the notion of a non-linear system as defined in eq. (3.1) as the dynamics of a multi-dimensional flow field, where  $\dot{\mathbf{x}}$  describes the multi-dimensional velocity field with initial condition,  $\mathbf{x}_0(t_0)$  at initial time,  $t_0$ , the basic idea of contraction analysis is that if any two neighbouring trajectories of this flow field converge to each other – in the meaning that the distance between them vanishes over time –, it can be concluded that eventually all system trajectories will converge to a single system state.

This slightly different concept of stability is more precisely referred to as convergence and the corresponding system behaviour as contracting [43]. Note that the dynamics of eq. (3.1) might again also refer to a closed-loop system subject to state feedback  $\mathbf{u}(\mathbf{x})$ , such that contraction analysis is applicable to unforced and closed-loop systems likewise. While contraction theory as presented in its original form in [32, 43] allows the evaluation of non-autonomous systems, for the context of this work it will only be employed to analyse the TWIP’s autonomous dynamics and therefore only the slightly reduced version as presented in [2] will be further discussed.

In order to provide a mathematical condition for a system to be contracting, the virtual displacement,  $\delta\mathbf{x}$ , – an infinitesimal displacement at fixed time – between two neighbouring trajectories is introduced. For this virtual displacement the following differential relation holds:

$$\delta\dot{\mathbf{x}} = \frac{\partial \mathbf{f}}{\partial \mathbf{x}} \delta\mathbf{x}. \quad (3.11)$$

Defining the distance between two trajectories as the squared Euclidean displacement vector allows to evaluate how this distance evolves over time:

$$\frac{d}{dt}(\delta\mathbf{x}^T \delta\mathbf{x}) = 2 \delta\mathbf{x}^T \delta\dot{\mathbf{x}} = 2 \delta\mathbf{x}^T \frac{\partial \mathbf{f}}{\partial \mathbf{x}} \delta\mathbf{x}. \quad (3.12)$$

Denoting  $\lambda_{f,\max}$  as the largest eigenvalue of the symmetric part of the system's Jacobian, i.e. the largest eigenvalue of  $\frac{1}{2}(\frac{\partial \mathbf{f}}{\partial \mathbf{x}} + \frac{\partial \mathbf{f}}{\partial \mathbf{x}}^T)$ , permits the definition of an upper bound for this correlation:

$$\frac{d}{dt}(\delta \mathbf{x}^T \delta \mathbf{x}) \leq 2 \lambda_{f,\max} \delta \mathbf{x}^T \delta \mathbf{x}. \quad (3.13)$$

and the solution of this differential equation:

$$\delta \mathbf{x}^T \delta \mathbf{x} \leq (\delta \mathbf{x}_0^T \delta \mathbf{x}_0) e^{\int_0^t \lambda_{f,\max} dt} \quad (3.14)$$

yields the conclusion that if the largest eigenvalue of the system's Jacobian,  $\lambda_{f,\max}$ , is uniformly strictly negative any distance between two trajectories converges to zero exponentially. This motivates the following definition according to [43]:

**Definition 3.5** (Contraction Region). For a given system,  $\dot{\mathbf{x}} = \mathbf{f}(\mathbf{x})$ , a region within the state-space where the system's Jacobian,  $\frac{\partial \mathbf{f}}{\partial \mathbf{x}}$ , is uniformly negative-definite, is referred to as a contraction region.  $\blacktriangle$

Note that eq. (3.12) describes a quadratic form which is always equal to zero for the skew-symmetric part of a square matrix [42] and in consequence only the symmetric part of the Jacobian is relevant in this consideration. With the definition of contraction regions and the introduction of a  $r_\delta$ -sphere – already familiar from Lyapunov theory –, local system behaviour can be defined:

**Definition 3.6** (Exponential Convergence to a Single Trajectory). Any trajectory,  $\mathbf{x}$ , starting in a sphere of constant radius,  $r_\delta$ , centred about a given trajectory,  $\mathbf{x}_d$ , and for all times,  $t \geq 0$ , contained in a contraction region, remains in that  $r_\delta$ -sphere and converges to the given trajectory,  $\mathbf{x}_d$ , exponentially.  $\blacktriangle$

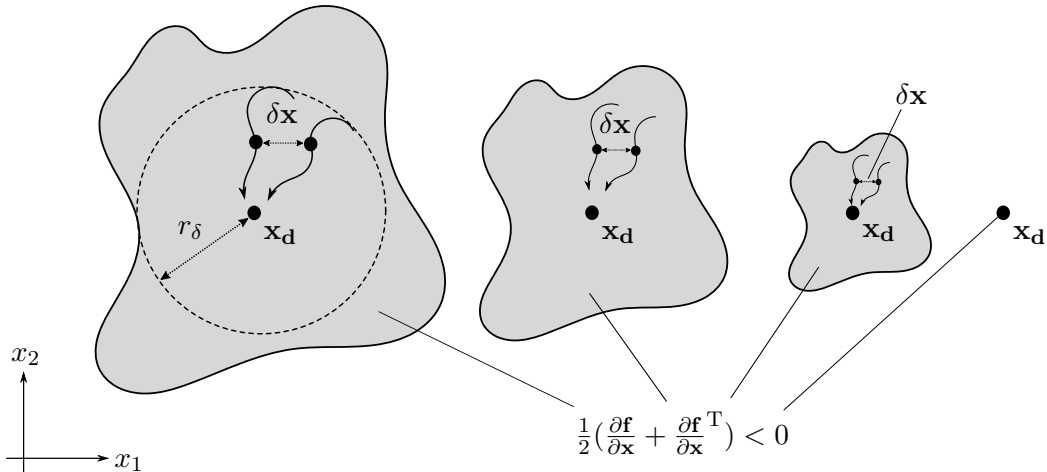


Figure 3.4: The system contracts within the region of the state-space where its Jacobian's symmetric part is strictly negative-definite. As all differential lengths between neighbouring trajectories vanish over time within this contraction region, convergence to a single trajectory is assured.

The expansion to global exponential contraction is straight-forward:

**Definition 3.7** (Global Exponential Convergence to a Single Trajectory). If the entire state-space is a contraction region, global exponential convergence to this given trajectory,  $\mathbf{x}_d$ , is guaranteed.  $\blacktriangle$

Notice that the notion of a system contracting can be considered a more general conception than stability in the sense of Lyapunov and does per se not imply convergence to an equilibrium point. While the single trajectory,  $\mathbf{x}_d$ , the system is converging to might be an equilibrium,  $\mathbf{x}_{eq}$ , it might as well describe a limit-cycle or likewise. As illustrated in fig. 3.4 contraction only guarantees for all system trajectories to exponentially tend to a single system state which is contained in the defined contraction region, however not required to be defined a priori. If on the other hand it is known that a specific equilibrium point of interest,  $\mathbf{x}_{eq}$ , is contained in a contraction region, exponential converge towards it can directly be concluded for all other trajectories within this region.

### 3.4.2 Generalization of Coordinates and Contraction Metrics

While the definition of contracting behaviour is straight-forward, for higher-dimensional systems the conditions on the system's Jacobian,  $\frac{\partial \mathbf{f}}{\partial \mathbf{x}}$ , might be hard to prove to hold for all  $\mathbf{x}$ . The results from contraction analysis can however be vastly extended [32] by introducing a differential state transformation,  $\Theta(\mathbf{x})$ , to so-called local coordinates,  $\delta \mathbf{z}$ . The virtual displacement in local coordinates,  $\delta \mathbf{z}$ , is then defined through the following differential relation:

$$\delta \mathbf{z} = \Theta(\mathbf{x})\delta \mathbf{x}, \quad (3.15)$$

where the state transformation,  $\Theta(\mathbf{x})$ , denotes a state-dependent square matrix. This allows for the generalization of the squared distance between two trajectories:

$$\delta \mathbf{z}^T \delta \mathbf{z} = \delta \mathbf{x}^T \Theta(\mathbf{x})^T \Theta(\mathbf{x}) \delta \mathbf{x} = \delta \mathbf{x}^T \mathbf{M}(\mathbf{x}) \delta \mathbf{x}, \quad (3.16)$$

where the square matrix,  $\mathbf{M}(\mathbf{x})$ , represents a symmetric and continuously differentiable metric. If the state transformation,  $\Theta(\mathbf{x})$ , is chosen such that this metric is strictly positive-definite, exponential convergence of  $\delta \mathbf{z}$  to  $\mathbf{0}$  also guarantees convergence of  $\delta \mathbf{x}$  to  $\mathbf{0}$ . Additionally, the metric,  $\mathbf{M}(\mathbf{x})$ , is required to be initially bounded such that an initially bounded virtual displacement,  $\delta \mathbf{x}$ , guarantees for its representation in local coordinates,  $\delta \mathbf{z}$ , to be bounded, as well<sup>3</sup>.

Having introduced an alternate but equivalent way of describing the differential distance between two trajectories in eq. (3.16), the evolution of this squared distance can now be evaluated in local coordinates,  $\delta \mathbf{z}$ , as well. Firstly, the time derivative in local coordinates is defined as:

---

<sup>3</sup>Crucial to the concepts of contraction theory are the notions of Riemannian metrics and manifolds, which is why they will be further discussed in sec. 6. Additionally, the introduction of this state transformation,  $\Theta(\mathbf{x})$ , requires the definition of distances between two points in local coordinates with respect to the defined metric,  $\mathbf{M}(\mathbf{x})$ . This can be computed by finding the smallest path integral between those two points and will also be addressed in the same section.

$$\begin{aligned}\frac{d}{dt}\delta\mathbf{z} &= \dot{\Theta}(\mathbf{x})\delta\mathbf{x} + \Theta(\mathbf{x})\delta\dot{\mathbf{x}} = (\dot{\Theta}(\mathbf{x}) + \frac{\partial\mathbf{f}}{\partial\mathbf{x}}\Theta(\mathbf{x}))\delta\mathbf{x} \\ &= (\dot{\Theta}(\mathbf{x}) + \frac{\partial\mathbf{f}}{\partial\mathbf{x}}\Theta(\mathbf{x}))\Theta^{-1}(\mathbf{x})\delta\mathbf{z}\end{aligned}\quad (3.17)$$

which by introducing the so-called generalized Jacobian,  $\mathbf{F}$ , as:

$$\mathbf{F} = (\dot{\Theta}(\mathbf{x}) + \frac{\partial\mathbf{f}}{\partial\mathbf{x}}\Theta(\mathbf{x}))\Theta^{-1}(\mathbf{x})\quad (3.18)$$

yields the following definition of rate of change:

$$\frac{d}{dt}(\delta\mathbf{z}^T\delta\mathbf{z}) = 2\delta\mathbf{z}^T\frac{d}{dt}\delta\mathbf{z} = 2\delta\mathbf{z}^T\mathbf{F}\delta\mathbf{z}.\quad (3.19)$$

Analogously to def. 3.6 a contraction region can be defined where the generalized Jacobian,  $\mathbf{F}$ , is strictly negative-definite. Alternatively, referring to the rate of change in the original differential coordinates,  $\delta\mathbf{x}$ , again:

$$\frac{d}{dt}(\delta\mathbf{z}^T\delta\mathbf{z}) = \frac{d}{dt}(\delta\mathbf{x}^T\mathbf{M}(\mathbf{x})\delta\mathbf{x}) = \delta\mathbf{x}^T\left(\frac{\partial\mathbf{f}}{\partial\mathbf{x}}^T\mathbf{M}(\mathbf{x}) + \mathbf{M}(\mathbf{x})\frac{\partial\mathbf{f}}{\partial\mathbf{x}} + \dot{\mathbf{M}}(\mathbf{x})\right)\delta\mathbf{x}\quad (3.20)$$

yields the condition for a found metric,  $\mathbf{M}(\mathbf{x})$ , to be a contraction metric [2].

**Definition 3.8** (Contraction Metrics for Autonomous Systems). For an autonomous system,  $\dot{\mathbf{x}} = \mathbf{f}(\mathbf{x})$ , of dimension  $n$ , a  $n$ -by- $n$  matrix,  $\mathbf{M}(\mathbf{x})$ , is a contraction metric if it is uniformly positive-definite and additionally the expression,  $\left(\frac{\partial\mathbf{f}}{\partial\mathbf{x}}^T\mathbf{M}(\mathbf{x}) + \mathbf{M}(\mathbf{x})\frac{\partial\mathbf{f}}{\partial\mathbf{x}} + \dot{\mathbf{M}}(\mathbf{x})\right)$ , is uniformly negative-definite.  $\blacktriangle$

The contraction metric's time derivative,  $\dot{\mathbf{M}}(\mathbf{x})$ , is computed as:

$$\dot{\mathbf{M}}(\mathbf{x}) = \left(\frac{\partial\mathbf{M}(\mathbf{x})^T}{\partial\mathbf{x}}\mathbf{f}(\mathbf{x})\right)\quad (3.21)$$

and this condition can be extended to define exponential contraction:

**Definition 3.9** (Contraction Metrics Assuring Exponential Convergence). If additionally,  $\left(\frac{\partial\mathbf{f}}{\partial\mathbf{x}}\mathbf{M}(\mathbf{x}) + \mathbf{M}(\mathbf{x})\frac{\partial\mathbf{f}}{\partial\mathbf{x}} + \dot{\mathbf{M}}(\mathbf{x})\right) \leq -\beta_c\mathbf{M}(\mathbf{x})$  holds where  $\beta_c$  is a strictly positive constant, the system is contracting exponentially.  $\blacktriangle$

Again, depending on whether these conditions on the metric,  $\mathbf{M}(\mathbf{x})$ , can be fulfilled within some  $r_\delta$ -sphere or within the entire state-space the system is (exponentially) contracting locally or globally. The remarks that can be drawn from a system contracting in local coordinates are identical to the ones obtained from defining a contraction region by evaluating the system's Jacobian,  $\frac{\partial\mathbf{f}}{\partial\mathbf{x}}$ , in def. 3.6 and def. 3.7.

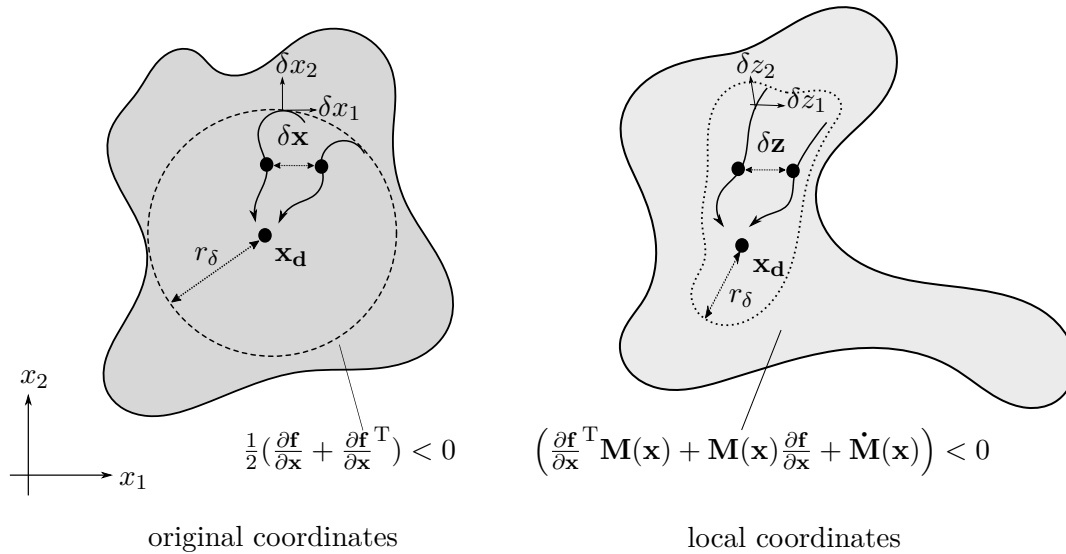


Figure 3.5: The extension of results through the introduction of local coordinates. If contraction can be proven in arbitrary local coordinates contracting behaviour and therefore convergence to a single trajectory can also be concluded for the original system.

The introduction of local coordinates,  $\delta \mathbf{z}$ , however allows a far less restrictive approach, as now any generalized Jacobian,  $\mathbf{F}$ , can be employed to prove system convergence. The consideration of differential lengths within contraction theory permits the conclusion of global system properties from local properties evaluated in local differential coordinates. This is unique to contraction theory and only valid due to its differential approach as it can be considered as taking into account “all possible directions” the system could evolve to. On the contrary, note that proving global asymptotic stability through Lyapunov’s direct method as discussed in sec. 3.3.2 required additional steps besides verifying that the definiteness-conditions on the Lyapunov-function,  $V(\mathbf{x})$ , hold in the entire state-space. Consequently, proving local asymptotic stability in the sense of Lyapunov for all possible system states is not sufficient to conclude global asymptotic stability as Lyapunov theory only evaluates how the system evolves in the directions defined through the Lyapunov-function-candidate.

While this marks a fundamental difference between Lyapunov theory and contraction theory, still contraction analysis can be considered an extension of Lyapunov direct method of proving exponential stability. In order to illustrate this connectedness, let us reconsider the sufficient conditions according to Lyapunov:  $\beta_1 \|\mathbf{x}\|^k \leq V(\mathbf{x}) \leq \beta_2 \|\mathbf{x}\|^k$  and  $\dot{V}(\mathbf{x}) \leq -\beta_3 V(\mathbf{x})$ .

Noticeably, this condition differs from the ones for local asymptotic stability in the way that it not only demands the Lyapunov-function,  $V(\mathbf{x})$ , to have certain definiteness properties but also to be bounded in relation to some  $k$ -vector-norm of the state trajectories. This notion of bounded and decreasing trajectory lengths is unique and crucial to the property of exponential stability – and consequently it also defines the basis of contrac-

tion analysis. By defining some differential Lyapunov-like scalar function,  $\delta V(\mathbf{x})$ , and its time derivative,  $\delta \dot{V}(\mathbf{x})$ , as:

$$\delta V(\mathbf{x}) = \delta \mathbf{x}^T \mathbf{M}(\mathbf{x}) \delta \mathbf{x} \quad (3.22)$$

$$\delta \dot{V}(\mathbf{x}) = \delta \mathbf{x}^T \left( \frac{\partial \mathbf{f}^T}{\partial \mathbf{x}} \mathbf{M}(\mathbf{x}) + \mathbf{M}(\mathbf{x}) \frac{\partial \mathbf{f}}{\partial \mathbf{x}} + \dot{\mathbf{M}}(\mathbf{x}) \right) \delta \mathbf{x} \quad (3.23)$$

parallels between Lyapunov theory and contraction theory can further be highlighted. Clearly, the differential Lyapunov-function-candidate,  $\delta V(\mathbf{x})$ , is bounded through the strictly positive eigenvalues of the contraction metric,  $\mathbf{M}(\mathbf{x})$ :

$$\delta \mathbf{x}^T \lambda_{\mathbf{M},\min} \delta \mathbf{x} \leq \delta \mathbf{x}^T \mathbf{M}(\mathbf{x}) \delta \mathbf{x} \leq \delta \mathbf{x}^T \lambda_{\mathbf{M},\max} \delta \mathbf{x} \quad (3.24)$$

$$\lambda_{\mathbf{M},\min} \|\delta \mathbf{x}\|_2^2 \leq \delta V(\mathbf{x}) \leq \lambda_{\mathbf{M},\max} \|\delta \mathbf{x}\|_2^2 \quad (3.25)$$

where  $\lambda_{\mathbf{M},\min}, \lambda_{\mathbf{M},\max} > 0$  holds for all system states,  $\mathbf{x}$ , due to  $\mathbf{M}(\mathbf{x})$  being a positive-definite contraction metric. Additionally, the following inequality holds:

$$\delta \mathbf{x}^T \left( \frac{\partial \mathbf{f}^T}{\partial \mathbf{x}} \mathbf{M}(\mathbf{x}) + \mathbf{M}(\mathbf{x}) \frac{\partial \mathbf{f}}{\partial \mathbf{x}} + \dot{\mathbf{M}}(\mathbf{x}) \right) \delta \mathbf{x} \leq -\beta_c \left( \delta \mathbf{x}^T \mathbf{M}(\mathbf{x}) \delta \mathbf{x} \right) \quad (3.26)$$

$$\delta \dot{V}(\mathbf{x}) \leq -\beta_c \delta V(\mathbf{x}). \quad (3.27)$$

This contemplation allows the interpretation of contraction theory as a differential form of Lyapunov's direct method through the introduction of generalized coordinates.

### 3.4.3 Remarks on Contraction Analysis

Concluding about non-linear stability analysis, Lyapunov theory and contraction theory both provide tools that if applied successfully allow legitimate system classification and powerful controller design. Contraction analysis is less restrictive as it does not require a specific location of the equilibrium – or even the predefinition of some invariant solution at all – which can be considered a major drawback of Lyapunov analysis when dealing with systems with uncertainty [2]. Additionally, contraction theory permits the inference of global properties within a defined contraction region from local analysis, while on the contrary a system that is proven to be locally stable in the sense of Lyapunov for all possible system states, is still not guaranteed to be globally stable. This makes Lyapunov's direct method non-applicable if a system's dynamics are not explicitly known – and consequently for most higher-order SDRE-controlled systems.

Also, if the finding of exponential stability over asymptotic stability is of relevancy, contraction theory might be the more natural approach. However, just as with Lyapunov's direct method an open quest remains in finding a suitable contraction metric fulfilling the necessary conditions. While often for simple and especially scalar systems a solid understanding of the system's dynamics can yield in a successful evaluation, no general rules to construct a corresponding metric exist. Especially for higher-order systems, a trial-and-error approach will yield in a non-feasible computational effort and a systematic approach is therefore highly relevant.

### 3.5 Controllability of Non-linear Systems

Closely related to the notion of stability is the controllability of a dynamical system subject to the input,  $\mathbf{u}$ . Figuratively speaking, controllability defines whether a certain physical excitation of a system can drive it to any desired state within the state-space – neglecting possible modelling errors, disturbances or other inconveniences arising from dealing with real technical systems over mathematical models. More precisely, in [8] controllability is defined in the following way:

**Definition 3.10** (Controllability of Dynamical Systems). A dynamical system is said to be controllable if for any initial state,  $\mathbf{x}_0$ , and any final state,  $\mathbf{x}_e$ , there exists an input that transfers  $\mathbf{x}_0$  to  $\mathbf{x}_e$ . Otherwise, the system is said to be uncontrollable. ▲

This definition of controllability only requires the existence of some input,  $\mathbf{u}$ , allowing any possible system transformations and does not make any further demands, like e.g. for this input to be bounded. Obviously, if a system is fully controllable, in theory one can assure for its states to stay bounded for all times and consequently assure stability.

#### Controllability of LTI-Systems

For an LTI-system of the form:

$$\dot{\mathbf{x}} = \mathbf{A}\mathbf{x} + \mathbf{B}\mathbf{u} \quad (3.28)$$

that some system input,  $\mathbf{u}$ , is applied to, controllability can be determined systematically by evaluating the system matrices,  $\mathbf{A}$  and  $\mathbf{B}$ . The most popular controllability-criterion is the one formulated by Kalman [8]:

$$\text{rank} \left( \begin{bmatrix} \mathbf{B} & \mathbf{A}\mathbf{B} & \mathbf{A}^2\mathbf{B} & \dots & \mathbf{A}^{n-1}\mathbf{B} \end{bmatrix} \right) \stackrel{!}{=} n \quad (3.29)$$

where,  $n$  is the dimension of the state-space vector of the evaluated system. If eq. (3.29) holds, the system is fully controllable, otherwise the system is not fully controllable but no notion of the extend to which the system is “uncontrollable” can be provided.

An alternate criterion is the one by Hautus which technically executes the same mathematical evaluation as the Kalman-criterion but considers each eigenvalue of the system matrix individually. According to Hautus, if for all eigenvalues,  $\lambda_i$ , of the system matrix,  $\mathbf{A}$ , the following condition:

$$\text{rank} \left( \begin{bmatrix} \mathbf{A} - \lambda_i\mathbf{I} & \mathbf{B} \end{bmatrix} \right) \stackrel{!}{=} n \quad (3.30)$$

holds, the system is fully controllable. The condition in eq. (3.30) checks whether any left eigenvector of the system-matrix,  $\mathbf{A}$ , corresponding to an eigenvalue,  $\lambda$ , is orthogonal to the image of the input matrix,  $\mathbf{B}$ . If the system matrix had one such eigenvector, this eigenvalue could not possibly be influenced with any linear combination of the input matrix’s basis vectors and consequently could not be controlled in this direction for the given system input [45].

Other than the Kalman-criterion, the application of the Hautus-criterion not only provides a binary classification of an entire system as controllable or not but instead allows to specifically determine which eigenvalues of the system are controllable or not. Due to its favourable capability, the Hautus-criterion additionally allows for classifying systems as stabilizable: for a not fully controllable system, still a stabilizing control law can be found as long as all its uncontrollable eigenvalues are stable, i.e. only have negative real-parts.

### Controllability of Non-linear Autonomous Systems

As the concept of eigenvalues and -vectors is exclusive to linear systems, the Kalman- or Hautus-criterion clearly can not directly be applied to non-linear systems. However, a generalization of the Kalman-criterion can be formulated, as derived in more detail in [42, 49]. In order to state this controllability condition for non-linear systems, first the Lie-bracket of two vector fields,  $\mathbf{f}(\mathbf{x})$  and  $\mathbf{g}(\mathbf{x})$ , needs to be defined:

$$[\mathbf{f}, \mathbf{g}] = \frac{\partial \mathbf{g}}{\partial \mathbf{x}} \mathbf{f} - \frac{\partial \mathbf{f}}{\partial \mathbf{x}} \mathbf{g}. \quad (3.31)$$

The Lie-bracket-operator defines a third vector field which if the original vector fields,  $\mathbf{f}(\mathbf{x})$  and  $\mathbf{g}(\mathbf{x})$ , are interpreted as flow fields, can be understood as the directional derivative of the fields along each other's flow [42]. This resulting vector field is commonly referred to as  $\text{ad}_{\mathbf{f}} \mathbf{g}$  and can be defined recursively:

$$\text{ad}_{\mathbf{f}}^0 \mathbf{g} = \mathbf{g} \quad \text{ad}_{\mathbf{f}}^1 \mathbf{g} = [\mathbf{f}, \text{ad}_{\mathbf{f}}^0 \mathbf{g}] \quad \text{ad}_{\mathbf{f}}^i \mathbf{g} = [\mathbf{f}, \text{ad}_{\mathbf{f}}^{i-1} \mathbf{g}]. \quad (3.32)$$

With the help of this notation, a non-linear controllability condition can be formulated. An autonomous non-linear system in input-affine form:

$$\dot{\mathbf{x}} = \mathbf{f}(\mathbf{x}) + \mathbf{g}(\mathbf{x})\mathbf{u} \quad (3.33)$$

can be considered fully controllable in the linear sense if the vector fields defined by:

$$\{\mathbf{g} \quad \text{ad}_{\mathbf{f}} \mathbf{g} \quad \text{ad}_{\mathbf{f}}^2 \mathbf{g} \quad \dots \quad \text{ad}_{\mathbf{f}}^{n-1} \mathbf{g}\} \quad (3.34)$$

are linearly independent for all  $\mathbf{x}$  [49]. In order to make the duality with the Kalman-criterion obvious, the condition could also be rephrased to claiming that a matrix with the Lie-brackets given in eq. (3.34) as columns has full rank,  $n$ , for all system states,  $\mathbf{x}$ . In fact, for a linear system the following holds:

$$\mathbf{g} = \mathbf{B} \quad \frac{\partial \mathbf{f}}{\partial \mathbf{x}} = \mathbf{A} \quad \frac{\partial \mathbf{g}}{\partial \mathbf{x}} = \mathbf{0}. \quad (3.35)$$

Consequently, for any LTI-system the set of vector fields of eq. (3.34) reduces to the columns of the Kalman-controllability-matrix of eq. (3.29):



$$\{\mathbf{g} \quad \text{ad}_f \mathbf{g} \quad \text{ad}_f^2 \mathbf{g} \quad \dots \quad \text{ad}_f^{n-1} \mathbf{g}\} \rightarrow \{\mathbf{B} \quad \mathbf{AB} \quad \mathbf{A}^2 \mathbf{B} \quad \dots \quad \mathbf{A}^{n-1} \mathbf{B}\} \quad (3.36)$$

and the demand for these columns to be linearly independent is equivalent to requiring them to span a full-rank matrix.

So similarly as with stability, evaluating a system's controllability results in strongly differing tasks depending on whether its dynamics are linear or not. Though a generally valid – and in this case necessary and sufficient – condition for a non-linear system to be fully controllable can be formulated, it can only be proven through the evaluation of a series of state-dependent terms. Showing that eq. (3.34) defines a set of linearly independent vectors in the entire state-space or at least a relevant subset of it, defines an arduous task. For higher order systems with more complex dynamics, this will in most cases result in computationally non-feasible problems.

Reconsidering the TWIP's dynamics of order six, the lie-brackets of eq. (3.34) require derivatives of order up to five. With the many trigonometric terms included in the dynamic model introduced in sec. 2 not vanishing through repeated derivation but resulting in more and more complex trigonometric formulae, it is easily fathomed that proving controllability for the non-linear system will denote a tremendous task. In [38] a reduced version of the TWIP's dynamics are evaluated in terms of controllability in the non-linear sense. However, to make this analysis possible, strong assumptions about the system dynamics, e.g. stability of internal dynamics, have to be made such that even if this property can be determined, controller design based on the achieved results might not yield in a robust control law.

### 3.6 Remarks on Non-linear System Analysis

Overall, the examples of stability and controllability analysis showcase two major difficulties exemplary for non-linear system analysis in general: Firstly, the generally valid conditions often are of sufficient kind and do not state whether they also have necessary character [42, 24]. Secondly, theorems for non-linear systems generally result in state-dependent formulations that additionally need to be proven to hold in relevant regions of the defined state-space. This amounts to a drastically increased complexity compared to a single evaluation of a numerical matrix as in for LTI-systems. Consequently, making non-linear tools applicable often requires strong assumptions about the system's dynamics which in return can jeopardize controller robustness if these do not hold to the presumed extend.

Alongside the mentioned eigenvalue analysis, a multitude of methods has been established to characterize LTI-system, e.g. in regards of controllability or observability. These linear tools have been applied successfully in analysis and design resulting in high-performing controllers for a wide range of industrial applications [42]. Great progress has been made in the field of non-linear control theory, as well, and a variety of powerful design techniques, e.g. feedback linearization, backstepping, or sliding mode control, have been introduced and applied successfully to specific technical problems. Nevertheless, most of these techniques remain only applicable to a very restricted class of systems [9, 29], such that a range of considerations remains necessary in order to employ them to control a specific non-linear system.

These described complications of non-linear system analysis motivate the introduction of a quasi-linear representation of the TWIP's dynamics through so-called state-dependent coefficient (SDC)-parametrization. This transformation to a quasi-linear system will allow the pointwise application of linear system analysis tools. Before employing it to the TWIP's dynamics however, in the next section the concepts and properties of SDC-parametrization will be introduced first.

## Chapter 4

# SDRE-based Controller Synthesis

Within control theory, a common approach to handle balancing problems, e.g. inverted pendula, is to first design a controller to execute the swing-up motion and subsequently a separate one stabilizing the linearized system about the desired balancing point [14]. In this work however, in order to find a single stabilizing state feedback controller for the TWIP providing sufficient performance within a relevant range about its upright equilibrium, in sec. 5 a control law is defined by pointwisely solving the so-called State-Dependent-Riccati-Equation (SDRE). The SDRE-based design technique can be interpreted as a non-linear approach mimicking the popular linear quadratic regulator (LQR)-design method [19] which is restricted to systems defined through linear dynamics.

Before its application to the TWIP, the following chapter will give a quick overview of the ideas behind SDRE-based synthesis. In addition, some conditions to be met for successful application are listed in sec. 4.2.1 as well as guaranteed properties of the closed-loop dynamics in sec. 4.3. While the closed-loop characteristics obtained from SDRE-synthesis are not as strong as those from LQR-design, it nevertheless has shown sufficient performance in a range of applications as for example listed in [9, 19, 11]. As SDRE-based controller synthesis is closely related to LQR-design in its systematic approach, first of all in sec. 4.1 the fundamentals of the LQR-technique and its generalization to non-linear systems will be outlined.

### 4.1 The LQR-Problem and its Generalization to Non-linear Systems

One of the most extensively applied techniques of controller synthesis for LTI-systems is the LQR-method [12]. Instead of having to explicitly choose poles of the closed-loop system and then placing these poles through some linear design methods, the LQR-approach implicitly executes pole placement by minimizing some predefined performance index [49]. When employing the LQR-method, a feedback control law:

$$\mathbf{u}(\mathbf{x}) = -\mathbf{K}\mathbf{x} \tag{4.1}$$

regulating the system to the origin,  $\mathbf{x} = \mathbf{0}$ , is found such that the quadratic index:

$$J = \frac{1}{2} \int_0^{\infty} \mathbf{x}^T \mathbf{Q} \mathbf{x} + \mathbf{u}^T \mathbf{R} \mathbf{u} \, dt \tag{4.2}$$

is minimized. The optimization problem defined by the performance index of eq. (4.2) constrained through the system dynamics,  $\dot{\mathbf{x}} = \mathbf{A}\mathbf{x} + \mathbf{B}\mathbf{u}$ , is referred to as the infinite-horizon LQR-problem. Within the performance index, the symmetric positive-semi-definite matrix,  $\mathbf{Q}$ , penalizes the state variables being different to zero and the symmetric positive-definite matrix,  $\mathbf{R}$ , weights the inputs applied to the system. Thus, the first term of eq. (4.2) tries to keep the components of the state vector close to the origin, while the second term tries to limit the input required to do so. Naturally, these define two conflicting tasks [49], such that through adjustment of the weighting matrices,  $\mathbf{Q}$  and  $\mathbf{R}$ , the designer can put quantitative emphasis on either effort and define a compromise solution.

Once concrete weighting matrices have been chosen, applying optimality conditions to the infinite-horizon LQR-problem yields the optimal feedback controller:

$$\mathbf{u}(\mathbf{x}) = -\mathbf{R}^{-1}\mathbf{B}^T\mathbf{P}\mathbf{x} \quad (4.3)$$

being constructed through the symmetric positive-definite matrix,  $\mathbf{P}$ , found by solving the Algebraic Riccati Equation (ARE):

$$\mathbf{A}^T\mathbf{P} + \mathbf{P}\mathbf{A} - \mathbf{P}\mathbf{B}\mathbf{R}^{-1}\mathbf{B}^T\mathbf{P} + \mathbf{Q} = 0. \quad (4.4)$$

For a controllable (stabilizable) pair of system matrices,  $(\mathbf{A}, \mathbf{B})$ , the resulting control law assures global asymptotic stability alongside robustness properties sufficient for most applications [37]. The LQR-technique not only allows a rather intuitive approach to define desired closed-loop dynamics through the formulation of a weighted performance index but additionally implicitly guarantees desirable closed-loop characteristics. In conclusion, the LQR-synthesis makes up a methodologically sound technique also applicable to high-dimensional systems which paved the way for it becoming one of the most popular design techniques since it has been introduced in today's form in the 1960s [23]. Although LQR-design as presented so far is restricted to LTI-systems, it can be generalized to the infinite-horizon non-linear optimal controller problem.

For an autonomous input-affine non-linear system as defined in eq. (3.33), an optimal feedback control law:

$$\mathbf{u}(\mathbf{x}) = -\mathbf{R}^{-1}(\mathbf{x})\mathbf{g}^T(\mathbf{x})\left(\frac{\partial W}{\partial \mathbf{x}}\right) \quad (4.5)$$

minimizing the performance index:

$$J = \frac{1}{2} \int_0^\infty \mathbf{x}^T\mathbf{Q}(\mathbf{x})\mathbf{x} + \mathbf{u}^T\mathbf{R}(\mathbf{x})\mathbf{u} \, dt \quad (4.6)$$

is obtained by solving the Hamilton-Jacobi-Equation (HJE):

$$\frac{1}{2}\mathbf{x}^T\mathbf{Q}(\mathbf{x})\mathbf{x} + \left(\frac{\partial W}{\partial \mathbf{x}}\right)^T \mathbf{f}(\mathbf{x}) - \frac{1}{2}\left(\frac{\partial W}{\partial \mathbf{x}}\right)^T \mathbf{g}(\mathbf{x})\mathbf{R}^{-1}(\mathbf{x})\mathbf{g}^T(\mathbf{x})\left(\frac{\partial W}{\partial \mathbf{x}}\right) = 0 \quad (4.7)$$

for the positive-definite scalar function  $W(\mathbf{x})$ . The weighting matrices,  $\mathbf{Q}(\mathbf{x})$  and  $\mathbf{R}(\mathbf{x})$ , still are required to be positive-(semi-)definite but can now be chosen state-dependent. Consequently, the performance index as defined in eq. (4.6) remains quadratic in the input but not necessarily in the state vector [9]. Unfortunately, there exists no efficient algorithm to solve the HJE for systems of order larger than one or two [21, 5], and consequently – unlike the ARE – it is very restricted in its application for controller design [37].

## 4.2 Significance of SDC-Parametrization in SDRE-based Controller Design

In an attempt to make the simplicity of optimal control techniques accessible to a variety of non-linear systems [39], in 1962 Pearson first suggested to investigate what today is called the State-Dependent-Riccati-Equation:

$$\mathbf{A}^T(\mathbf{x})\mathbf{P}(\mathbf{x}) + \mathbf{P}(\mathbf{x})\mathbf{A}(\mathbf{x}) - \mathbf{P}(\mathbf{x})\mathbf{B}(\mathbf{x})\mathbf{R}^{-1}(\mathbf{x})\mathbf{B}^T(\mathbf{x})\mathbf{P}(\mathbf{x}) + \mathbf{Q}(\mathbf{x}) = 0. \quad (4.8)$$

Within this approach, a state-dependent “version” of the ARE is solved for the positive-definite matrix,  $\mathbf{P}(\mathbf{x})$ , instead of trying to find a solution to the HJE. Analogously to the LQR-case, the obtained feedback control law is then defined by:

$$\mathbf{u}(\mathbf{x}) = -\mathbf{R}^{-1}(\mathbf{x})\mathbf{B}^T(\mathbf{x})\mathbf{P}(\mathbf{x})\mathbf{x}. \quad (4.9)$$

Generally speaking, the SDRE-scheme “ignores” the condition on the solution,  $\mathbf{P}(\mathbf{x})\mathbf{x}$ , to be the gradient of some scalar positive-definite function,  $W(\mathbf{x})$ , and instead simply chooses it to be a symmetric positive-definite matrix [9].

### 4.2.1 State-Dependent-Coefficient Form of Non-linear Systems

Obviously, the non-linear system dynamics as defined in eq. (3.33) do not contain any matrices,  $\mathbf{A}(\mathbf{x})$  and  $\mathbf{B}(\mathbf{x})$ , such that in order to execute SDRE-based controller synthesis, first a quasi- or pseudo-linear representation needs to be found through SDC-parametrization such that for all system states,  $\mathbf{x}$ , the following relation holds:

$$\dot{\mathbf{x}} = \mathbf{f}(\mathbf{x}) + \mathbf{g}(\mathbf{x})\mathbf{u} = \mathbf{A}(\mathbf{x})\mathbf{x} + \mathbf{B}(\mathbf{x})\mathbf{u}. \quad (4.10)$$

A SDC-parametrization fulfilling this condition exists if and only if the non-linear system vector,  $\mathbf{f}(\mathbf{x})$ , is continuously differentiable and the origin defines an equilibrium point,  $\mathbf{f}(\mathbf{0}) = \mathbf{0}$  [18]. For the state-dependent input matrix,  $\mathbf{B}(\mathbf{x})$ , the trivial choice lies in:

$$\mathbf{B}(\mathbf{x}) = \mathbf{g}(\mathbf{x}), \quad (4.11)$$

for which  $\mathbf{g}(\mathbf{x}) \neq \mathbf{0}$  has to hold for all system states,  $\mathbf{x}$ . However, the system matrix,  $\mathbf{A}(\mathbf{x})$ , is defined uniquely only in the scalar case and for systems of order larger than one it can easily be shown that there always exist an infinite number of feasible parametrizations [11] such that  $\mathbf{f}(\mathbf{x}) = \mathbf{A}(\mathbf{x})\mathbf{x}$  holds within the entire state-space.

The design step of finding a quasi-linear representation of the system’s dynamics marks a fundamental difference to LQR-synthesis, as it denotes an additional degree of freedom in the process of controller design. As a proper choice of the state-dependent system matrix,  $\mathbf{A}(\mathbf{x})$ , plays a significant role in obtaining a well-performing controller [21, 30], it will be discussed in more detail in the upcoming section.

### 4.2.2 Uniqueness and Optimality

Clearly, a different choice of state-dependent system matrix,  $\mathbf{A}(\mathbf{x})$ , will yield a different solution of the SDRE,  $\mathbf{P}(\mathbf{x})$ , and in consequence a control law found by solving the SDRE will in general not be optimal in the sense that it minimizes the performance index of eq. (4.6) [21, 18]. For the solution of the SDRE divided by the system state,  $\frac{\mathbf{P}(\mathbf{x})}{\mathbf{x}}$ , to be optimal, it must coincide with the gradient of a solution of the HJE,  $\frac{\partial W}{\partial \mathbf{x}}$ . In general this will not hold, however in [21] the proof is illustrated that within the set of feasible parametrizations for the state-dependent system matrices, the one yielding the optimal solution is always contained.

Consequently, the solution of the SDRE is optimal in regards of the performance index defined through the weighting matrices,  $\mathbf{Q}(\mathbf{x})$  and  $\mathbf{R}(\mathbf{x})$ , only in the scalar case but generally suboptimal in the multi-variable case [9]. However, in [12] it is demonstrated that as the system state is driven to the origin, optimality is asymptotically satisfied at an quadratic rate. This behaviour of SDRE-controlled systems has also been observed in applications where the system trajectories converged to the optimal trajectories while approaching the equilibrium state. Consequently, if the system states can be kept reasonably small during usage, near optimal multi-variable feedback control can be achieved through SDRE-synthesis.

Note that in the same paper [12], two approaches to exploit the additional degree of freedom in choosing a SDC-parametrization to recover optimality in SDRE-design are introduced. However, these are not easily applicable in general as one is dependent on the initial condition and the other involves the computationally expensive solving of a partial differential equation (PDE). In consequence, optimality is a criterion that may be considered when choosing a SDC-representation, however a variety of successful applications of the SDRE-scheme have been executed with suboptimal solutions and shown steady performance.

### 4.2.3 Controllability and Stabilizing Solutions

Similar as with the LQR-method for the SDRE-scheme to yield a stabilizing control law, the chosen SDC-parametrization must be controllable (stabilizable). In consequence, controllability can be considered a crucial property to take into account when choosing a quasi-linear representation to execute SDRE-design. For this purpose, let us introduce the following classifications as defined in [9, 12]:

**Definition 4.1** (Controllable SDC-Parametrization). A valid SDC-representation as defined in eq. (4.10) is said to be a controllable parametrization of the non-linear system in the region,  $\Omega \subseteq \mathbb{R}^n$ , if the pair,  $(\mathbf{A}(\mathbf{x}), \mathbf{B}(\mathbf{x}))$ , is pointwise controllable in the linear sense for all  $\mathbf{x} \in \Omega$ . ▲

**Definition 4.2** (Strongly Controllable SDC-Parametrization). A valid SDC-representation as defined in eq. (4.10) is said to be a strongly controllable parametrization of the non-linear system in the region,  $\Omega \subseteq \mathbb{R}^n$ , if there exists some  $\kappa > 0$  such that  $\sigma_{\text{CO},\min} \geq \kappa$  for all  $\mathbf{x} \in \Omega$ , where  $\sigma_{\text{CO},\min}$  denotes the smallest singular value of a controllability matrix based on the pair,  $(\mathbf{A}(\mathbf{x}), \mathbf{B}(\mathbf{x}))$ . ▲

Note that these notions allow no conclusions about the non-linear system itself, and especially pointwise controllability of a chosen SDC-parametrization must not be misinterpreted as controllability of the non-linear system as introduced in sec. 3.5.

Analogously to the ARE, in a region where the set of system matrices,  $(\mathbf{A}(\mathbf{x}), \mathbf{B}(\mathbf{x}))$ , is controllable<sup>1</sup>, the closed-loop dynamics resulting from SDRE-based synthesis:

$$\dot{\mathbf{x}} = (\mathbf{A}(\mathbf{x}) - \mathbf{B}(\mathbf{x})\mathbf{K}(\mathbf{x}))\mathbf{x} = \mathbf{A}_{\text{cl}}(\mathbf{x})\mathbf{x} \quad (4.12)$$

define a pointwise stabilizing solution [9, 10]. For every state,  $\mathbf{x} \neq \mathbf{0}$ , a stabilizing solution for the system “frozen” in its current state is found through solving the ARE that the SDRE collapses to at this specific point. Additionally, under the assumption that all entries of the state-dependent matrices are continuously differentiable with respect to  $\mathbf{x}$ , the SDRE-method produces closed-loop dynamics that are locally asymptotically stable with respect to the origin [9].

Generally, global asymptotic stability can not be guaranteed through SDRE-design even if all eigenvalues of the closed-loop system matrix,  $\mathbf{A}_{\text{cl}}(\mathbf{x})$ , strictly lie in the left half complex plane. Only for symmetric closed-loop system matrices,  $\mathbf{A}_{\text{cl}}(\mathbf{x}) = \mathbf{A}_{\text{cl}}^{\text{T}}(\mathbf{x})$ , a Lyapunov-function can be constructed to proof global asymptotic stability as deduced in [9]. However, as this is a rather restrictive condition and additionally global stability can not hold for systems with several isolated equilibria like the TWIP, in the context of this work an alternate approach relying on contraction analysis to determine stability margins will be introduced in sec. 6.

#### 4.2.4 Guideline on Defining a SDC-Representation

Overall, for non-scalar systems there exists no generally applicable approach to find a proper SDC-parametrization of the non-linear dynamics. In [13] a number of examples are provided illustrating how the chosen pseudo-linear representation influences resulting controller performance and feasibility of the SDRE. In the same paper, beneficial properties for quasi-linear dynamics that still represent the state intercouplings of the original non-linear system are underlined. In consequence, as a rule-of-thumb the state-dependent coefficient matrix,  $\mathbf{A}(\mathbf{x})$ , can be demanded to contain a non-zero entry,  $a_{ij}(\mathbf{x})$ , if the  $i$ th state derivative depends on the  $j$ th state [11]. Note however that this is a design guideline exclusively based on empirical investigation and not on any mathematical proofs.

Further complications, e.g. constant state-independent terms, can occur when the system dynamics are not provided in input-affine form, however in many cases still a work-around can be found to successfully define a feasible SDC-parametrization. Among others this issue is addressed in [11], does however not apply to the TWIP’s dynamics and will accordingly not be discussed in more detail.

In conclusion, choosing a suitable SDC-parametrization can be considered the designer’s main task when employing SDRE-based synthesis. On one hand the introduction of a SDC-representation marks an additional degree of freedom to be exploited by the designer, while on the other hand one has to likewise assure to not yield in non-feasibility of the SDRE due to deficient parametrization.

---

<sup>1</sup>Note that in addition to controllability, another essential condition for successful LQR- or SDRE-based controller design likewise is for the system to be observable, as both design techniques rely on full state feedback. As for the TWIP subject to this work all system states can be assumed measured through appropriate sensors, observability will not be addressed in further discussions. If the proposed design technique is however to be used on systems not providing full state feedback, pointwise observability in the linear sense as defined in [45] needs to be assured for a stabilizing SDRE-based control law.

### 4.3 Further Design Steps in SDRE-based Controller Synthesis

After having found a favourable SDC-parametrization, few additional steps remain within SDRE-based synthesis. First, the designer has to determine weighting matrices to complete the non-linear regulator problem to be addressed through the SDRE. Eventually, a method to solve the resulting SDRE needs to be found to obtain an explicit control law.

#### 4.3.1 Choosing Weighting Matrices, $\mathbf{Q}(\mathbf{x})$ and $\mathbf{R}(\mathbf{x})$

While SDC-parametrization is an aspect of SDRE-based controller design broadly discussed in the literature, the choice of possibly state-dependent weighting matrices is often only touched on or in many cases not addressed at all [26, 4, 3]. Even though the concrete choice of penalty matrices is known to have great influence on system performance and input effectiveness [28], within a variety of applications they are still chosen as identity or constant matrices [17, 20, 30, 13]. Obviously, this will simplify computations and is consequently especially desirable if one intends to find an analytical solution to the SDRE. However, in [28] examples are provided where a state-dependent choice of penalty matrices significantly improved the resulting controller performance indicating that if computationally possible the state-dependency of the penalty matrices should be exploited.

Just as in LQR-synthesis, there exists no generally valid method to make this choice, and most designers rely on a trial-and-error-approach to achieve desired closed-loop behaviour [37, 27]. However, as most solvers used for solving the SDRE will rely on the performance index to be convex, a rule-of-thumb as in [28] can be defined to choose:

$$\mathbf{Q}(\mathbf{x}) = \mathbf{Q}_0 + \mathbf{Q}_1(\mathbf{x}) \quad \mathbf{R}(\mathbf{x}) = \mathbf{R}_0 + \mathbf{R}_1(\mathbf{x}). \quad (4.13)$$

The suggestion is to compose the weighting matrices of a constant diagonal matrix:

$$\mathbf{Q}_0 = \text{diag}(c_0, \dots, c_n), \quad (4.14)$$

with strictly positive coefficients,  $c_i > 0$ , and a state-dependent matrix:

$$\mathbf{Q}_1(\mathbf{x}) = \text{diag}(q_1(x_1), \dots, q_n(x_n)), \quad (4.15)$$

where the entries,  $q_i(x_i)$ , are chosen as exclusively even degree polynomials of the corresponding system state:

$$q_i(x_i) = k_{i2} x_i^2 + k_{i4} x_i^4 + k_{i6} x_i^6 + \dots \quad (4.16)$$

where again the coefficients,  $k_{im}$ , are strictly positive. The construction of the input weighting matrix,  $\mathbf{R}(\mathbf{x})$ , is executed analogously, however the state-dependent matrix,  $\mathbf{R}_1(\mathbf{x})$ , might be chosen as mixed even degree monomials of several system states.

Besides the matrices being positive-(semi)definite and defining a convex performance index, there are no further restrictions and the concrete choice solely depends on the desired closed-loop dynamics. Sec. 5.3.2 will demonstrate the influence of weighting matrices and motivate the choice made with regards to the TWIP's dynamics.



### 4.3.2 Solving the SDRE

With all state-dependent matrices fixed, the SDRE is completely defined and the only remaining task is solving it. The ideal method is to analytically solve the matrix equation with the help of some symbolic software package offline to obtain some directly applicable state-dependent control law. However, as this will only work for low order systems or ones exhibiting specific structures, another approach is to pointwisely solve the SDRE online at a relatively high Hertz-rate [10]. With the SDRE-approach – even though the full non-linearities of the system are taken into account – the controller solely has to solve the linear AREs obtained from evaluating the SDRE for the current system state. As especially for higher-order systems linear equations are solved at a remarkably lower computational effort than non-linear problems, this allows fast online computation. Consequently, the SDRE-method can be – and mostly has been – applied to systems with fast dynamics and significantly high system order [26, 3, 20]. A last option would be to compute point solutions of the SDRE offline and then execute gain scheduling during applications [10].

## 4.4 Remarks on SDRE-based Controller Synthesis

Finally, a couple of conclusions can be drawn about controller synthesis based on the SDRE-technique. First of all, despite of its close relatedness to the LQR-technique, generally the SDRE-method can neither guarantee global stability nor optimality in regards of the predefined performance index. However, it has been showcased that both of these properties are locally provided in some proximity to the origin. Nevertheless, for a suitable SDC-parametrization the resulting suboptimal and locally stabilizing SDRE-controller has proven sufficient performance in many applications.

The non-unique choice of a quasi-linear SDC-parametrization as well as possibly state-dependent weighting matrices mark additional degrees of freedom within the process of controller design. This might be considered an advantage if these flexibilities can be exploited to achieve some further closed-loop qualities. Likewise, the necessity of introducing a pseudo-linear representation can be interpreted as a restriction as certain conditions have to be met by the SDC-parametrization to ensure a stabilizing controller.

Unlike many other approaches of exploiting linear tools for non-linear controller design, SDRE-based controllers do not forcefully cancel out all of the system's non-linearities. As with these kind of controllers usually beneficial non-linear system properties are eliminated as well, according design techniques often result in significantly increased control efforts [12, 13]. Additionally, through appropriate choice of weighting matrices within the SDRE, soft input bounds can be imposed by the designer.

A remarkable property of SDRE-based controller design is its applicability to a variety of non-linear systems. The restrictions on the system's dynamics to be provided in input-affine form are mild when compared to other non-linear design methods like backstepping or feedback linearization [16]. Additionally, in many cases work-arounds can be found to also apply the SDRE-approach to systems that initially were not given in input-affine form [11]. Even if no analytical solution to the SDRE can be found, it can nevertheless be applied to higher-order systems with fast dynamics as the online computations required are solely linear and can consequently be executed with high frequency.

Lastly, another advantage of the SDRE-technique is the ability to benefit from the extensive research already conducted on the field of linear optimal control by for instance employing one of the many advanced algorithms for solving the ARE.

## Chapter 5

# Application of SDRE-based Controller Synthesis to the TWIP

The SDRE-approach as presented in sec. 4 was used to design a non-linear controller stabilizing the TWIP introduced in sec. 2 in its upright position. The design process and resulting controller performance will be discussed in the following chapter which can be considered split in two halves. The first half is dedicated to the procedure of finding a suitable SDRE to use in controller synthesis for the TWIP and accordingly sec. 5.1 will motivate the exact SDC-representation chosen within this work. Even though addressed in the last section, optimality will not be of particular interest within this work, and instead the focus will merely be set on controller performance. Likewise, as for the TWIP discussed within this work all states are assumed to be measured, observability will not be debated, either. Particular attention however was drawn to finding a controllable and continuously differentiable parametrization to assure a stabilizing solution within a relevant state-space region. Additionally, in sec. 5.2 the state-dependent weighting matrices will be defined and physically motivated through the TWIP's dynamics to complete the employed SDRE.

The second half will focus on performance and input efficiency achieved by the controller based on the resulting SDRE and how these are affected by certain design parameters. The relevancy of a proper parametrization as well as the influence of state-dependent penalty matrices will be further highlighted by direct comparison of different feasible SDC-representations in sec. 5.3.1 and varying weighting matrices in sec. 5.3.2. Lastly, the SDRE-based controller found within this paper will be compared to a LQR-controller based on the linearized dynamics about the upright equilibrium point in sec. 5.4. The two controllers will be investigated in various scenarios, e.g. subject to non-linear friction not included in the dynamic model or arising disturbances, to also exhibit their robustness properties.

### 5.1 SDC-Parametrization of the TWIP's Non-linear Dynamics

As the first step of SDRE-design, the found SDC-parametrization is introduced and quickly debated why this particular choice was made. No major issues arose when parametrizing the TWIP's dynamics as the way they are introduced in [25] already

allows for sufficiently easy handling. Accordingly, within this paper a parametrization was found that has similarities to the one used within [26], however it is not identical. After the introduction of the chosen SDC-representation in sec. 5.1.1, it will be examined in regards of controllability to assure stabilizing controller synthesis and a negative example will be provided on how faulty parametrization can yield in an inherently non-controllable SDC-representation in sec. 5.1.2.

### 5.1.1 Constructing a Continuously Differentiable System Matrix, $\mathbf{A}(\mathbf{x})$

#### Applied Methods for Concrete Choice of SDCs

Generally, when trying to parametrize a system's non-linear dynamics, the easiest case imaginable are dynamics exclusively polynomial in the system states. In such a case, the corresponding monomials can simply be lowered in their degree by one and written to the according entry in the state-dependent system matrix,  $\mathbf{A}(\mathbf{x})$ . Mixed monomials of two or more system states can be split up in equal parts and distributed over the according matrix entries to represent the state intercoupling with a non-zero entry at each index of the corresponding system states as proposed in [11]. For the most part, this approach can be applied successfully, e.g. for damping terms, and it was broadly executed within this paper.

However, this method no longer exclusively works if the system dynamics contain terms that are not polynomial in the system states but instead trigonometric or constant – which will often be the case, e.g. for gravity or centrifugal terms. Special attention has to be drawn to trigonometric terms due to two reasons. First, if the dynamics contain terms that exclusively include system variables in the context of some trigonometric expression, the corresponding term needs to be divided by some system variable before it is added to the state-dependent system matrix such that later when the system matrix is multiplied with the state vector,  $\mathbf{A}(\mathbf{x})\mathbf{x} = \mathbf{f}(\mathbf{x})$ , still holds. However, this division obviously amounts to a singularity for the divisor state being equal to zero such that this case needs to be considered separately. Secondly, close attention needs to be drawn to cosine terms as they do not vanish as the corresponding state approaches zero such that a transformation needs to be found for  $\mathbf{f}(\mathbf{0}) = \mathbf{0}$  to still hold. Usually this can be obtained through employing some trigonometric identity to replace cosine expressions with a set of constant and sine terms and subsequently treating constant terms as proposed in [10].

Fortunately, with the TWIP's dynamics as derived in [25] there remain no merely constant terms and only the  $a_{11}(\mathbf{x})$ -coefficient of the inertia matrix of [25] contained an isolated cosine term which however ends up as a mixed sine-cosine terms when eq. (28) of [25] is solved for the second order derivatives. In conclusion, all trigonometric terms contain some sine coefficient, such that no further transformation was necessary to assure for  $\mathbf{f}(\mathbf{0}) = \mathbf{0}$  to always hold.

### Resulting SDC-Parametrization

For the yaw acceleration,  $\ddot{\psi}$ , the pitch-dependent trigonometric expressions were treated as parameters such that the approach of splitting-up and distributing monomials could be applied, and the following parametrization was found:

$$\ddot{\psi} = \frac{\sin(\theta)}{\rho_2(\theta)} \left( -2K_2 \cos(\theta) \dot{\theta} \dot{\psi} - K_4 \dot{x} \dot{\psi} \right) = a_{62}(\mathbf{x}) \dot{x} + a_{64}(\mathbf{x}) \dot{\theta} + a_{66}(\mathbf{x}) \dot{\psi} \quad (5.1)$$

where the state-dependent coefficients were chosen to:

$$a_{62}(\mathbf{x}) = \frac{\sin(\theta)}{\rho_2(\theta)} \left( -\frac{1}{2} K_4 \dot{\psi} \right) \quad (5.2)$$

$$a_{64}(\mathbf{x}) = \frac{\sin(\theta)}{\rho_2(\theta)} \left( -K_2 \cos(\theta) \dot{\psi} \right) \quad (5.3)$$

$$a_{66}(\mathbf{x}) = \frac{\sin(\theta)}{\rho_2(\theta)} \left( -\frac{1}{2} K_4 \dot{x} - K_2 \cos(\theta) \dot{\theta} \right). \quad (5.4)$$

For the the driving and pitch acceleration,  $\ddot{x}$  and  $\ddot{\theta}$ , however this method alone was not sufficient, as they both contain a gravity term solely depending on a trigonometric expression of the pitch angle. In consequence, those terms needed to be divided by some system state and as they exclusively depend on the pitch angle it made sense to choose this system state as a divisor, like also suggested in [26]. Consequently, the following parametrizations resulted for the driving acceleration:

$$\ddot{x} = \frac{\sin(\theta)}{\rho_1(\theta)} K_4 \left( -K_4 g \cos(\theta) + K_3 \dot{\theta}^2 + (K_3 - K_2 \cos^2(\theta)) \dot{\psi}^2 \right) \quad (5.5)$$

$$= a_{23}(\mathbf{x}) \theta + a_{24}(\mathbf{x}) \dot{\theta} + a_{26}(\mathbf{x}) \dot{\psi} \quad (5.6)$$

where the state-dependent coefficients were chosen to:

$$a_{23}(\mathbf{x}) = \frac{\sin(\theta)}{\rho_1(\theta)} \frac{1}{\theta} \left( -K_4^2 g \cos(\theta) \right) \quad (5.7)$$

$$a_{24}(\mathbf{x}) = \frac{\sin(\theta)}{\rho_1(\theta)} K_3 K_4 \dot{\theta} \quad (5.8)$$

$$a_{26}(\mathbf{x}) = \frac{\sin(\theta)}{\rho_1(\theta)} \left( K_3 - K_2 \cos^2(\theta) \right) K_4 \dot{\psi} \quad (5.9)$$

and the pitch acceleration:

$$\ddot{\theta} = \frac{\sin(\theta)}{\rho_1(\theta)} \left( K_1 K_4 g - K_4^2 \cos(\theta) \dot{\theta}^2 + (K_1 K_2 - K_4^2) \cos(\theta) \dot{\psi}^2 \right) \quad (5.10)$$

$$= a_{43}(\mathbf{x}) \theta + a_{44}(\mathbf{x}) \dot{\theta} + a_{46}(\mathbf{x}) \dot{\psi} \quad (5.11)$$

with the state-dependent coefficients:

$$a_{43}(\mathbf{x}) = \frac{\sin(\theta)}{\rho_1(\theta)} \frac{1}{\theta} (K_1 K_4 g) \quad (5.12)$$

$$a_{44}(\mathbf{x}) = \frac{\sin(\theta)}{\rho_1(\theta)} \left( -K_4^2 \cos(\theta) \right) \dot{\theta} \quad (5.13)$$

$$a_{46}(\mathbf{x}) = \frac{\sin(\theta)}{\rho_1(\theta)} \left( K_1 K_2 - K_4^2 \right) \cos(\theta) \dot{\psi} \quad (5.14)$$

This parametrization of trigonometric gravity terms is particularly preferable and has been used in preceding works [26, 28] as the corresponding expression,  $\frac{\sin(\theta)}{\theta}$ , tends to one as the angle,  $\theta$ , tends to zero such that no special attention needs to be drawn to values of the divisor being numerically close to zero. In order to rule out numerical problems, the according entries,  $a_{23}(\mathbf{x})$  and  $a_{43}(\mathbf{x})$ , are set to  $\frac{1}{\rho_1(0)}$  as the value of the pitch angle approaches the MATLAB machine precision<sup>1</sup>.

For the input matrix the trivial choice,  $\mathbf{B}(\mathbf{x}) = \mathbf{g}(\mathbf{x})$ , was made as it can easily be shown that  $\mathbf{g}(\mathbf{x}) \neq \mathbf{0}$  holds for all system states. The resulting SDC-representation chosen to define a SDRE-based control law has the following structure:

$$\dot{\mathbf{x}} = \begin{bmatrix} 0 & 1 & 0 & 0 & 0 & 0 \\ 0 & 0 & a_{23}(\mathbf{x}) & a_{24}(\mathbf{x}) & 0 & a_{26}(\mathbf{x}) \\ 0 & 0 & 0 & 1 & 0 & 0 \\ 0 & 0 & a_{43}(\mathbf{x}) & a_{44}(\mathbf{x}) & 0 & a_{46}(\mathbf{x}) \\ 0 & 0 & 0 & 0 & 0 & 1 \\ 0 & a_{62}(\mathbf{x}) & 0 & a_{64}(\mathbf{x}) & 0 & a_{66}(\mathbf{x}) \end{bmatrix} \mathbf{x} + \begin{bmatrix} 0 & 0 \\ b_2(\mathbf{x}) & b_2(\mathbf{x}) \\ 0 & 0 \\ b_4(\mathbf{x}) & b_4(\mathbf{x}) \\ 0 & 0 \\ b_6(\mathbf{x}) & -b_6(\mathbf{x}) \end{bmatrix} \mathbf{u} \quad (5.15)$$

where the exact matrix entries are once again listed in detail in the appendix (A.4).

### Remarks on Found SDC-Parametrization

Note that the resulting system matrix,  $\mathbf{A}(\mathbf{x})$ , has two zero columns corresponding to the states,  $x$  and  $\psi$ . This illustrates more prominently what could have already been inferred from the non-linear state-space model – the TWIP’s dynamics are completely independent of these two system states and they consequently do not play a role within the task of stabilizing the TWIP in its upright position. Giving this observation some further thought, it makes sense that the TWIP’s current position and orientation on the ground do not influence its postural stability.

In [35] the subdivision of system states into so-called shape variables and external variables is proposed. While shape variables influence the system’s kinetic energy and therefore appear in the inertia matrix when executing Lagrangian dynamic modelling, external variables do not. This differentiation is worth keeping in mind when executing SDC-parametrization, as no inappropriate relevancy should be denoted to external variables through the found quasi-linear representation. In sec. 5.3.1 an example will be provided showcasing how overvaluing of external variables can negatively influence controller performance.

Lastly, in order to demonstrate that the found parametrization defines dynamics identical to the non-linear system’s, simulations were executed with a small constant inputs,  $\tau_i = 0.01 \text{ N m}$ , on each wheel to allow the simulations to run longer for comparison. Again at pitch angles,  $\theta > \frac{\pi}{3}$ , the simulations were stopped and the resulting trajectories are provided in fig. 5.1.

<sup>1</sup>Note that the exact value the coefficient is set to for  $\theta \cong 0$  is not of great importance as the matrix entry will be multiplied by  $\theta$  during simulations and numerically vanish as  $\theta$  reaches values below machine precision. Setting the matrix entry itself to zero however has to be avoided as this would yield in a non-controllable system matrix,  $\mathbf{A}(\mathbf{0})$ , with all state-dependent coefficients being equal to zero, and consequently would be detected as non-feasible by the employed ARE-solver.

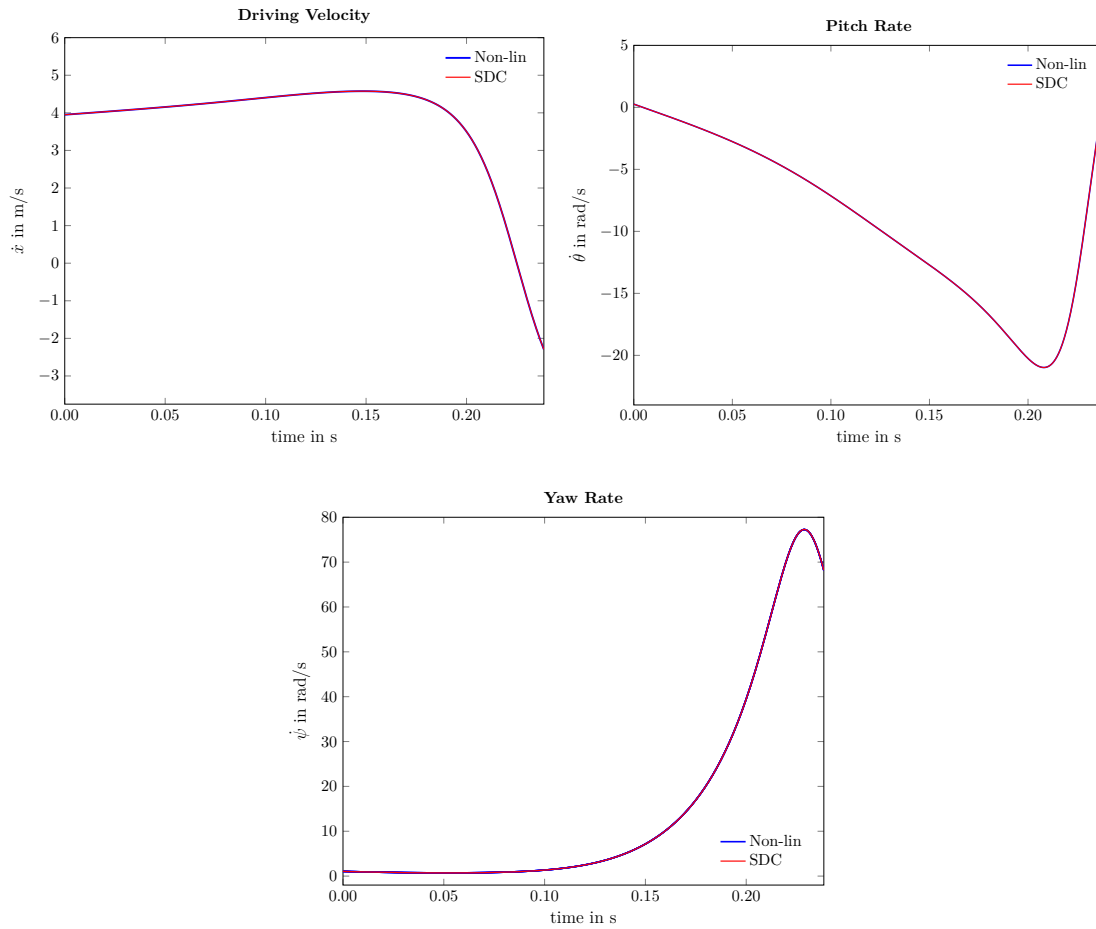


Figure 5.1: Comparison of the simulated dynamics of the SDC-parametrization to the non-linear state-space model. According simulations were executed for several initial states and within none of them a deviation of the SDC-model from the original non-linear one could be detected.

### 5.1.2 Pointwise Controllability of SDC-Parametrizations

#### Controllability of Chosen SDC-Parametrization

Once a quasi-linear representation is found that fulfills the preliminaries of being continuously differentiable and not containing any singularities, the next step to assure successful SDRE-based design is to investigate the found SDC-representation for controllability. The most desirable option is to analytically prove that the pair of system matrices,  $(\mathbf{A}(\mathbf{x}), \mathbf{B}(\mathbf{x}))$ , is controllable in the linear sense for all possible system states. Employing the Hautus-controllability-criterion as defined in eq. (3.30), for the chosen SDC-parametrization yields in proving that:

$$\text{rank} \left( \begin{bmatrix} \mathbf{A}(\mathbf{x}) - \lambda_i(\mathbf{x}) \mathbf{I} & \mathbf{B}(\mathbf{x}) \end{bmatrix} \right) \stackrel{!}{=} 6 \quad (5.16)$$

holds for all eigenvalues,  $\lambda_i(\mathbf{x})$ , and states,  $\mathbf{x}$ .

In detail, the Hautus-controllability-matrix is defined as:

$$\begin{bmatrix} -\lambda_i(\mathbf{x}) & 1 & 0 & 0 & 0 & 0 & 0 & 0 \\ 0 & -\lambda_i(\mathbf{x}) & a_{23}(\mathbf{x}) & a_{24}(\mathbf{x}) & 0 & a_{26}(\mathbf{x}) & b_2(\mathbf{x}) & b_2(\mathbf{x}) \\ 0 & 0 & -\lambda_i(\mathbf{x}) & 1 & 0 & 0 & 0 & 0 \\ 0 & 0 & a_{43}(\mathbf{x}) & a_{44}(\mathbf{x}) - \lambda_i(\mathbf{x}) & 0 & a_{46}(\mathbf{x}) & b_4(\mathbf{x}) & b_4(\mathbf{x}) \\ 0 & 0 & 0 & 0 & -\lambda_i(\mathbf{x}) & 1 & 0 & 0 \\ 0 & a_{62}(\mathbf{x}) & 0 & a_{64}(\mathbf{x}) & 0 & a_{66}(\mathbf{x}) - \lambda_i(\mathbf{x}) & b_6(\mathbf{x}) & -b_6(\mathbf{x}) \end{bmatrix} \quad (5.17)$$

Even though the controllability matrix of eq. (5.16) does not seem immoderately complex in its structure, proving that it has full rank for all state-dependent eigenvalues,  $\lambda_i(\mathbf{x})$ , results in complex equations no more analytically solvable.

In consequence, a pointwise approach of evaluating the state-dependent Hautus-controllability-matrix on a fine grid within a relevant region of the state-space was decided on. For each grid point,  $\mathbf{x}_g$ , the SDC-parametrization was evaluated and the resulting pair of constant matrices,  $(\mathbf{A}(\mathbf{x} = \mathbf{x}_g), \mathbf{B}(\mathbf{x} = \mathbf{x}_g))$ , examined for the Hautus-controllability-criterion. The rank of the constant Hautus-controllability-matrix for the corresponding grid points was determined through computing its singular values,  $\sigma_i$ , and checking that for all of them  $\sigma_i \gg 0$  holds, such that a margin for numerical robustness of the controllability property could be provided.

For the shape variables of the TWIP used within this paper, the limits as listed in tab. 5.1 have been experimentally determined in preceding works. Accordingly, the pointwise evaluation was executed within those limits and the chosen stepsizes are provided in tab. 5.1, as well. Note that the defined grid is not equidistant, as the number of grid points for the pitch angle and yaw rate was chosen higher as these two states can be considered to have the most significant influence on the system's non-linearities. Experimental results reaffirm this assumption, as high spinning and large pitch deviations have been observed to be most critical system states which often cause controllers to fail [26].

Table 5.1: The state limits, stepsizes, and number of grid points used for the pointwise examination for controllability. Due to the nature of the TWIP's dynamics all limits are symmetric with respect to the origin.

State	Lower Bound	Upper Bound	Stepsize	Grid Points
$\dot{x}$	-1 m/s	1 m/s	0.125 m/s	17
$\theta$	$-\frac{\pi}{3}$	$\frac{\pi}{3}$	$\frac{\pi}{25}$	51
$\dot{\theta}$	$-2\pi/s$	$2\pi/s$	$0.167\pi/s$	25
$\dot{\psi}$	$-7.5\pi/s$	$7.5\pi/s$	$0.5\pi/s$	31



For the entire set of 671,925 evaluated points within state-space, none was found to be non-controllable and all singular values determined within those computations remained larger than  $\sigma_{min} \geq 0.946$ , such that numerical concerns can be put aside and the found parametrization even be considered strongly controllable as defined in def. 4.2 within all grid points.

### Example of an Inherently Non-controllable SDC-Parametrization

Before further design steps will be discussed, at this point an example will be provided to showcase how there exist feasible representations in the sense that they are continuously differentiable and  $\mathbf{A}(\mathbf{x})\mathbf{x} = \mathbf{f}(\mathbf{x})$  holds for all system states but nevertheless can not be employed for SDRE-design due to their inherent uncontrollability. Consider for instance the following parametrization:

$$\mathbf{A}_{nc}(\mathbf{x}) = \begin{bmatrix} 0 & 1 & 0 & 0 & 0 & 0 \\ 0 & a_{nc,22}(\mathbf{x}) & 0 & a_{nc,24}(\mathbf{x}) & 0 & a_{nc,26}(\mathbf{x}) \\ 0 & 0 & 0 & 1 & 0 & 0 \\ 0 & a_{nc,42}(\mathbf{x}) & 0 & a_{nc,44}(\mathbf{x}) & 0 & a_{nc,46}(\mathbf{x}) \\ 0 & 0 & 0 & 0 & 0 & 1 \\ 0 & 0 & 0 & 0 & 0 & a_{nc,66}(\mathbf{x}) \end{bmatrix} \quad (5.18)$$

where the matrix entries,  $a_{nc,ij}(\mathbf{x})$ , are listed in the appendix (A.4). Transforming  $\mathbf{A}_{nc}(\mathbf{x})$  to lower triangular form by exchanging columns and eliminating the  $a_{26}(\mathbf{x})$ -entry:

$$\mathbf{A}_{nc}(\mathbf{x}) = \begin{bmatrix} 1 & 0 & 0 & 0 & 0 & 0 & 0 \\ a_{nc,22}(\mathbf{x}) & a_{nc,24}(\mathbf{x}) & 0 & 0 & 0 & 0 & 0 \\ 0 & 1 & \frac{-a_{nc,26}(\mathbf{x})}{a_{nc,24}(\mathbf{x})} & 0 & 0 & 0 & 0 \\ a_{nc,42}(\mathbf{x}) & a_{nc,44}(\mathbf{x}) & a_{nc,46}(\mathbf{x}) - \frac{a_{nc,44}(\mathbf{x})a_{nc,26}(\mathbf{x})}{a_{nc,24}(\mathbf{x})} & 0 & 0 & 0 & 0 \\ 0 & 0 & 1 & 0 & 0 & 0 & 0 \\ 0 & 0 & a_{nc,66}(\mathbf{x}) & 0 & 0 & 0 & 0 \end{bmatrix} \quad (5.19)$$

illustrates that  $\mathbf{A}_{nc}(\mathbf{x})$  has three eigenvalues  $\lambda_{nc,i} = 0$ . Now, again examining the Hautus-controllability-criterion:

$$\text{rank} \left( \left[ \mathbf{A}_{nc}(\mathbf{x}) - \lambda_{nc,i}(\mathbf{x}) \mathbf{I} \quad \mathbf{B}(\mathbf{x}) \right] \right) \stackrel{!}{=} 6 \quad (5.20)$$

for the eigenvalues  $\lambda_{nc,i} = 0$ :

$$\text{rank} \left( \begin{bmatrix} 0 & 1 & 0 & 0 & 0 & 0 & 0 & 0 \\ 0 & a_{nc,22}(\mathbf{x}) & 0 & a_{nc,24}(\mathbf{x}) & 0 & a_{nc,26}(\mathbf{x}) & b_2(\mathbf{x}) & b_2(\mathbf{x}) \\ 0 & 0 & 0 & 1 & 0 & 0 & 0 & 0 \\ 0 & a_{nc,42}(\mathbf{x}) & 0 & a_{nc,44}(\mathbf{x}) & 0 & a_{nc,46}(\mathbf{x}) & b_4(\mathbf{x}) & b_4(\mathbf{x}) \\ 0 & 0 & 0 & 0 & 0 & 1 & 0 & 0 \\ 0 & 0 & 0 & 0 & 0 & a_{nc,66}(\mathbf{x}) & b_6(\mathbf{x}) & -b_6(\mathbf{x}) \end{bmatrix} \right) = 5 < 6 \quad (5.21)$$

yields a rank deficient Hautus-controllability-matrix and in conclusion the system has three non-controllable eigenvalues. As this is the case for arbitrary system states, the SDC-parametrization through  $\mathbf{A}_{nc}(\mathbf{x})$  is not controllable for any state and consequently, passing this SDC-parametrization evaluated at a specific state to an ARE-solver will always throw an error.

## 5.2 Further Design Steps in SDRE Controller Synthesis

After having decided on a feasible and controllable quasi-linear SDC-representation, the choice of weighting matrices remained in order to define desired controller properties before solving the resulting SDRE and applying the found control law.

### 5.2.1 Choosing Weighting Matrices, $\mathbf{Q}(\mathbf{x})$ and $\mathbf{R}(\mathbf{x})$

In this work, the author aimed to exploit the additional degree of freedom in the choice of weighting matrices to achieve desired controller performance. Primary objective was to adjust the performance index to impose some “soft constraints” on the input. The maximum torque,  $\tau_{\max}$ , that can be applied to the either wheel of the TWIP is limited through its electrodynamics to about 0.6 Nm [1], such that the controller was adapted to remain within that range of required input even when recovering from critical states. Secondly, it was aimed to produce as little overshoot in the states as possible and allow a preferably smooth transition to the origin.

Roughly the guideline discussed in sec. 4.3.1 was consulted, in the sense that each penalty matrix was chosen as a superposition of a constant and a state-dependent diagonal matrix. However to reflect the state intercouplings within the TWIP’s dynamics, the state-dependent coefficients are dependent on several system states and not just the one state to be weighted through the matrix entry. Still, the performance index is assured to be convex as all state-dependent terms exclusively define polynomials of even degree.

After an initial configuration was chosen, it was adapted consecutively after executing several simulations with predefined initial conditions that were set to represent certain critical states to be stabilized. This process resulted in the following set of matrices:

$$\mathbf{Q}(\mathbf{x}) = \text{diag}(q_1, q_2(\theta, \dot{x}, \dot{\psi}), q_3(\theta), q_4(\theta, \dot{\theta}, \dot{\psi}), q_5, q_6(\theta, \dot{x}, \dot{\theta}, \dot{\psi})) \quad (5.22)$$

$$\mathbf{R}(\mathbf{x}) = \text{diag}(r(\dot{\theta}, \dot{\psi}), r(\dot{\theta}, \dot{\psi})) \quad (5.23)$$

where the coefficients were adapted to:

$$q_1 = 4.5 \tag{5.24}$$

$$q_2(\theta, \dot{x}, \dot{\psi}) = 3 + \frac{\theta^2}{\pi^2}(200\dot{x}^2 + 400\dot{\psi}^2) \tag{5.25}$$

$$q_3(\theta) = 10 + 2000\frac{\theta^2}{\psi^2} \tag{5.26}$$

$$q_4(\theta, \dot{\theta}, \dot{\psi}) = 2 + \frac{\theta^2}{\pi^2}(1500\dot{\theta}^2 + 500\dot{\psi}^2) \tag{5.27}$$

$$q_5 = 4 \tag{5.28}$$

$$q_6(\theta, \dot{x}, \dot{\theta}, \dot{\psi}) = 1 + \frac{\theta^2}{\pi^2}(100(\dot{x}^2 + \dot{\theta}^2) + 20\dot{\psi}^2) \tag{5.29}$$

$$r(\dot{\theta}, \dot{\psi}) = 0.5 + 150\dot{\theta}^2 + 400\dot{\psi}^4. \tag{5.30}$$

The coefficients,  $q_1$  and  $q_5$ , corresponding to the external variables were chosen to not contain any state-dependencies as they are completely decoupled and consequently do not pose a threat for the system being destabilized. For the same reason, their values were determined smaller compared to the state-dependent coefficients, while larger in comparison to the constant factors of the remaining state weighting coefficients,  $q_i$ , to allow the controller to also drive the external variables to the origin whenever the system is in an overall stable state.

The numerically largest coefficient,  $q_3$ , corresponds to the pitch angle as it is the most critical state when trying to stabilize the robot in its upright position. A too large pitch deviation is a system state the controller will not be able to recover from such that there lies importance in reacting fast and aggressively to significant pitch deviations. Also the sine-terms appearing in all second-order derivatives demonstrate that the system's non-linearities emerge only for pitch angles larger than zero. In consequence, all remaining weights were chosen to be scaled with the current pitch angle, as well, as any highly dynamic system state can be considered critical when coupled with a large pitch deviation.

The entries,  $q_2$  and  $q_4$ , were chosen dependent on the state they are penalizing on the one hand and additionally on the current yaw rate as the TWIP's driving and pitch acceleration are strongly influenced by spinning motions. The  $q_6$ -entry weighting the yaw rate itself, reflects all intercouplings of the system's dynamics. The exact numerical values chosen within the matrix entries are the mere result of an approach of trying-out-and-adjusting.

Concerning the input weighting matrix, identical terms,  $r$ , are chosen to penalize either torque, as there is no apparent reason to make the input to one wheel more expensive than to the other. The motivation behind choosing  $r$  only dependent on the pitch and yaw rate, is to impose the aforementioned soft constraint on the input. As described above, the detection of a high pitch or yaw rate alone is not to be considered a critical state, as long as the TWIP remains reasonably close to its upright equilibrium. In order to prevent the controller from overshooting, in such situations the input penalty is set reasonably high compared to the state weightings. As soon as the robot experiences an additional pitch deviation, the state weightings will however dominate again.

### 5.2.2 Solving the SDRE

As for the higher-order dynamics of the TWIP an analytical closed-form solution was not obtainable, in the context of this paper the approach of solving the “frozen” SDRE online at a relatively high Hertz-rate was decided on. The preimplemented implicit LQR-solver of MATLAB, `icare`, was used to solve the ARE resulting from evaluating the SDRE at the present state and to determine the current gain matrix. Further information about the MATLAB `icare`-solver can be found online, e.g. on the MathsWorks documentation website. For the integration of the system states, a simple fixed-stepsize Runge-Kutta-method was used that had been applied successfully on the TWIP for online state integration in the context of previous works at the Chair of Automatic Control. The exact stepsizes used for the simulation runs varied and are therefore provided individually for each of the following examples.

## 5.3 Significance of Design Flexibilities Within SDRE-based Controller Synthesis

Before concluding about SDRE-based controller synthesis, the following examples will showcase several issues within SDRE-based design discussed so far and demonstrate how design flexibilities within the SDRE-method influence the resulting controller performance. For easier comparison of the results, four initial states as provided in tab. 5.2 were determined to represent common “critical situations” of the TWIP in real-life scenarios and to later be used in simulations.

Table 5.2: The initial states used within simulations presented in the following. Each state was chosen to represent some specific “dynamically critical” situation the TWIP might face in applications.

Symbol	$x$	$\dot{x}$	$\theta$	$\dot{\theta}$	$\psi$	$\dot{\psi}$
$\mathbf{x}_{0,m}$	0 m	0.25 m/s	$0.2\pi$ rad	$0.75\pi$ rad/s	$0.25\pi$ rad	$\pi$ rad/s
$\mathbf{x}_{0,p}$	0 m	0.5 m/s	$0.3\pi$ rad	$\pi$ rad/s	0 rad	$\pi$ rad/s
$\mathbf{x}_{0,y}$	0 m	1 m/s	$0.1\pi$ rad	$0.75\pi$ rad/s	0 rad	$5.75\pi$ rad/s
$\mathbf{x}_{0,c}$	0 m	1 m/s	$0.333\pi$ rad	$2\pi$ rad/s	$0.5\pi$ rad	$5.75\pi$ rad/s

The initial state,  $\mathbf{x}_{0,m}$ , denotes an overall still moderately critical state, however the TWIP is already subject to a pitch deviation and significant pitch and yaw rate at the same time. The initial vector,  $\mathbf{x}_{0,p}$ , describes a state critical due to its high pitch deviation,  $\mathbf{x}_{0,y}$  a critical high spinning state, and finally  $\mathbf{x}_{0,c}$  a most critical initial states as all shape variables are almost chosen at their limits as defined in tab. 5.1. Clear reference will be provided for each simulation run which initial state and stepsize was used.

### 5.3.1 Comparison of Different Feasible SDC-Parametrizations

First of all, the debated influence of a physically meaningful SDC-parametrization will be highlighted. For this purpose, a quasi-linear representation hereafter referred to as TP-SDC-parametrization was defined. The state-dependent system matrix of the TP-SDC-parametrization was chosen to have the following structure:

$$\mathbf{A}_{\text{tp}}(\mathbf{x}) = \begin{bmatrix} 0 & 1 & 0 & 0 & 0 & 0 \\ 0 & 0 & 0 & 0 & a_{\text{tp},25}(\mathbf{x}) & 0 \\ 0 & 0 & 0 & 1 & 0 & 0 \\ 0 & 0 & 0 & 0 & a_{\text{tp},45}(\mathbf{x}) & 0 \\ 0 & 0 & 0 & 0 & 0 & 1 \\ 0 & 0 & 0 & 0 & a_{\text{tp},65}(\mathbf{x}) & 0 \end{bmatrix} \quad (5.31)$$

where the individual matrix entries are again provided in the appendix (A.4). Obviously, this matrix does not represent any dynamical intercouplings as all state-dependent coefficients were placed in the column representing the yaw angle which as an external variable has no influence on the system's remaining dynamics. Nevertheless, the SDC-representation of eq. (5.31) is feasible as it defines a continuously differentiable quasi-linear representation and  $\mathbf{A}(\mathbf{x})\mathbf{x} = \mathbf{f}(\mathbf{x})$  holds for all system states. Additionally, executing the pointwise controllability analysis as described in sec. 5.1.2 on the  $\mathbf{A}_{\text{tp}}(\mathbf{x})$ -parametrization only yields in non-controllability for  $\theta \equiv 0^2$ . The singularity arising for  $\psi = 0$  was handled by switching to another simple structured SDC-parametrization introduced in [26] for  $\psi < 10^{-12}$ :

$$\mathbf{A}_{\text{Kim}}(\mathbf{x}) = \begin{bmatrix} 0 & 1 & 0 & 0 & 0 & 0 \\ 0 & 0 & a_{\text{Kim},23}(\mathbf{x}) & 0 & 0 & 0 \\ 0 & 0 & 0 & 1 & 0 & 0 \\ 0 & 0 & a_{\text{Kim},43}(\mathbf{x}) & 0 & 0 & 0 \\ 0 & 0 & 0 & 0 & 0 & 1 \\ 0 & 0 & a_{\text{Kim},63}(\mathbf{x}) & 0 & 0 & 0 \end{bmatrix} \quad (5.32)$$

where again the property of  $\frac{\sin(\theta)}{\theta} \rightarrow 1$  as  $\theta \rightarrow 0$  is exploited and the matrix entries are provided in the appendix (A.4), as well. The simulation results shown in fig. 5.2 correspond to the modest,  $\mathbf{x}_{0,m}$ , and critical,  $\mathbf{x}_{0,c}$ , initial states. As the TP-SDC-parametrization was found to have weak numerical properties, all simulations were executed at a small stepsize of  $\Delta t = 0.025$  ms to factor out instability due to numerical issues as much as possible. The weighting matrices employed within the simulations were the ones defined in sec. 5.2.1 and identical for either parametrization. The trajectories of the corresponding inputs are provided in fig. 5.3.

---

<sup>2</sup>Note that this issue would need to be further addressed if one actually planned to use this representation for controller synthesis and had to be handled by e.g. switching to another SDC-matrix for non-controllable system states.

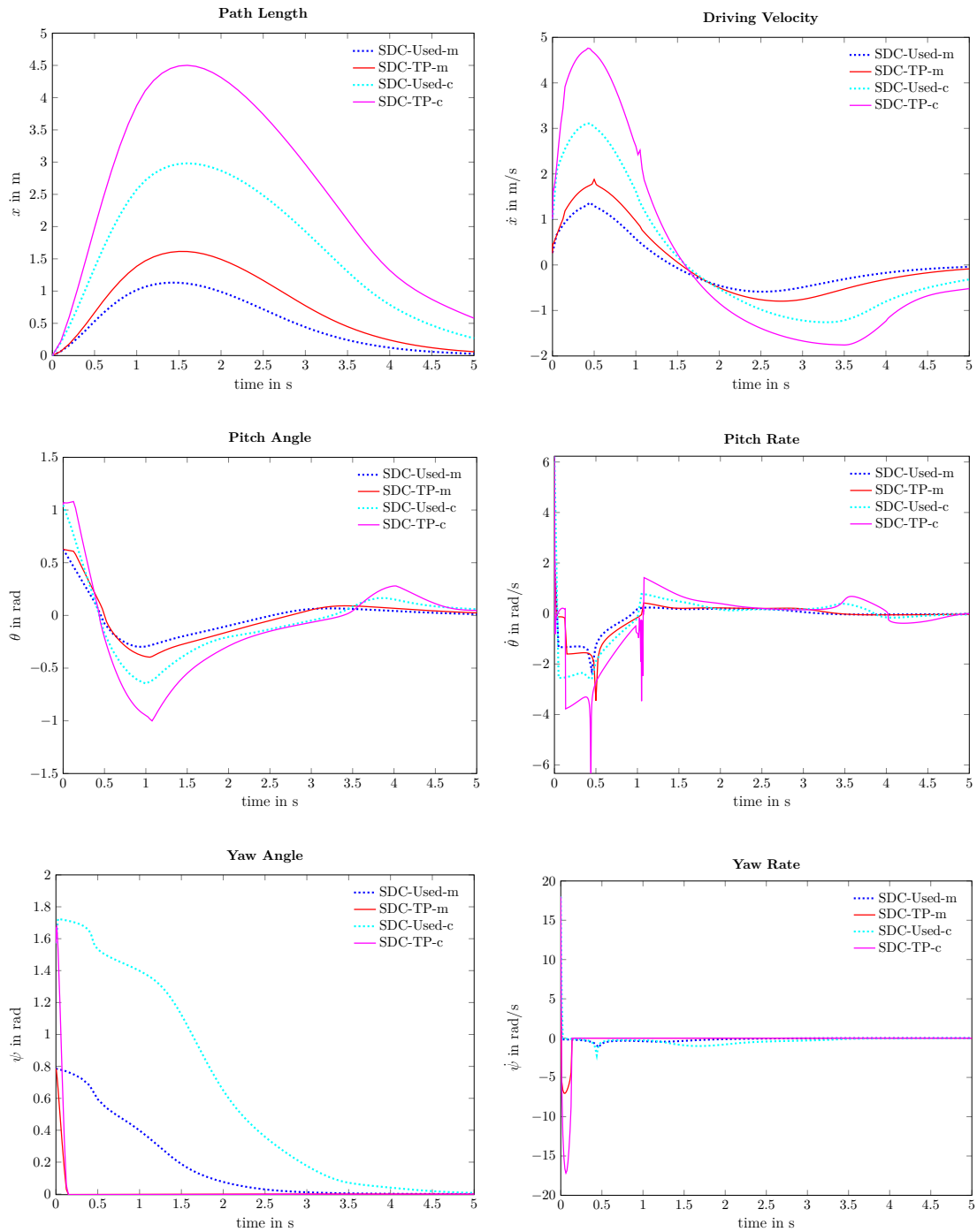


Figure 5.2: Comparison of the simulated dynamics of the SDC-parametrization chosen for controller synthesis, Used-SDC, and an alternate feasible SDC-representation, TP-SDC, that pays no attention to the TWIP’s dynamical intercouplings.

While the state trajectories qualitatively look similar, for all system states the overshoot is drastically higher for the TP-SDC-parametrization and in consequence state convergence is achieved at a slower rate. Additionally, significantly noticeable in the pitch rate the controller based on the TP-SDC-parametrization struggles with the dynamically

critical initial state,  $\mathbf{x}_{0,c}$ , and experiences not only strong overshooting but also minor oscillations at about  $t = 1.2$ s despite the small stepsize which do not appear with the Used-SDC-parametrization.

The TP-SDC-parametrization however manages to drive the yaw angle to the origin faster than the Used-SDC-parametrization does. As this can be considered a non-crucial task when stabilizing the TWIP in its upright equilibrium, it can be concluded that the TP-SDC-Parametrization over-emphasizes on the yaw dynamics while producing unwanted overshoot in more relevant states like the pitch angle which then causes the controller to struggle when trying to restabilize the system dynamics.

The beneficial choice of the Used-SDC-Representation becomes even more prominent when taking a closer look at the input trajectories of fig. 5.3. While the Used-SDC-representation in the beginning also requires larger torques to stabilize the dynamically critical initial state,  $\mathbf{x}_{0,c}$ , it still remains within the range of technical feasibility, while the TP-SDC-Parametrization not only by far exceeds the viable range but also exhibits strong chattering when trying to restabilize the drastic pitch rate overshoot. For the dynamically modest initial state,  $\mathbf{x}_{0,m}$ , the inputs remain within a non-problematic scale, however they experience shoot-ups from time to time while the Used-SDC-parametrization provides a much smoother transition.

Another reason to favour the Used-SDC-Parametrization are its numerical properties. The stepsize within these simulations had to be chosen significantly small to allow the TP-SDC-Parametrization to run at all without exhibiting major numerical issues, while the Used-SDC-Parametrization exhibits no complications even for stepsizes twenty times as large of  $\Delta t = 0.5$  ms – which will be a remarkable advantage when having to solve the SDRE online in future applications as a stepsize of  $\Delta t = 0.025$  ms would most likely not be realisable in online computations.

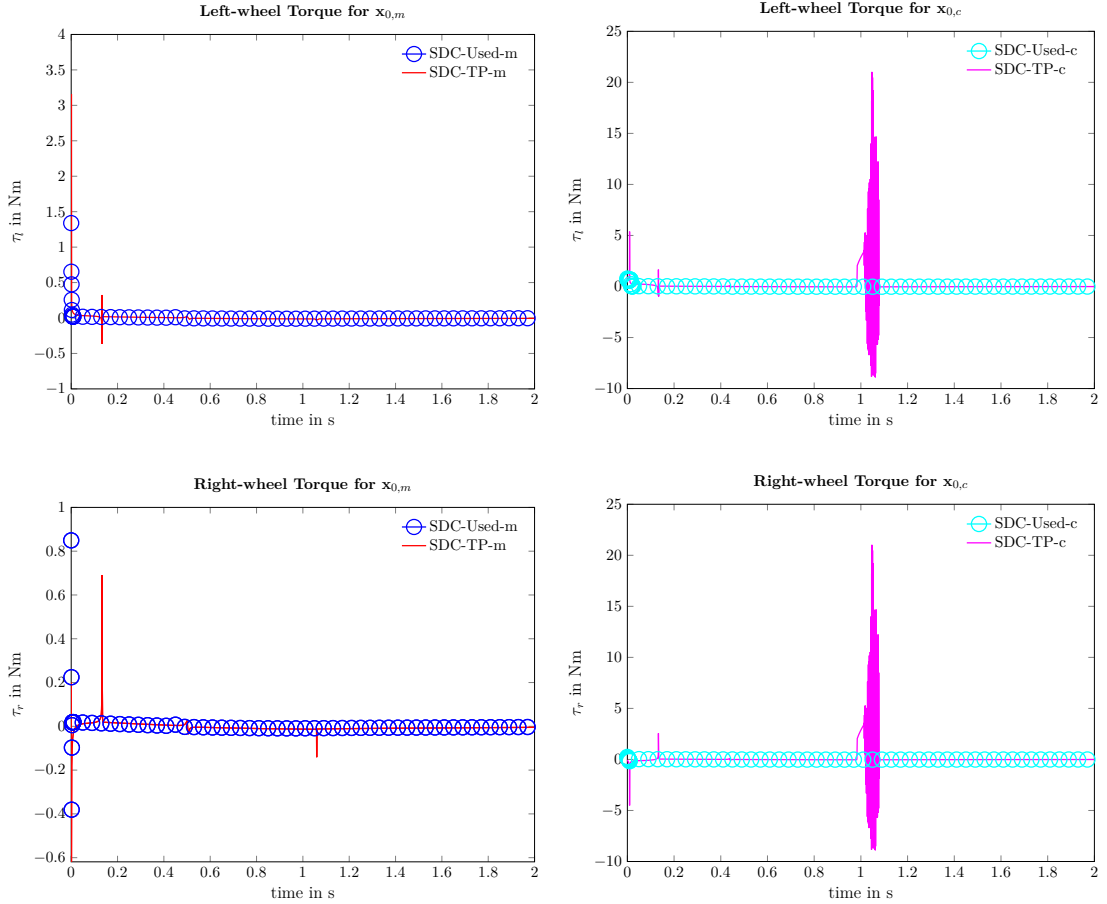


Figure 5.3: Comparison of the inputs of the SDC-parametrization, Used-SDC, chosen for controller synthesis and an alternate feasible SDC-representation, TP-SDC, that pays no attention to the TWIP’s dynamical intercouplings. Note that the inputs have been plotted separately for each initial state and additionally the Used-SDC trajectories in circles to allow better visible distinction. Also, the plots are truncated at  $t = 2$  s as all inputs remain in close proximity to the zero-axis from there on.

### 5.3.2 Comparison of State-Dependent and Constant Penalty Matrices

Also addressed within previous sections has been the possibility to influence state convergence and input effectiveness through adapting the state-dependent weighting matrices,  $\mathbf{Q}(\mathbf{x})$  and  $\mathbf{R}(\mathbf{x})$ . Especially, the idea of limiting the torques required to stabilize the robot was suggested. This capacity will now be demonstrated by comparing the controller performance resulting from constant and state-dependent penalty matrices while using the same Used-SDC-Representation as defined in sec. 5.1.1. The state-dependent matrices are the ones introduced in sec. 5.2.1, while the constant matrices were chosen based on the constant terms within the state-dependent matrices, however the coefficients,  $q_1$ ,  $q_5$ , and  $q_6$ , were slightly adapted to not over- or underweight the corresponding system states in the absence of the state-dependent terms of the original penalty matrices:

$$\mathbf{Q} = \text{diag}(1 \ 3 \ 10 \ 2 \ 1 \ 2.5) \quad (5.33)$$

$$\mathbf{R} = \text{diag}(0.5 \ 0.5). \quad (5.34)$$



The simulation results included in fig. 5.4 correlate to the high pitch deviation,  $\mathbf{x}_{0,p}$ , and high yaw rate,  $\mathbf{x}_{0,y}$ , initial states and were executed at a stepsize of  $\Delta t = 0.1$  ms. Again, the input trajectories are provided separately to allow better distinction of the individual plots and are listed in fig. 5.5. Investigating the state trajectories resulting from the employment of constant weighting matrices reveals no evidently undesirable behaviour. Quite the contrary, except for the pitch rate all states actually converge faster and with less overshoot than the state trajectories corresponding to the SDRE-based controller defined through state-dependent penalty matrices. Besides quite sharp transitions in some system states, merely judging from the trajectories of fig. 5.4 there are no apparent downsides to the simplifying choice of constant weighting matrices.

Examining however the input trajectories plotted in fig. 5.5, the disadvantage of constant penalty matrices becomes obvious. While the state-dependent weighting matrices for the most part rely on inputs within the feasible range of about 1 N m to stabilize the high pitch initial state,  $\mathbf{x}_{0,p}$ , the constant weighting matrices produce inputs off that range by a factor of ten. For the high yaw rate initial state,  $\mathbf{x}_{0,y}$ , this effect becomes even more prominent as the required left-wheel torque shoots up to about 37 N m, while the controller under the employment of state-dependent weighting matrices manages to stabilize the TWIP by applying a maximum torque of about 1 N m.

Recalling the motivation behind choosing state-dependent coefficients of the weighting matrices in sec. 5.2.1, for the high yaw initial state,  $\mathbf{x}_{0,y}$ , far superior efficiency can be expected, as this is the exact situation that the performance index was adapted for. As the TWIP experiences a high spinning rate but no severe pitch deviation, the controller subject to the state-dependent penalty matrices detects the overall system state to not be critical and consequently does not overreact. The minor shoot-up of the applied torque leaving the feasible range, when employing the state-dependent weighting matrices-based controller for the high pitch initial state can be argued as a result of having decided to let the controller act most drastically on high pitch deviations.

The provided examples reaffirm that per se constant matrices do not imply worse controller performance in terms of assuring smooth and fast convergence to the origin. However, these simulations underline the reasoning of the chosen state-dependent weighting matrices in sec. 5.2.1 where the importance of making the inputs more expensive for highly dynamical system states that nevertheless do not threaten postural stability was highlighted. Especially the constant-weighted trajectory corresponding to the high yaw rate initial state,  $\mathbf{x}_{0,y}$ , exhibits this kind of overreaction of the controller resulting in required inputs far off the technically viable range.

In conclusion good performance can be obtained when executing SDRE-based design with constant matrices – and many examples are provided in the literature where this approach was applied successfully. When however the system’s input are subject to technical limitations, the state-dependencies of the penalty matrices make for an easy and low-effort opportunity to guide the inputs to remain within a technical feasible range. The choice of state-dependent weighting matrices allows to make inputs more expensive in certain system states or “situations” of the plant where for example non-linear intercouplings are less present and the overall system state can therefore be considered non-critical.

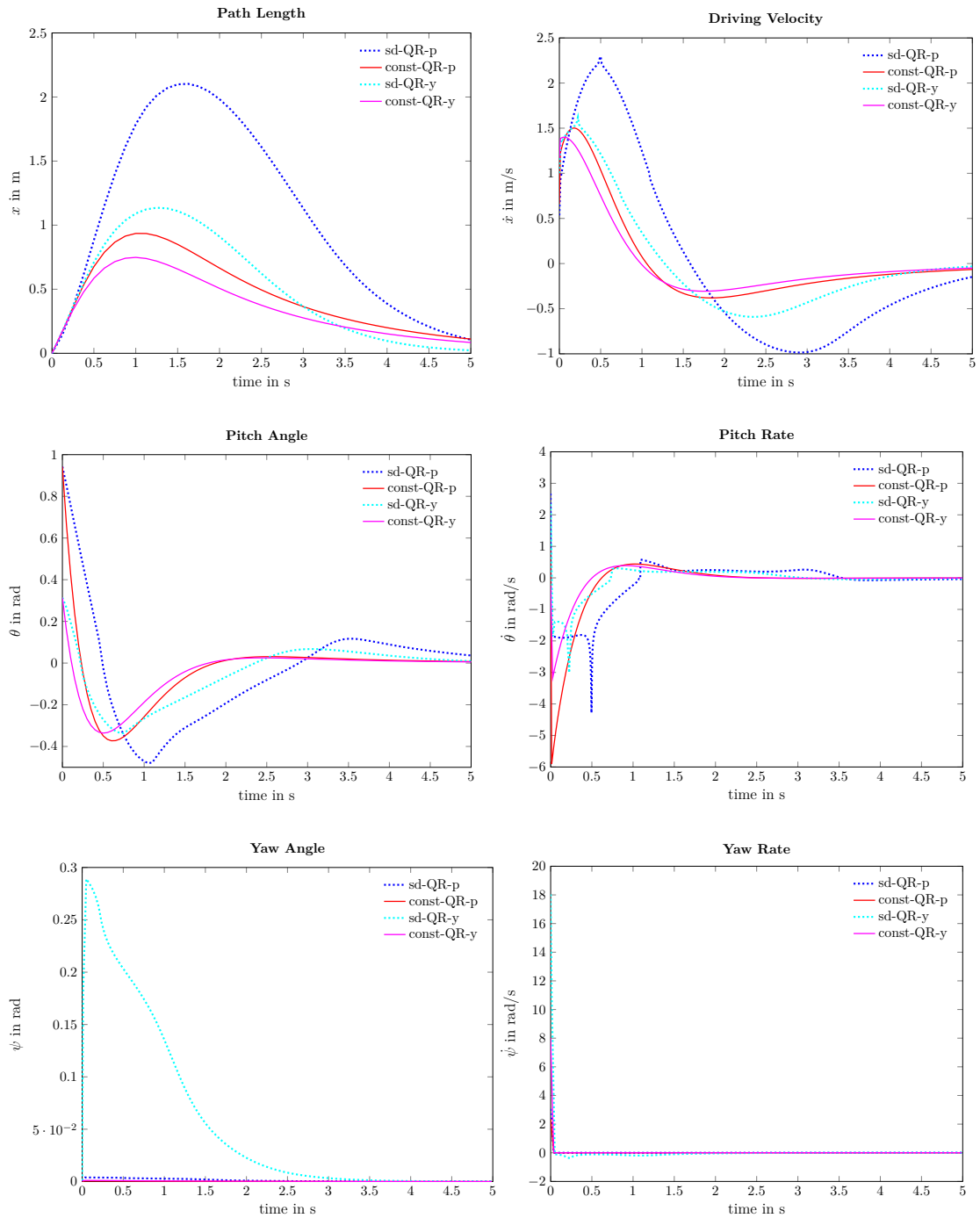


Figure 5.4: Comparison of the dynamics of the SDC-parametrization chosen for controller synthesis when using state-dependent weighting matrices or constant ones. While the constant weighting matrices result in fast state convergence and even less overshoot in all states but the pitch rate, the required inputs to achieve stabilization as shown in fig. 5.5 are off the feasible range.

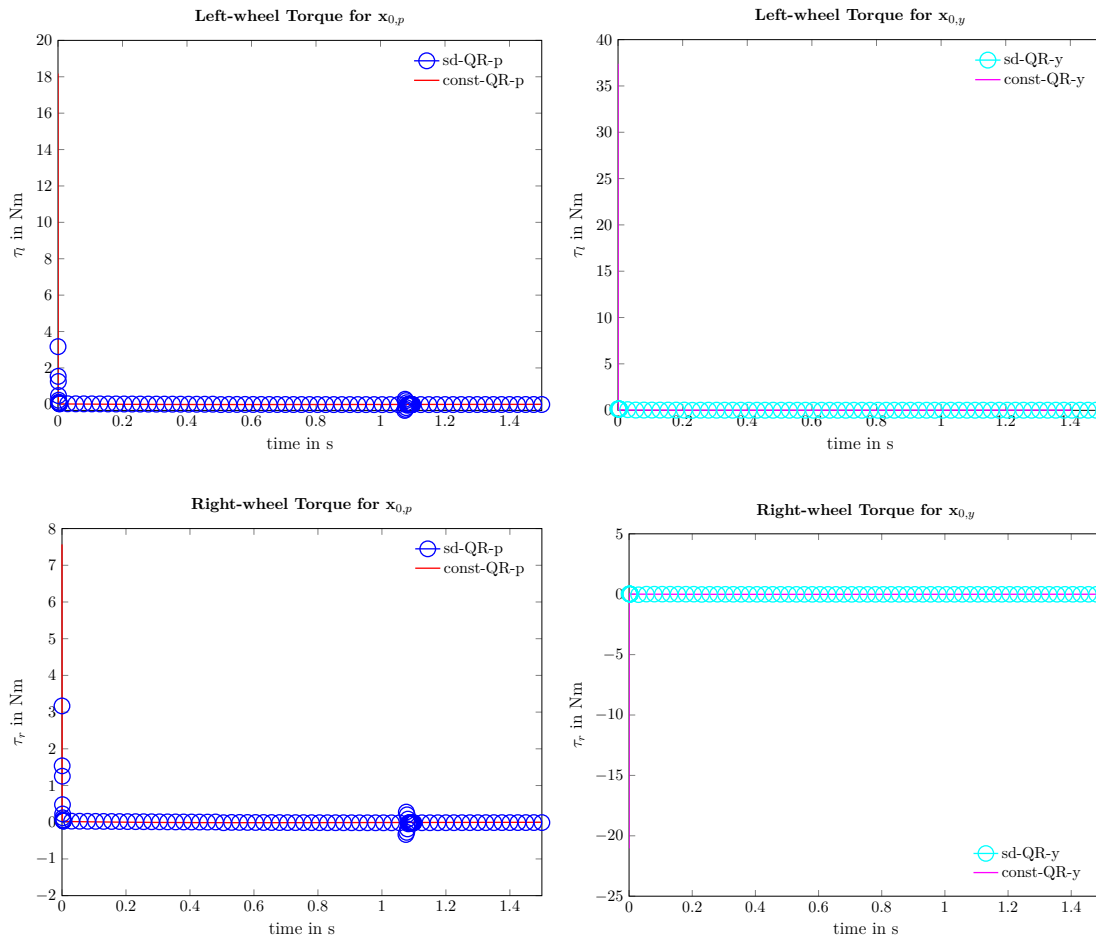


Figure 5.5: Comparison of the inputs required for stabilizing the system states depending on whether constant or state-dependent weighting matrices are employed. While the inputs for the state-dependent weighting remain within the technically viable range except for a minor peak in the very beginning when stabilizing the high pitch initial state, the required inputs for constant weighting shoot up to a technically non-realisable range. The provided trajectories were truncated at  $t = 1.5$  s, as all inputs remained close to zero from there on.

## 5.4 Comparative Study of SDRE-based and LQR-based Controllers for the TWIP

As the SDRE-method can be interpreted as the non-linear mimicry of LQR-synthesis, an obvious choice for comparing it in regards of obtainable controller performance lies in a LQR-controller based on the system's linearized dynamics. Accordingly, the TWIP's dynamics were linearized about their upright equilibrium point and the resulting constant system matrices are provided in the appendix (A.5). Again the built-in MATLAB LQR-solver was used to compute a now constant feedback gain matrix,  $\mathbf{K}$ , for the linearized dynamics subject to the performance index defined through the constant weighting matrices as provided in eq. (5.33). The obtained linear controller was subsequently applied to the TWIP and its closed-loop behaviour compared to the SDRE-controlled system.

### 5.4.1 Controller Performance when Stabilizing Different Initial States

First of all, the two controllers will be compared in regards of state convergence and input efficiency when stabilizing the dynamically moderate,  $\mathbf{x}_{0,m}$ , and critical,  $\mathbf{x}_{0,c}$ , initial states without any additional configurations or perturbations applied. The computed state trajectories for the two controllers are presented in fig. 5.6. The simulations were executed with a fixed stepsize of  $\Delta t = 0.1$  ms and the corresponding input trajectories are provided in fig. 5.7. Qualitatively, the trajectories for the LQR-controlled system resemble the ones given in fig. 5.4 obtained from the SDRE-controller subject to constant weighting matrices and consequently similar conclusions can be drawn about the LQR-controlled system.

While the LQR-controller manages to briefly drive the states to the origin while exhibiting comparable or even less overshoot than the non-linear SDRE-controller, the shoot up of the required inputs to do so is even more drastic than in the SDRE-case with constant weighting matrices as the input trajectories of fig. 5.7 showcase. In order to stabilize the highly dynamical initial state,  $\mathbf{x}_{0,c}$ , the linear controller relies on imposing torques of almost up to 50 N m, while the non-linear controller manages to remain within the technical feasible range of 1 N m. After the simulation time of 5 s the SDRE-controller has nevertheless been able to drive the system states similarly close to the origin while having consumed a fraction of the energy the LQR-controller would have required.

This effect is common for linear controllers and repeatedly discussed in papers on SDRE-based controller synthesis. As among others pointed out in [12, 13, 16], linear controllers tend to try and brutally cancel out all non-linearities within the system's dynamics which often amounts to vast energy consumptions when trying to stabilize a non-linear system. While the moderately dynamical initial state,  $\mathbf{x}_{0,m}$ , can already only be stabilized with inputs ten times as large as feasible, for the critically dynamical state,  $\mathbf{x}_{0,c}$ , the linear controller would demand inputs of up to fifty times of the viable maximum torque applicable. In conclusion, as the robot would not be able to produce torques within that scale the linear controller can be expected to likely fail in applications when subject to dynamically critical conditions. The non-linear SDRE-based controller on the other hand can exploit the systems "natural" dynamics and consequently restore postural stability far less aggressively even in critical situations.

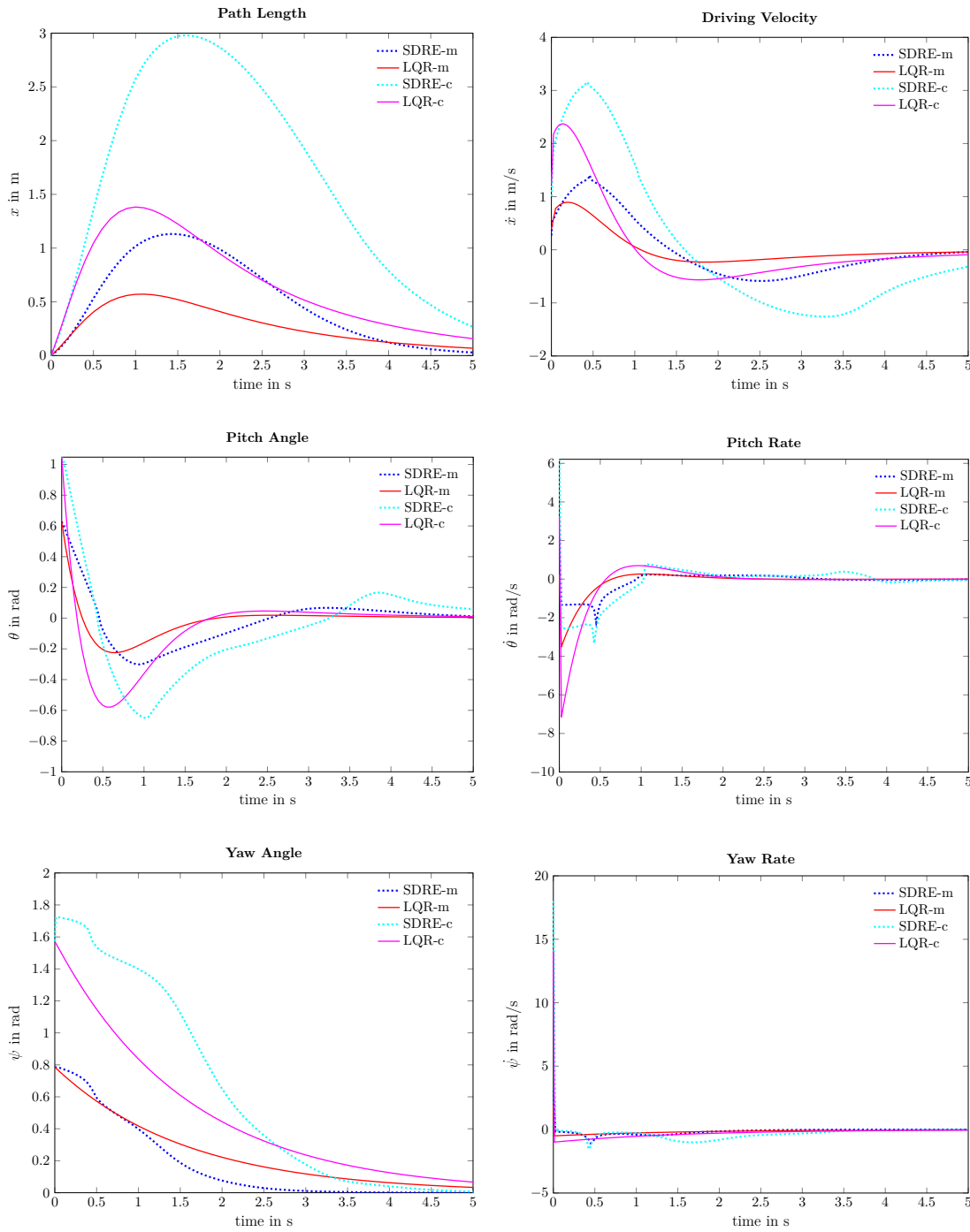


Figure 5.6: Comparison of the obtained state trajectories when either a linear LQR-controller or non-linear SDRE-controller is applied. Even though convergence can be achieved marginally faster for most states when employing the LQR-controller, the inputs required to do so as plotted in fig. 5.7 exceed the technical realisable scale.

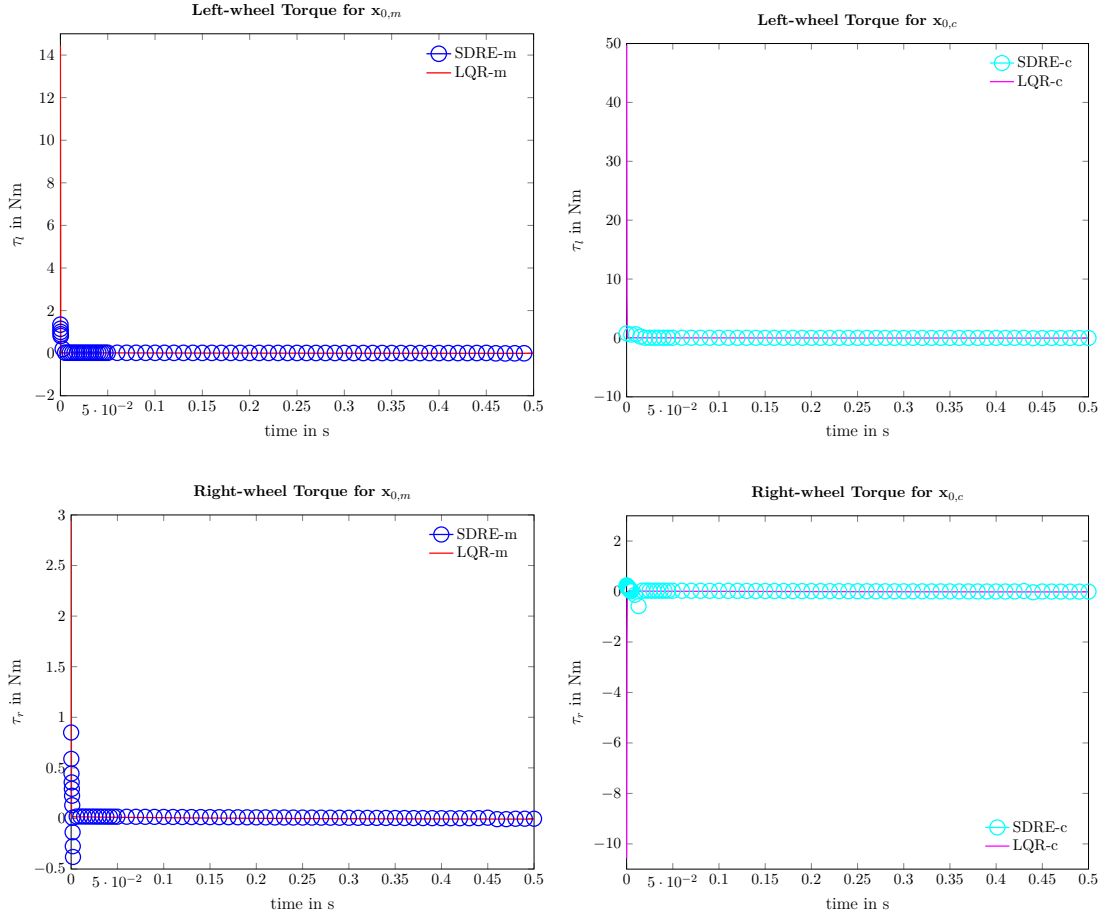


Figure 5.7: Comparison of the inputs required to stabilize the TWIP when using a linear LQR-controller versus the proposed SDRE-controller. While the SDRE-controller manages to restore a stable system state while not ever exceeding the technical viable input range, the LQR-controller would rely on inputs off by a factor of up to fifty to restabilize the dynamically critical initial state.

#### 5.4.2 Controller Performance in the Presence of Disturbance

The remaining two examples are aimed to provide further insight on robustness properties of the LQR- and SDRE-controller respectively by evaluating how they can be expected to perform in “unexpected” scenarios. For this purpose, first the controllers were examined when subject to arising step-disturbances as for instance when driving over a small obstacle. Similar experiments were executed in [26] and did not pose a threat to destabilize the robot with the SDRE-controller applied – however the TWIP used within this publication has strongly differing parameters such that for a slender-body TWIP as employed within this work, the results might considerably deviate.

In order to simulate the step-disturbance, within the simulation time of  $t \in [0.5 \text{ s}, 1.0 \text{ s}]$  a constant torque of  $\tau_{dis} = 0.4 \text{ Nm}$  was added to the right wheel. The chosen time frame describes the TWIP bending over at a large pitch distortion and can consequently be considered a critical moment for an external disturbance to arise. The resulting

trajectories as presented in fig. 5.8 again correspond to the dynamically modest,  $\mathbf{x}_{0,m}$ , and critical initial states,  $\mathbf{x}_{0,c}$ , and were executed at a fixed stepsize of  $\Delta t = 0.05$  ms.

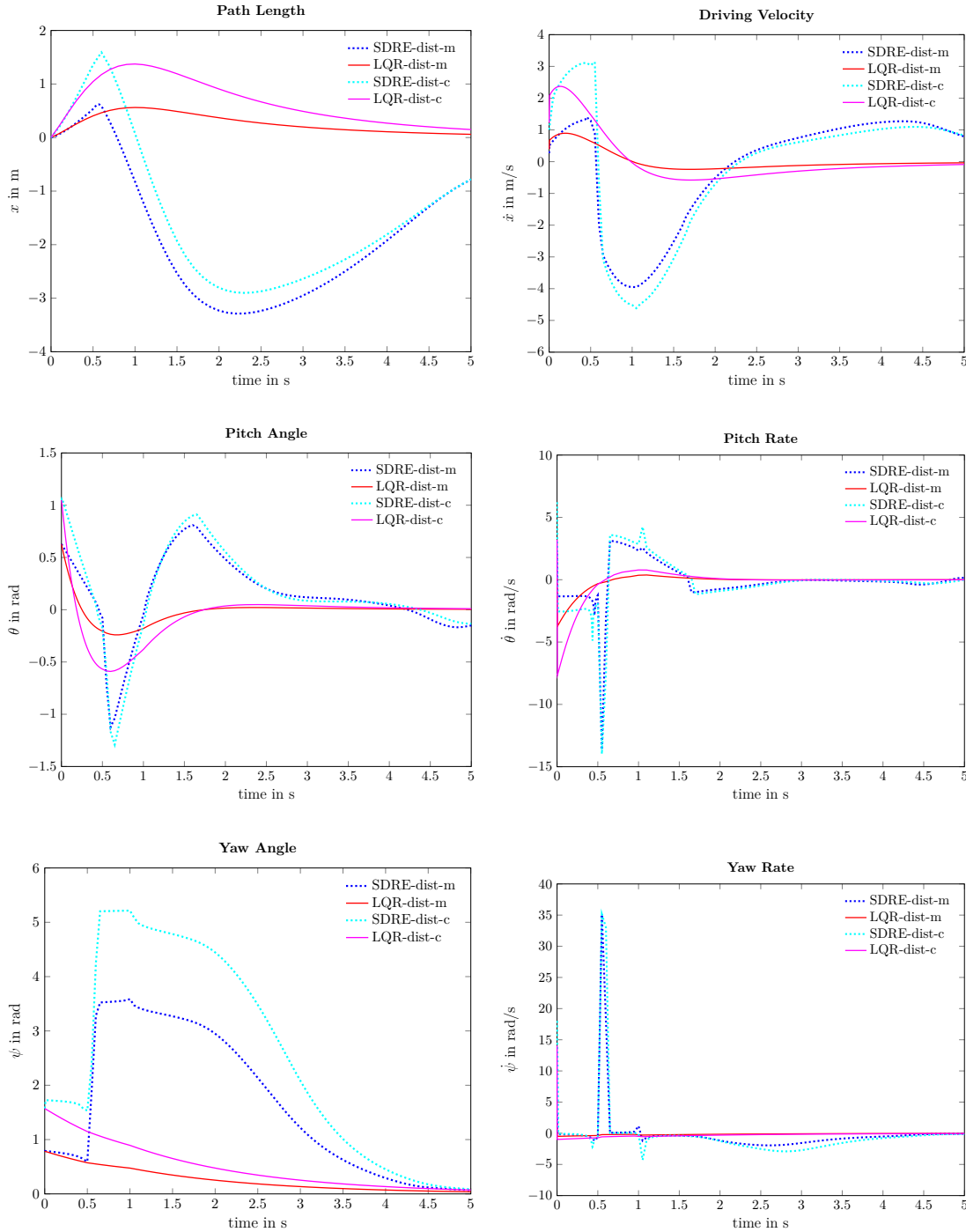


Figure 5.8: The resulting state trajectories when a constant disturbance of 0.4 N m is applied between simulation times,  $t = 0.5$  s and  $t = 1.0$  s. While the SDRE-based controller manages to restabilize the system while experiencing some oscillations, the LQR-controller hardly seems to be affected by the step-disturbance.

The computed state trajectories of the LQR-controlled system are almost indistinguishable to the ones of fig. 5.6 corresponding to the system subject to no disturbance. The same can be observed for the input trajectories provided in fig. 5.9 of the LQR-controlled system – the occurring disturbance is compensated within a single timestep and consequently no significantly increased control effort can be determined.

For the SDRE-controlled system remarkably different state convergence can be observed when compared to the non-disturbed trajectories of fig. 5.6. The disturbance occurs as the system is deviated from the upright equilibrium by almost  $-\frac{\pi}{3}$  and consequently the system is experiencing strong non-linear state intercouplings. Therefore the system experiences shoot-ups and some oscillation in the inputs when the disturbance is applied and withdrawn as displayed in fig. 5.9. Nevertheless, the SDRE-controller restabilizes the disturbed system and regulates the yaw dynamics and pitch rate to the origin within the remaining simulation time, as well. While after the predefined simulation time of 5 s the pitch deviation and driving velocity are still larger than zero, they are kept within a non-critical range and can be expected to converge within short time. While the inputs the SDRE-controller applies to maintain stability are higher than for the non-disturbed examples of the last section, they still remain within the feasible range at all times showcasing that the input efficiency determined through the chosen performance index can also be preserved in unexpected situations.

The executed simulations reaffirm the excellent robustness properties of LQR-design [37] and prove the SDRE-design to be inferior in this regard. However, as with the examples provided in the last section, the LQR-controller relies on applying torques far off the feasible range to stabilize the system. Even though the SDRE-controlled system exhibits drastic overshooting, the controller still manages to restabilize the system in a dynamically critical situation while maintaining the required inputs in the technically viable range persistently.



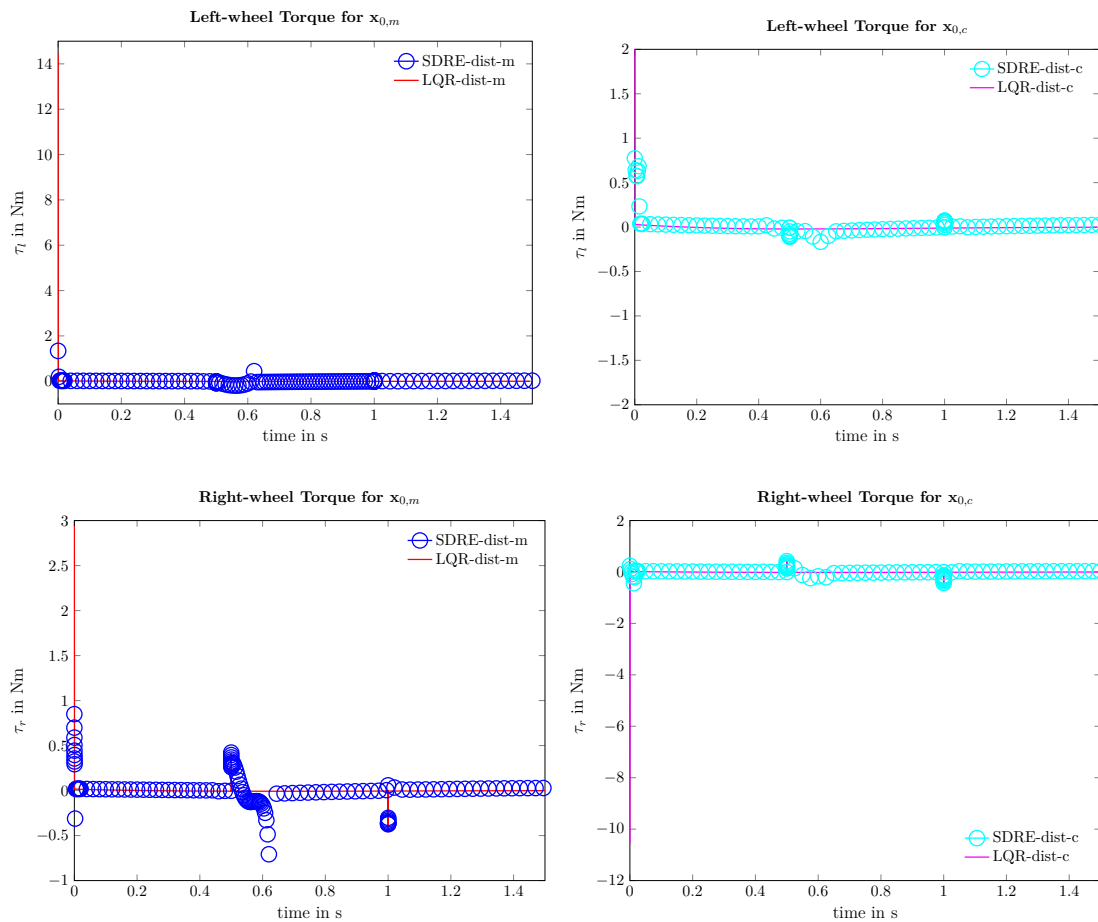


Figure 5.9: The corresponding inputs when the LQR- and SDRE-based controllers are subject to a step-disturbance. While the inputs required by the SDRE-controller slightly shoot-up when the disturbance is applied and withdrawn, they quickly converge back to low effort stabilization afterwards while remaining in the feasible range at all times.

### 5.4.3 Controller Performance on Model with Non-linear Friction

Lastly, in order to test the two controllers in terms of their robustness regarding modelling inaccuracies, examples will be provided of how the LQR-based and SDRE-based controllers perform on an extended dynamic model of the robot taking into account non-linear friction effects. The model used within the following simulations incorporates friction between the wheels and the ground as well as between individual components of the TWIP. The resulting state trajectories after simulation at a stepsize of  $\Delta t = 0.1$  ms for the dynamically modest,  $\mathbf{x}_{0,m}$ , and fast spinning initial states,  $\mathbf{x}_{0,y}$ , are provided in fig. 5.10.

While the SDRE-based controller still manages to drive the pitch deviation to the origin smoothly without any significant overshoot and within reasonable time, the controller struggles with regulating the driving velocity and yaw rate back to the equilibrium state. While the yaw rate seems to converge to a constant spinning mode, the driving velocity starts to diverge to non-physical values.

These results can be reasoned as the SDRE-controller as proposed within this work sets a strong focus on reestablishing the TWIP in its upright zero-pitch deviation and explicitly demands to not react too drastically to high yaw rates or driving velocities alone. Additionally, the friction terms directly influence the unstable system states while their effect on the pitch deviation is only indirect through dynamical decoupling. However, to achieve sufficient controller performances when subject to friction as implemented in the presented model, the controller would most likely have to be redesigned based on a non-linear model taking into account according effects.

Note that only trajectories corresponding to the SDRE-controlled system are plotted in fig. 5.10, as the LQR-controlled system diverges within the first ms of simulation time as indicated in the plots of fig. 5.11. This again highlights the LQR-controller's alienness to the system's natural dynamics, while the SDRE-controller "being aware" of the system's inherent non-linearities can still stabilize some system states even in the presence of the unknown effects of non-linear friction terms.

Additionally, notice that nevertheless the inputs required to partially stabilize the TWIP also start to diverge to physically non-reasonable values after about 2s of simulation time when employing the SDRE-based controller, as well. For this reason, no input trajectories are provided and the SDRE-controller can likely be expected to fail if friction effects this strong were to be present. The examples nevertheless showcase how the predefined performance index majorly affects resulting controller performance even if subject to unfamiliar dynamics.

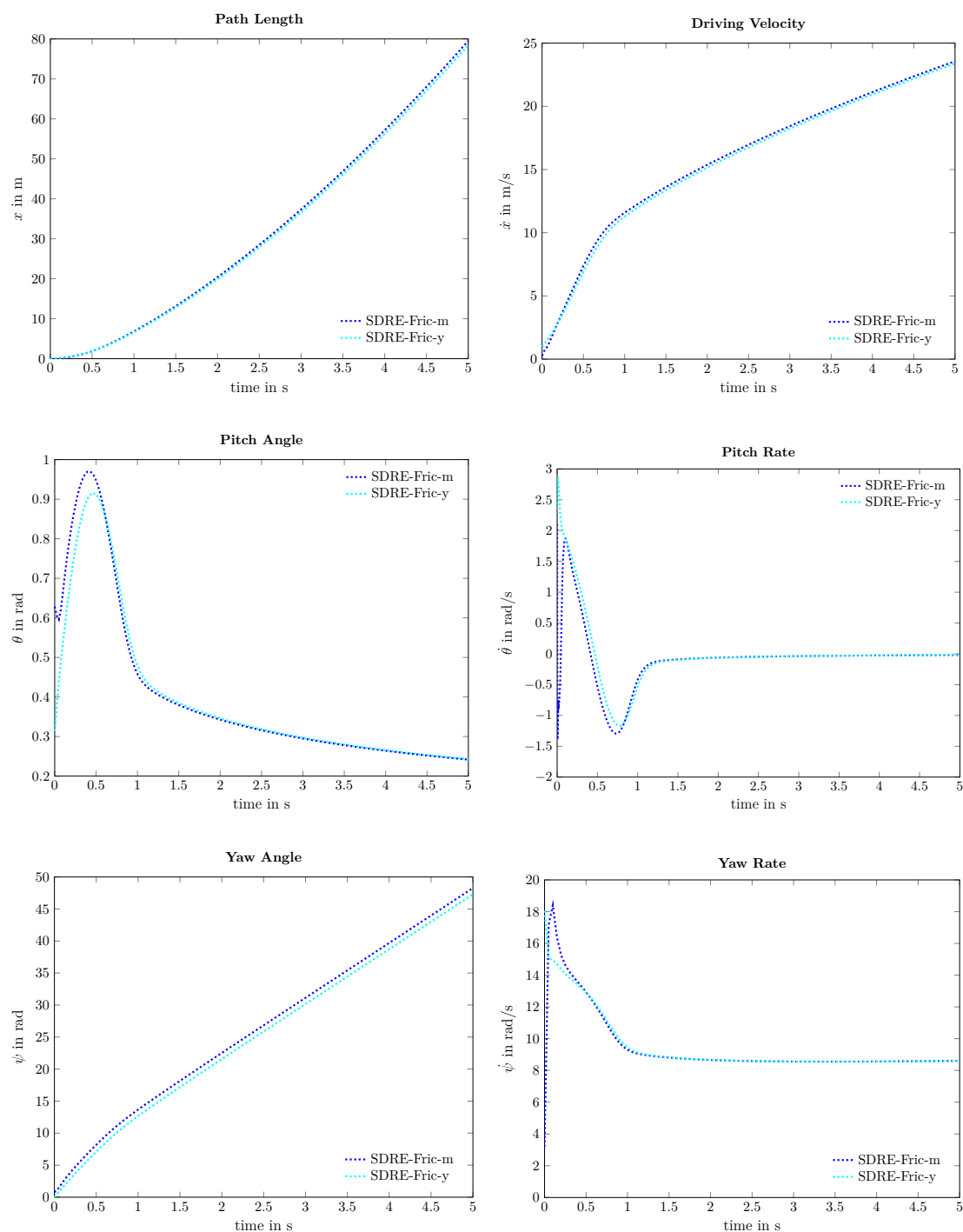


Figure 5.10: The resulting state trajectories when applying the SDRE-controller based on a frictionless model to an extended model taking into account non-linear friction effects. While the controller still manages to stabilize the TWIP's pitch deviation, it can no longer get hold of its driving velocity and spinning motion. In order to improve controller performance, the performance index could be adjusted or a completely new controller taking into account the friction effects designed.

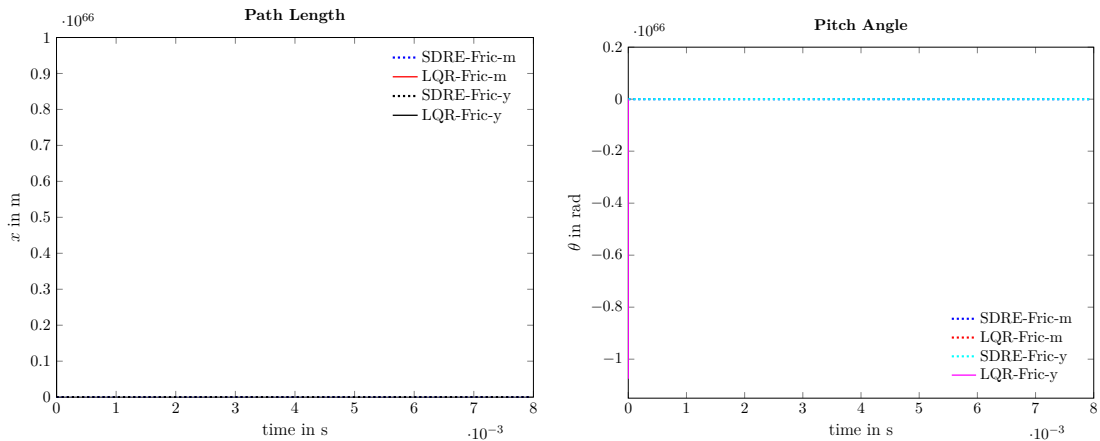


Figure 5.11: The state trajectories of the LQR-controlled system start to diverge within the first couple of steps of simulation time. Here the simulated path length and pitch deviation are provided as examples.

## 5.5 Remarks on SDRE-based Controller Synthesis for the TWIP

Through the SDRE-approach, a controller was found that manages to stabilize the TWIP in its upright position for a large region within the state-space. The additional degrees of freedom arising from defining a quasi-linear SDC-representation and state-dependent weighting matrices were exploited to allow predominantly smooth state convergence, while keeping the applied inputs within a technically realisable scale of 1 N m even in dynamically critical situations. Through more intensive studies, these parameters could probably be adapted to further improve the corresponding closed-loop dynamics and input efficiency.

The proposed SDRE-based controller taking into account the robot's inherent nonlinearities proved superior energy efficiency when compared to a LQR-controller based on the linearized dynamics and an alternate SDRE-controller based on a differing SDC-parametrization. While the linear controller already exceeded the feasible input range for non-critical states, it relies on tremendous input efforts to be able to stabilize the system in highly dynamical situations, such that it reasonably can be expected to fail in application.

Additionally, note that the proposed SDRE-controller allowed for the simple Runge-Kutta-solver to run without numerical issues at a significantly larger stepsize compared to the alternate SDRE-controller based on the TP-SDC-parametrization and the LQR-controller. As stepsizes significantly smaller than 1 ms will be problematic to realize when applying the controller to the actual robot, this will be a critical advantage of the proposed SDRE-controller.

Subject to step-disturbances in the input, the SDRE-based controller – while not exhibiting robustness properties as strong as the LQR-controller – still managed to restabilize the system without exhibiting drastic oscillations. Additionally, the SDRE-controller remained within in the viable input range at all times. Employing the found controller on a model taking into account non-linear friction terms showed sufficient performance

in stabilizing the pitch deviation but failed to regulate the driving velocity and yaw rate to the origin. In order to achieve better performance on the friction model, the state-dependent weighting matrices could be adjusted accordingly – as in its current configuration the controller is defined to act aggressively only if large pitch deviations arise. When trying to regulate the friction model with the LQR-controller, the system diverged within a short time frame. Further real-life experiments would have to be conducted to judge controller performance and robustness in application.

During simulations no non-controllable system state as well as no initial state was found for that the proposed SDRE-controller failed to restore the equilibrium state within reasonable time and effort – even when all system states are chosen at their physical limits as defined in tab. 5.1. However, even though a significant number of simulations was executed in the context of this work, these can not yet be considered technical proof of closed-loop stability. For this reason, the next chapter will introduce an approach to characterize the closed-loop dynamics in regards of stability based on contraction analysis, while facilitating computations by using the results already obtained from pointwisely solving the SDRE.



## Chapter 6

# Contraction-based Stability Analysis of SDRE-controlled Systems

While the last chapter introduced a controller based on the SDRE-technique and empirically analysed its performance through different simulation set-ups, in this chapter a systematic approach will be proposed to evaluate the obtained closed-loop dynamics. In order to determine stability properties of the closed-loop system, contraction theory will be employed and a method introduced to fit a contraction metric, while making use of the fact that during SDRE-synthesis pointwisely some positive-definite metric has already been found in the solution of the SDRE.

First however, a short overview on the topic of stability margins and analysis for SDRE-based controllers is provided in sec. 6.1. Hereinafter, the idea of exploiting the solution of the SDRE to help guide the quest for a suitable contraction metric is first motivated in sec. 6.2 and subsequently the resulting method introduced in sec. 6.3. Lastly, the obtained contraction metric and corresponding contraction region will be showcased and discussed in sec. 6.4. This concluding application of contraction analysis should provide further insights on how the evaluation of local properties in local coordinates allows characterization of the original system – which is unique for contraction theory and therefore makes it an attractive tool to examine SDRE-controlled systems.

### 6.1 Stability Characteristics and Analysis for SDRE-controlled Systems

A general drawback of SDRE-based controller design is that it does not implicitly guarantee stability margins of the closed-loop dynamics as other design techniques do. For higher-order or in other regards complex systems, the solution to the SDRE and therefore by implication also the closed-loop dynamics:

$$\dot{\mathbf{x}} = (\mathbf{A}(\mathbf{x}) - \mathbf{B}(\mathbf{x})\mathbf{K}(\mathbf{x}))\mathbf{x} = \mathbf{A}_{cl}(\mathbf{x})\mathbf{x} \quad (6.1)$$

are generally not explicitly known [18] such that only local asymptotic stability about the origin can be assured. As the solution of the ARE in  $\mathbf{x} = \mathbf{0}$  defines closed-loop

dynamics,  $\mathbf{A}_{\text{cl}}(\mathbf{0})$ , exclusively containing eigenvalues with strictly negative real-parts [17], employing Lyapunov’s indirect method yields local asymptotic stability about the equilibrium,  $\mathbf{x}_{\text{eq}} = \mathbf{0}$ . Additionally, the local solution of the SDRE in a certain system state,  $\mathbf{x}$ , is assured to define a locally stabilizing solution, however these solutions can never assure global stability – even if the closed-loop dynamic matrix,  $\mathbf{A}_{\text{cl}}(\mathbf{x})$ , is known to only have eigenvalues in the left complex half-plane within the entire state-space<sup>1</sup>.

Consequently, stability analysis of SDRE-controlled systems can be considered a crucial as well as challenging task in evaluating the obtained controller. Several publications can be found addressing themselves to this task: Erdem and Alleyne propose an analytical approach in [17] and one based on “overvaluing” vector norms in [18] solved numerically, however both can be considered to only be feasible for low order systems. Two further numerical approaches based on Lyapunov theory are the ones by Bracci in [5] and by Seiler who employs sum-of-squares programming in [40]. However Seiler’s method is quite restrictive as it for examples assumes all state-dependent system matrices to be exclusively polynomial in the system states and Bracci’s approach again is computationally expensive for higher-order systems.

Thus, as the investigated TWIP is a six-dimensional system and the solution of the SDRE is only accessible pointwise, an alternate approach based on contraction theory is presented in the context of this work. In [7] Chang first presented the idea of using contraction theory to examine closed-loop stability properties of SDRE-controlled systems. Consequently, the procedure of [7] might at first appear similar to the method proposed within this paper as it also seeks to define stability margins by evaluating the contraction conditions as provided in def. 3.9. However, Chang does not explain how he numerically approaches the problem and also exclusively discusses a system of order two when applying his method. Additionally, in [7] the condition of def. 3.9 is relaxed to a critical extend, which will be further discussed in sec. 6.3 where the applied method is introduced in detail. Prior to this, some concepts of Riemannian geometry which are essential within contraction theory will be quickly outlined in order to further motivate the proposed method.

## 6.2 Motivation of Fitting a Contraction Metric Based on Frozen SDRE-Solutions

When employing contraction theory for stability analysis, one tries to find a symmetric positive-definite and generally state-dependent metric,  $\mathbf{M}(\mathbf{x})$ , defining a transformation to local differential coordinates,  $\delta\mathbf{z}$ . For the system dynamics described by these local coordinates,  $\delta\mathbf{z}$ , exponential convergence can be deduced to hold for all system states in which the found metric fulfills the condition of def. 3.9 as within that entire region, it can be concluded that all differential distances,  $\sqrt{\delta\mathbf{z}^T \delta\mathbf{z}} = \sqrt{\delta\mathbf{x}^T \mathbf{M}(\mathbf{x}) \delta\mathbf{x}}$ , between neighbouring trajectories will vanish at an exponential rate. This observation then allows the corollary that if the system is contracting in local coordinates,  $\delta\mathbf{z}$ , the original system represented by differential coordinates,  $\delta\mathbf{x}$ , exhibits exponential convergence to a single trajectory, as well.

<sup>1</sup>Recalling Lyapunov’s direct method as discussed in sec. 3.3.2, proving that local asymptotic stability holds for the entire state-space is not sufficient to confirm global asymptotic stability. Within Lyapunov theory matters like finite escape time and invariant sets do not allow such conclusions for non-linear system by exclusively examining local properties [16]. For further information refer to [16, 42, 24].



The open quest remains in finding some approach to determine a contraction metric,  $\mathbf{M}(\mathbf{x})$ , suggesting to discuss the definition of a metric and the ideas linked to it in some more detail. Contraction theory is based on two key concepts of Riemannian geometry: Riemannian manifolds,  $\Upsilon$ , described through Riemannian metrics,  $\mathbf{M}(\mathbf{x})$ , which is why those notions will be minimalistically outlined in the upcoming section. Note that the following explanations will only be to an extend necessary to motivate the proposed method and have the mere purpose to ease understanding, however by no means claim to be complete. The following definitions are adapted from [48] – for exact and more detailed derivations the author refers to this material.

A tuple,  $(X, d)$ , of a set,  $X$ , and a mapping,  $d$ , defined as

$$d : X \times X \rightarrow K(\mathbf{x}_1, \mathbf{x}_2) \quad \mathbf{x}_1, \mathbf{x}_2 \in X, \quad K \in \mathbb{R}, \quad (6.2)$$

define a metric space if for the mapping certain criteria (positiveness, zero distance, symmetry, and triangle inequality) hold. The mapping,  $d$ , is then referred to as the corresponding distance function or metric [48].

Euclidean space defines a metric space where distances within the set of  $\mathbb{R}^n$  are measured through the mapping defined by the well-know Euclidean norm:

$$\text{dist}(\mathbf{x}_1, \mathbf{x}_2) = \sqrt{(x_{1,1} - x_{2,1})^2 + (x_{1,2} - x_{2,2})^2 + \dots + (x_{1,n} - x_{2,n})^2}. \quad (6.3)$$

The term manifold defines a metric space that locally resembles an open subset of Euclidean space where however globally properties from Euclidean space no longer hold [48]. Examples of such characteristics that do not need to be satisfied on a manifold are the shortest distance being defined through a straight line and triangles having an constant angle sum of  $\pi$ . These kind of properties are also covered in the notion of “curvilinear” coordinates contrary to Cartesian coordinates. Consequently, to put points on a manifold into context, e.g. in terms of the distance separating them, tools from Euclidean geometry are no longer sufficient.

A Riemannian metric,  $\mathbf{M}(\mathbf{x})$ , equips a continuously differentiable manifold,  $\Upsilon$ , with an inner product on each tangent space [29], providing a local concept of lengths:  $\sqrt{\delta\mathbf{x}^T \mathbf{M}(\mathbf{x}) \delta\mathbf{x}}$ . In order to allow such a definition of length, the Riemannian metric must be symmetric positive-definite and continuously differentiable. Note that the Riemannian metric per se is not a metric in the sense of metric spaces as it does not yet define a global distance function. The Riemannian metric can however be employed to measure distances between two points on the manifold, by first computing a curve connecting them along the curvilinear coordinates of the manifold:

$$\gamma : [0, 1] \rightarrow \Upsilon \quad \frac{d\gamma(s)}{ds} \neq 0 \quad \forall s \in [0, 1], \quad (6.4)$$

where  $\gamma(s = 0) = \mathbf{x}_1$  and  $\gamma(s = 1) = \mathbf{x}_2$  define the two points on the manifold to be connected. Hereinafter, the distance can be determined by integration along this curve [29]:

$$\text{dist}_{\mathbf{M}}(\mathbf{x}_1, \mathbf{x}_2) = l(\gamma(s)) = \int_0^1 \sqrt{\frac{d\gamma(s)}{ds}^T \mathbf{M}(\gamma(s)) \frac{d\gamma(s)}{ds}} ds. \quad (6.5)$$

Consequently the Riemannian metric can be understood as inducing a distance function and the tuple of a Riemannian manifold,  $\Upsilon$ , and metric,  $\mathbf{M}(\mathbf{x})$ , then interpreted as a

metric space. The minimal-length connection of two points on the Riemannian manifold can be described through so-called geodesics [48]. In [29] one possible approach is presented to compute geodesics, however a variety of methods exist.

Reinterpreting Euclidean space considered in most engineering tasks as a Riemannian manifold, the corresponding Riemannian metric is the identity matrix,  $\mathbf{I}$ , and the distance function collapses to the Euclidean norm – the differentiation between local lengths and global distance diffuses. The shortest distance between two points always yields a straight line:

$$\text{dist}_{\mathbf{I}}(\mathbf{x}_1, \mathbf{x}_2) = \sqrt{(\mathbf{x}_1 - \mathbf{x}_2)^T \mathbf{I} (\mathbf{x}_1 - \mathbf{x}_2)}. \quad (6.6)$$

Now, from optimal control theory it is known that the solution of the SDRE,  $\mathbf{P}(\mathbf{x})$ , defines a continuously differentiable symmetric positive-definite matrix that when applied as a control law,  $\mathbf{u}(\mathbf{x}) = -\mathbf{R}^{-1}(\mathbf{x})\mathbf{B}^T(\mathbf{x})\mathbf{P}(\mathbf{x})\mathbf{x}$ , guarantees local stability. Additionally, one can determine that this solution in fact describes a Riemannian metric inducing the local notion of length,  $\sqrt{\delta\mathbf{x}^T \mathbf{P}(\mathbf{x}) \delta\mathbf{x}}$ .

In conclusion, stability analysis based on contraction theory implies the search for a Riemannian metric locally assuring exponential convergence. When having solved the SDRE, pointwise a positive-definite metric has been found that locally guarantees asymptotic convergence and is additionally known to locally have optimality properties in regards of the system dynamics and the predefined performance index. This finding motivates the fitting method proposed in the context of this paper employing the gridded solution of the SDRE to provide some local guidance in finding a contraction metric.

### 6.3 Introduction and Comparison of a Fitting Method for Contraction Metrics

#### Proposed Method to Fit a Polynomial Contraction Metric

The proposed fitting method is based on the concepts of semi-definite programming which encompasses optimization problems where decision variables are symmetric matrices instead of vectors. Generally, so-called semi-definite programs (SDPs) define optimization problems involving semi-definite constraint, i.e. linear matrix inequalities (LMIs) or bi-linear matrix inequalities (BMIs) [31]. A LMI demands some definiteness properties for a given linear matrix expression and can always be denoted by:

$$\mathbf{L}(\mathbf{x}) = \mathbf{L}_0 + \sum_{i=1}^m y_i \mathbf{L}_i > 0 \quad (6.7)$$

where  $\mathbf{y}$  defines an  $m$ -dimensional vector and  $\mathbf{L}_i$   $n \times n$ -symmetric matrices [31]. The extension to BMIs is straight-forward and can for instance be found in [46]. Typical SDPs usually define feasibility problems where a symmetric matrix fulfilling the given constraints is searched for but can as well be extended by some objective, e.g. additionally minimizing the matrix's trace or likewise. For further information on SDPs as well as examples and properties of LMIs, refer to [31, 46].

Again recalling the contraction condition of def. 3.9, yields that applying contraction analysis to the SDRE-controlled systems defined through closed-loop dynamics as in eq. (6.1), results in finding some metric,  $\mathbf{M}(\mathbf{x})$ , such that:

$$\mathbf{M}(\mathbf{x}) > \mathbf{0} \quad (6.8)$$

$$\left( \frac{\partial \mathbf{A}_{\text{cl}}(\mathbf{x}) \mathbf{x}}{\partial \mathbf{x}} \right)^{\text{T}} \mathbf{M}(\mathbf{x}) + \mathbf{M}(\mathbf{x}) \left( \frac{\partial \mathbf{A}_{\text{cl}}(\mathbf{x}) \mathbf{x}}{\partial \mathbf{x}} \right) + \dot{\mathbf{M}}(\mathbf{x}) \leq -\beta \mathbf{M}(\mathbf{x}) \quad (6.9)$$

holds for a as large as possible region of the state-space. These conditions define two LMIs in the contraction metric,  $\mathbf{M}(\mathbf{x})$ , and consequently what at first seems like a simple feasibility SDP. In fact for a constant metric, this feasibility problem could easily be solved, however as the desired metric,  $\mathbf{M}(\mathbf{x})$ , is state-dependent and additionally the closed-loop dynamics,  $\mathbf{A}_{\text{cl}}(\mathbf{x}) \mathbf{x}$ , are not known analytically known but only accessible pointwise, a more advanced procedure as described in the following is required.

First of all to describe the state-dependency of the contraction metric, a polynomial approach was chosen. Consequently, all metric entries were defined as polynomial in the TWIP's shape variables,  $[\dot{x}, \theta, \dot{\theta}, \dot{\psi}]$ , with a maximum degree of  $m$ , meaning that any metric entry:

$$M_{pq}(\dot{x}, \theta, \dot{\theta}, \dot{\psi}) = \sum_{i=0}^m \sum_{j=0}^m \sum_{k=0}^m \sum_{l=0}^m c_{pq,ijkl} \dot{x}^i \theta^j \dot{\theta}^k \dot{\psi}^l \quad i + j + k + l \leq m \quad (6.10)$$

contains any possible products of system states defining monomials with a degree of smaller than or equal to  $m$ . The set of decision variables is consequently made up of the coefficients of the monomials,  $c_{pq,ijkl}$ , of each metric entry,  $M_{pq}$ .

Additionally, as the contraction conditions can not be evaluated analytically, a gridding-approach analogously to the controllability analysis of the found SDC-parameterization in sec. 5.1.2 was decided on. Again, the shape variable limits as defined in tab. 5.1 were used as a guideline and a grid equidistant within state-space was chosen - the exact parameters of the grid used will be provided in sec. 6.4. Within these predefined grid points,  $\mathbf{x}_{\mathbf{g}}$ , ineq. (6.9) was evaluated and the resulting LMIs:

$$\left. \frac{\partial (\mathbf{A}_{\text{cl}} \mathbf{x})^{\text{T}}}{\partial \mathbf{x}} \right|_{\mathbf{x}=\mathbf{x}_{\mathbf{g}}} \mathbf{M}(\mathbf{x} = \mathbf{x}_{\mathbf{g}}) + \mathbf{M}(\mathbf{x} = \mathbf{x}_{\mathbf{g}}) \left. \frac{\partial (\mathbf{A}_{\text{cl}} \mathbf{x})}{\partial \mathbf{x}} \right|_{\mathbf{x}=\mathbf{x}_{\mathbf{g}}} + \dot{\mathbf{M}}(\mathbf{x} = \mathbf{x}_{\mathbf{g}}) \leq -\beta \mathbf{M}(\mathbf{x} = \mathbf{x}_{\mathbf{g}}) \quad (6.11)$$

were added to the optimization problem individually to demand some local property for the metric to be fitted. Due to the polynomial form of the metric,  $\mathbf{M}(\mathbf{x})$ , its time derivative defined as:

$$\dot{\mathbf{M}}(\mathbf{x}) = \left( \frac{\partial \mathbf{M}(\mathbf{x})^{\text{T}}}{\partial \mathbf{x}} \mathbf{A}_{\text{cl}}(\mathbf{x}) \mathbf{x} \right) \quad (6.12)$$

can easily be computed as the Jacobian of the metric,  $\frac{\partial \mathbf{M}(\mathbf{x})}{\partial \mathbf{x}}$ , again is polynomial in  $\mathbf{x}$ . However, more difficultly lay in defining the Jacobian of the closed-loop system,  $\frac{\partial \mathbf{A}_{\text{cl}}(\mathbf{x}) \mathbf{x}}{\partial \mathbf{x}}$ .

Considering the closed-loop dynamics in detail:

$$\begin{aligned} \frac{\partial \mathbf{A}_{cl}(\mathbf{x})}{\partial \mathbf{x}} \mathbf{x} &= \frac{\partial (\mathbf{A}(\mathbf{x}) - \mathbf{B}(\mathbf{x}) \mathbf{K}(\mathbf{x}))}{\partial \mathbf{x}} \mathbf{x} \\ &= \mathbf{A}(\mathbf{x}) + \frac{\partial \mathbf{A}(\mathbf{x})}{\partial \mathbf{x}} \mathbf{x} - \mathbf{B}(\mathbf{x}) \mathbf{K}(\mathbf{x}) - \frac{\partial (\mathbf{B}(\mathbf{x}) \mathbf{K}(\mathbf{x}))}{\partial \mathbf{x}} \mathbf{x}, \end{aligned} \quad (6.13)$$

the addends defining the Jacobian can be addressed individually. While the first two terms can be determined analytically by evaluating the state-dependent system matrix,  $\mathbf{A}(\mathbf{x})$ , as defined in sec.5.1.1, the third term was at least accessible pointwise as the state-dependent gain-matrix for a certain grid-point,  $\mathbf{K}(\mathbf{x} = \mathbf{x}_g)$ , can be obtained from solving the corresponding ARE. However, for the last partial derivative:

$$\frac{\partial (\mathbf{B}(\mathbf{x}) \mathbf{K}(\mathbf{x}))}{\partial \mathbf{x}} \mathbf{x} = \frac{\partial \mathbf{B}(\mathbf{x})}{\partial \mathbf{x}} \mathbf{K}(\mathbf{x}) \mathbf{x} + \mathbf{B}(\mathbf{x}) \frac{\partial \mathbf{K}(\mathbf{x})}{\partial \mathbf{x}} \mathbf{x} \quad (6.14)$$

the Jacobian of the gain matrix,  $\frac{\partial \mathbf{K}(\mathbf{x})}{\partial \mathbf{x}}$ , had to be assumed to be reasonably small compared to the Jacobians of the system's dynamic matrices<sup>2</sup> and consequently the second addend was neglected. The first term was again computed by determining the Jacobian of the input matrix,  $\frac{\partial \mathbf{B}(\mathbf{x})}{\partial \mathbf{x}}$ , analytically and employing the pointwise solution of the SDRE for  $\mathbf{K}(\mathbf{x} = \mathbf{x}_g)$ .

With the Jacobian of the closed-loop dynamics determined, ineq (6.9) could be evaluated for all grid-points and added to the optimization problem. However, in order to assure contracting behaviour, additionally the positive-definiteness condition of ineq. (6.8) needs to be fulfilled, as well. As already suggested in the last section, within this work an attempt to benefit from the positive-definite metric already found in the solution of the SDRE was applied. Consequently, it was not solely demanded for the metric to be positive-definite within all predefined grid-points:

$$\mathbf{M}(\mathbf{x} = \mathbf{x}_g) > \mathbf{0} \quad (6.15)$$

but instead pointwise the following LMI:

$$\mathbf{M}(\mathbf{x} = \mathbf{x}_g) \geq \mathbf{P}(\mathbf{x} = \mathbf{x}_g) \quad (6.16)$$

was added to constrain the optimization problem. Additionally, in the upright equilibrium point:

$$\mathbf{M}(\mathbf{x}_g = \mathbf{0}) = \mathbf{P}(\mathbf{x}_g = \mathbf{0}) \quad (6.17)$$

was defined to adapt desirable properties of the solution of the SDRE in the origin,  $\mathbf{P}(\mathbf{0})$ . As the TWIP is subject to almost linear dynamics within close proximity to the upright equilibrium point, and recalling that for LTI-systems asymptotic stability is synonymous with exponential stability, it can be assumed for  $\mathbf{P}(\mathbf{0})$  to not just guarantee asymptotic but exponential convergence to the origin.

---

<sup>2</sup>Note that if for example a finer state-space grid was employed, this Jacobian could be determined numerically e.g. through finite differences. As the proposed method gets computationally expensive for a large amount of grid points, a more coarse grid was employed and consequently the term omitted.

With ineq. (6.8) being addressed as well, on the defined state-space grid all conditions on the metric to assure contracting behaviour were met, and the resulting optimization problem could be handled by defining some optimistic constant contraction rate,  $\beta$ , and testing if the resulting feasibility problem yields a solution. If the solver fails, the contraction rate could be lowered and again the new feasibility problem tried to be solved. Instead of executing this trial-and-error approach by hand however, the pre-implemented bisection algorithm of YALMIP was employed. In order to do so, the contraction rate,  $\beta$ , was added to the set of decision variables and the optimization problem extended by the objective of  $-\beta$  to maximize the obtainable convergence rate. When approaching the resulting SDP, the bisection algorithm starts out by checking if  $\beta = 0$  yields a feasible solution and then increases the convergence rate in quite large steps until a feasible solution can no longer be obtained. This way having defined an upper and lower bound for the convergence rate, subsequently the solution is "fine-tuned" through a common bisection-approach.

### Comparing the Proposed Method to the Approach Presented in [7]

Comparing this approach to Chang's in [7] two major differences become obvious. Firstly, Chang assumes the time derivative of the metric,  $\dot{\mathbf{M}}$ , to be negligible and accordingly sets it to zero in ineq. (6.9). He argues this choice by stating that the velocity vector,  $\dot{\mathbf{x}}$ , can be assumed to be sufficiently small. This however does not necessarily seem reasonable as many of the systems SDRE-controllers have been designed for – like e.g. missiles, helicopters, or also the TWIP – inherently possess fast dynamics. Additionally, even if assuming that the velocity vector vanishes as the system approaches the origin, in general the designer would be interested in finding a contraction region as large as possible – not only in some close proximity to the origin. For this reason, within the proposed method the time derivative of the contraction metric was included in the optimization problem. Due to the polynomial approach, also taking into account the metric's time derivative yields in only minor additional computational expenses.

A further difference lies in Chang choosing the convergence rate to be state-dependent,  $\beta(\mathbf{x})$ , while within the proposed method the convergence rate is declared a constant decision variable. Recalling the definition of a contraction metric in def. 3.9, such a state-dependency is not included. Technically, a metric defining a contraction region can only correspond to a single constant convergence rate, as it defines a unique upper bound for the maximum time the system takes to converge on the contracting manifold. Consequently, Chang does not find one metric identifying one interconnected and contracting Riemannian manifold, but instead defines a different metric corresponding to a different contracting region for each evaluated grid-point.

Note that the deduction of global contraction properties for the entire manifold from properties examined in local coordinates is only feasible in the context of contraction theory as the entire tangent space of that manifold is evaluated. This simultaneous consideration of all differential directions allows to exclude phenomena like finite escape times et cetera that prohibit inference of global properties within Lyapunov analysis. If however no longer one interconnected set of a Riemannian manifold and metric is considered, an inference from local to global properties is no longer feasible. Chang's approach only showcases contracting behaviour of the system in some evaluated system state corresponding to a grid-point,  $\mathbf{x}_g$ . However as the origin is not assured to also be included in the pointwise defined contracting manifold, convergences to the particular trajectory

of the equilibrium located in the origin can not be concluded. In conclusion, the method introduced in [7] can locally prove contracting behaviour, however not necessarily to the equilibrium point of interest.

The proposed method on the other hand defines a single pair of corresponding contraction metric and region with a fixed convergence rate to be maximised. Therefore, the introduced fitting method does not violate the conditions that enable the deduction of global properties valid on the entire manifold from the evaluation in local coordinates. On the other hand, with the presented technique, special attention need to be drawn to the metric fulfilling the contraction conditions outside the chosen grid-points, as well. Phrased differently, with the proposed method additional checks need to be provided to assure for any point outside the chosen LMI-grid to be included on the manifold defined by the found metric. Chang's method however has the same issue of assuring contracting behaviour in between grid-points.

## 6.4 Obtained Metric and Remarks on Fitting Method

The fitting technique as introduced in sec. 6.3 was applied to the TWIP's dynamics for different sets of parameters, like polynomial degree  $m$ , state-space limits, or number of grid-point the LMIs are defined in. The best result was be obtained within the state-space region of:

$$\dot{x} \in [-1.0, 1.0] \quad \theta \in \left[-\frac{\pi}{3}, \frac{\pi}{3}\right] \quad \dot{\theta} \in [-2\pi, 2\pi] \quad \dot{\psi} \in [-6.0\pi, 6.0\pi], \quad (6.18)$$

when defining an equidistant  $7 \times 7 \times 7 \times 7$ -grid for the LMIs to be set in and choosing the maximum polynomial degree as two. The obtained metric defined a manifold contracting at a rate of  $\beta = 0.7476$ . After the solver converged, the found metric was examined on the predefined LMI-grid as well as on another  $13 \times 13 \times 13 \times 13$ -grid finer than the original one, to also assure contracting behaviour outside the states where the LMIs had been set. In those test-points,  $\mathbf{x}_t$ , the found metric was evaluated for positive-definiteness and the left site of ineq. (6.9) was investigated for negative-definiteness. Within the total of 28,561 evaluated test-states, no point was found where the chosen metric was not positive-definite and only 728 points were determined where the contraction condition of ineq. (6.9) was violated – these 728 points however only make up 2.54 % of all test-points.

Note that the  $\dot{\psi}$ -limit of the contraction region can be further expanded of up to  $\dot{\psi} = 6.325\pi$  and the solver does still converge, however the resulting contracting manifold can only guarantee a convergence rate of  $\beta = 0.0596$ . However, if the task was to solely find a region as large as possible, almost all of the relevant state-space could be covered. For yaw rates larger than,  $\dot{\psi} = 6.325\pi$ , the solver no longer converges to a positive convergence rate, such that with the proposed method exponential convergence can not be proven for this region of the state-space. Note however, that only exponential convergence – a far stronger characteristic than (asymptotic) stability – can not be shown any more, however the remaining set of the state-space might still be asymptotically stable.

The region of exponential stability being limited by the yaw rate,  $\dot{\psi}$ , has a solid physical interpretation as the TWIP's non-linearities become most prominent in high spinning states, such that stabilizing the system at an exponential rate might become impossible

for the controller. However, reducing the limits in another relevant system state like the pitch angle, did not yield in a manifold contracting at a faster rate. Consequently, it can be concluded that the limitation of the region of exponential contraction by the system's yaw rate is due to the weighting matrices discussed in sec. 5.2.1. The performance index was explicitly chosen such that the controller would not act too aggressively in high spinning situations, in order to prevent the required inputs exceeding the viable range – which marks a probable explanations for the SDRE-closed loop dynamics no longer converging exponentially when stabilizing high yaw rates.

In conclusion, the proposed method allows successful stability analysis of the SDRE-controlled system even though the closed-loop dynamics are only known pointwise. The technique can be considered non-restrictive as it does not demand the evaluated system to have a specific structure and additionally can be applied within reasonable computational effort to higher-order systems – like the six-dimensional example of the TWIP. Also, only minor simplifications had to be incorporated to evaluate ineq. (6.9) by assuming one of the addends within the closed-loop system's Jacobian to be negligible. Additionally, note the proposed method will not only guarantee asymptotic but exponential stability which shows far superior performance and robustness in the presence of perturbations [7].





## Chapter 7

# Conclusion and Perspective

### 7.1 Summary and Conclusion

In the context of this work, first in sec.2 dynamic models for the TWIP have been comparatively studied and in conclusion a non-linear input-affine model was found to be used in controller design. After outlining the basis of non-linear stability analysis in sec.3 and the ideas behind SDRE-based controller synthesis in sec.4, the SDRE-method was applied to define a control law to stabilize the found non-linear dynamics of the TWIP in its upright position in sec.5. Hereinafter, exponential stability of the closed-loop dynamics was investigated in sec.6.

When defining the proposed non-linear controller, the focus was set on two tasks: first parametrizing the system's dynamics to obtain a quasi-linear SDC-representation as presented in sec.5.1.1, and secondly adjusting the state-dependent weighting matrices to construct a suitable performance index in sec.5.2.1. The chosen SDC-parametrization was motivated by the inherent non-linear intercouplings within the TWIP's dynamics and exhibited several favourable characteristics in regards of controllability and numerical feasibility. The proposed SDC-representation was found to be strongly controllable in 671,925 evaluated system states with the smallest singular value of all investigated controllability-matrices being equal to 0.945. Beneficial numerical properties of the found SDC-representation could be reaffirmed during simulations where a significantly larger integration stepsize could stably be used on the SDRE-controller compared to the LQR-controller or an alternate SDRE-controller based on a less favourable SDC-representation.

A specific choice of state-dependent weighting matrices allowed to differentiate between "more or less critical" highly dynamical system states and through further adjustments remarkable input efficiency could be achieved. The additional degree of freedom in choosing state-dependent penalty matrices to impose soft constraints on the input was successfully implemented in the context of this work. While the resulting non-linear controller managed to restabilize all considered system states within physically relevant limits under low energy consumption, it experienced minor oscillations and overshoot when a constant disturbances was simulated in sec.5.4.2 and consequently turned out to have robustness properties inferior to the LQR-controller. When applied to a dynamic model including non-linear friction terms in sec.5.4.3, the SDRE-controller still managed to partially stabilize the TWIP, while the LQR-controller diverged within short time.

Finally, as first suggested by Chang in [7] with the employment of contraction theory, a valid technique to systematically analyse stability of SDRE-controlled systems with the closed-loop dynamics not explicitly known has been defined. However, several adjustments on the method proposed by Chang had to be made in order to assure that the mathematical requirements for defining a contraction region are not violated. Also, the approach proposed in the context of this work introduced the idea of locally guiding the fitting process of a contraction metric through the pointwise solution of the SDRE. Application of the proposed method allowed to prove exponential stability for 97.46 % of all 28,561 points evaluated within the relevant subset of the state-space. Additionally, the proposed technique can be considered non-restrictive due to its reasonable computational costs even when applied to higher-order systems.

## 7.2 Perspectives

In conclusion, the found SDRE-controller proved fast convergence in almost the entire relevant subset of the state-space while maintaining input efficient behaviour by exploiting the TWIP's inherent dynamics instead of brutally cancelling out any non-linearities. In the context of this work, a strong focus was set on stabilizing pitch deviations – in order to enhance controller performance for certain alternating system states, e.g. high-spinning modes or likewise, the chosen performance index could be further adapted and reviewed through according simulation. While the chosen SDC-parametrization with its focus on pitch stabilization proved sufficient controller performance within this paper, it might however also be adapted for differing applications.

As with the proposed fitting method in theory unification of computed contraction regions is possible, an extension to a multi-step fitting procedure could be implemented in order to define even larger contraction regions. For instance, after the first metric has been found and evaluated on a grid of test points, in a second computation round all points of the test grid that were not included in the contracting manifold of the first metric could be chosen as LMI-points such that the next metric is assured to include these points. If this second round fails due to the fact that some states might define a non-exponentially stable point within state-space, the set could be split in half and a third search for two new metrics could be executed and so on. Obviously, in all steps the equilibrium point of interest would have to be included in the set of LMIs to assure convergence to this particular trajectory.

As an alternate approach, it could be tried to apply some polynomial fitting approach to first determine a state-dependent expression for the solution of the SDRE and then solving the finding of a contraction metric through sum-of-squares programming to assure the contraction conditions to strictly be fulfilled – however in this case special attention would have to be drawn to handling non-linear terms as sum-of-squares programming only permits the usage of polynomial decision variables. However, trigonometric terms for examples could be approximated by some  $k$ -th order Taylor-series expansion to make this approach feasible.

Lastly, as all results found within this work are based on simulations exclusively, the primarily remaining task lies in trying out the found controller on the actual robot to see if the computed contraction region and observed input efficiency can be reaffirmed in real-life experiments.

# Appendix A

## Dynamic Models of the TWIP

### A.1 Parameters of the Employed TWIP

Table A.1: The numerical values of parameters describing the TWIP as introduced in sec. 2 and discussed in the remaining of this paper. The lower indices,  $b$  and  $w$ , indicate whether a parameter belongs to the pendulum's body or wheels. These parameters define a small and slender robot which will influence the controller requirements.

Model Parameter	Variable	Value
Gravitational acceleration	$g$	9.81 m/s <sup>2</sup>
Mass of pendulum-body	$m_b$	0.277 kg
Mass of either wheel	$m_w$	0.028 kg
MOI of the body w.r.t its driving axis	$I_{b1}$	$0.543 \cdot 10^{-3}$ kg m <sup>2</sup>
MOI of the body w.r.t the TWIP's axle	$I_{b2}$	$0.481 \cdot 10^{-3}$ kg m <sup>2</sup>
MOI of the body w.r.t its longitudinal axis	$I_{b3}$	$0.154 \cdot 10^{-3}$ kg m <sup>2</sup>
MOI of the wheels w.r.t their axis	$I_{w1}$	$0.741 \cdot 10^{-5}$ kg m <sup>2</sup>
MOI of the wheels w.r.t to their diameter	$I_{w2}$	$0.496 \cdot 10^{-5}$ kg m <sup>2</sup>
Height of the body's centre of mass	$l$	0.049 m
Radius of either wheel	$r$	0.033 m
Distance between the two wheels	$d$	0.098 m

## A.2 Constants and Auxiliary Variables

For easier readability, a set of auxiliary variables and constants was introduced:

$$K_1 = m_b + 2 m_w + 2 I_{w1}/r^2 \quad (\text{A.1})$$

$$K_2 = I_{b1} - I_{b3} + m_b l^2 \quad (\text{A.2})$$

$$K_3 = I_{b2} + m_b l^2 \quad (\text{A.3})$$

$$K_4 = m_b l \quad (\text{A.4})$$

$$K_5 = (m_w + I_{w1}/r^2) \quad (\text{A.5})$$

$$\rho_1(\theta) = K_4^2 \sin^2(\theta) + m_b I_{b2} + 2 K_3 K_5 \quad (\text{A.6})$$

$$\rho_2(\theta) = K_2 \sin^2(\theta) + I_{b3} + 2 I_{w2} + \frac{d^2}{2} K_5 \quad (\text{A.7})$$

$$\mu_1 = K_1 K_3 - K_4^2 \quad (\text{A.8})$$

$$\mu_2 = I_{b3} + 2 I_{w2} + \frac{d^2}{2} K_5. \quad (\text{A.9})$$

## A.3 Non-linear State-Space Model

The following state-space model of the TWIP is used within this work:

$$\begin{bmatrix} \dot{x} \\ \ddot{x} \\ \dot{\theta} \\ \ddot{\theta} \\ \dot{\psi} \\ \ddot{\psi} \end{bmatrix} = \begin{bmatrix} f_1(\mathbf{x}) \\ f_2(\mathbf{x}) \\ f_3(\mathbf{x}) \\ f_4(\mathbf{x}) \\ f_5(\mathbf{x}) \\ f_6(\mathbf{x}) \end{bmatrix} + \begin{bmatrix} 0 & 0 \\ g_{21}(\mathbf{x}) & g_{22}(\mathbf{x}) \\ 0 & 0 \\ g_{41}(\mathbf{x}) & g_{42}(\mathbf{x}) \\ 0 & 0 \\ g_{61}(\mathbf{x}) & g_{62}(\mathbf{x}) \end{bmatrix} \begin{bmatrix} \tau_l \\ \tau_r \end{bmatrix} \quad (\text{A.10})$$

where the individual vector entries are given in the following:

$$f_1(\mathbf{x}) = \dot{x} \quad (\text{A.11})$$

$$f_2(\mathbf{x}) = \frac{\sin(\theta)}{\rho_1(\theta)} K_4 \left( -K_4 g \cos(\theta) + K_3 \dot{\theta}^2 + (K_3 - K_2 \cos^2(\theta)) \dot{\psi}^2 \right) \quad (\text{A.12})$$

$$f_3(\mathbf{x}) = \dot{\theta} \quad (\text{A.13})$$

$$f_4(\mathbf{x}) = \frac{\sin(\theta)}{\rho_1(\theta)} \left( K_1 K_4 g - K_4^2 \cos(\theta) \dot{\theta}^2 + (K_1 K_2 - K_4^2) \cos(\theta) \dot{\psi}^2 \right) \quad (\text{A.14})$$

$$f_5(\mathbf{x}) = \dot{\psi} \quad (\text{A.15})$$

$$f_6(\mathbf{x}) = \frac{\sin(\theta)}{\rho_2(\theta)} \left( -2 K_2 \cos(\theta) \dot{\theta} \dot{\psi} - K_4 \dot{x} \dot{\psi} \right) \quad (\text{A.16})$$

$$g_{21}(\mathbf{x}) = \frac{1}{\rho_1(\theta)} (K_3/r + K_4 \cos(\theta)) \quad (\text{A.17})$$

$$g_{22}(\mathbf{x}) = g_{21}(\mathbf{x}) \quad (\text{A.18})$$

$$g_{41}(\mathbf{x}) = \frac{1}{\rho_1(\theta)} (-K_4 \cos(\theta)/r - K_1) \quad (\text{A.19})$$

$$g_{42}(\mathbf{x}) = g_{41}(\mathbf{x}) \quad (\text{A.20})$$

$$g_{61}(\mathbf{x}) = -\frac{d}{2r\rho_2(\theta)} \quad (\text{A.21})$$

$$g_{62}(\mathbf{x}) = -g_{61}(\mathbf{x}). \quad (\text{A.22})$$

## A.4 SDC-Parametrizations of the Non-linear State-Space Model

### A.4.1 SDC-Parametrization Used for Controller Design

The pseudo-linear representation chosen for SDRE-based controller synthesis is defined as:

$$\begin{bmatrix} \dot{x} \\ \ddot{x} \\ \dot{\theta} \\ \ddot{\theta} \\ \dot{\psi} \\ \ddot{\psi} \end{bmatrix} = \begin{bmatrix} 0 & 1 & 0 & 0 & 0 & 0 \\ 0 & 0 & a_{23}(\mathbf{x}) & a_{24}(\mathbf{x}) & 0 & a_{26}(\mathbf{x}) \\ 0 & 0 & 0 & 1 & 0 & 0 \\ 0 & 0 & a_{43}(\mathbf{x}) & a_{44}(\mathbf{x}) & 0 & a_{46}(\mathbf{x}) \\ 0 & 0 & 0 & 0 & 0 & 1 \\ 0 & a_{62}(\mathbf{x}) & 0 & a_{64}(\mathbf{x}) & 0 & a_{66}(\mathbf{x}) \end{bmatrix} \begin{bmatrix} x \\ \dot{x} \\ \theta \\ \dot{\theta} \\ \psi \\ \dot{\psi} \end{bmatrix} + \begin{bmatrix} 0 & 0 \\ b_2(\mathbf{x}) & b_2(\mathbf{x}) \\ 0 & 0 \\ b_4(\mathbf{x}) & b_4(\mathbf{x}) \\ 0 & 0 \\ b_6(\mathbf{x}) & -b_6(\mathbf{x}) \end{bmatrix} \begin{bmatrix} \tau_l \\ \tau_r \end{bmatrix}, \quad (\text{A.23})$$

where the matrix entries of the state-dependent system matrix,  $\mathbf{A}(\mathbf{x})$ , are:

$$a_{23}(\mathbf{x}) = \frac{\sin(\theta)}{\rho_1(\theta)} \frac{1}{\theta} \left( -K_4^2 g \cos(\theta) \right) \quad (\text{A.24})$$

$$a_{24}(\mathbf{x}) = \frac{\sin(\theta)}{\rho_1(\theta)} K_3 K_4 \dot{\theta} \quad (\text{A.25})$$

$$a_{26}(\mathbf{x}) = \frac{\sin(\theta)}{\rho_1(\theta)} \left( K_3 - K_2 \cos^2(\theta) \right) K_4 \dot{\psi} \quad (\text{A.26})$$

$$a_{43}(\mathbf{x}) = \frac{\sin(\theta)}{\rho_1(\theta)} \frac{1}{\theta} (K_1 K_4 g) \quad (\text{A.27})$$

$$a_{44}(\mathbf{x}) = \frac{\sin(\theta)}{\rho_1(\theta)} \left( -K_4^2 \cos(\theta) \dot{\theta} \right) \quad (\text{A.28})$$

$$a_{46}(\mathbf{x}) = \frac{\sin(\theta)}{\rho_1(\theta)} \left( K_1 K_2 - K_4^2 \right) \cos(\theta) \dot{\psi} \quad (\text{A.29})$$

$$a_{62}(\mathbf{x}) = \frac{\sin(\theta)}{\rho_2(\theta)} \left( -\frac{1}{2} K_4 \dot{\psi} \right) \quad (\text{A.30})$$

$$a_{64}(\mathbf{x}) = \frac{\sin(\theta)}{\rho_2(\theta)} \left( -K_2 \cos(\theta) \dot{\psi} \right) \quad (\text{A.31})$$

$$a_{66}(\mathbf{x}) = \frac{\sin(\theta)}{\rho_2(\theta)} \left( -\frac{1}{2} K_4 \dot{x} - K_2 \cos(\theta) \dot{\theta} \right) \quad (\text{A.32})$$

and the input matrix entries are identical to the one of the non-linear system:

$$b_2(\mathbf{x}) = g_{21}(\mathbf{x}) = \frac{1}{\rho_1(\theta)} (K_3/r K_4 \cos(\theta)) \quad (\text{A.33})$$

$$b_4(\mathbf{x}) = g_{41}(\mathbf{x}) = \frac{1}{\rho_1(\theta)} (K_4 \cos(\theta)/r + K_1) \quad (\text{A.34})$$

$$b_6(\mathbf{x}) = g_{61}(\mathbf{x}) = -\frac{d}{2r\rho_2(\theta)} \quad (\text{A.35})$$

#### A.4.2 Inherently Non-Controllable SDC-Parametrization

The matrix entries of the non-controllable example parametrization are listed in detail in the following:

$$a_{\text{nc},22}(\mathbf{x}) = \frac{\sin(\theta)}{\rho_1(\theta)} \frac{1}{\dot{x}} \left( -K_4^2 g \cos(\theta) \right) \quad (\text{A.36})$$

$$a_{\text{nc},24}(\mathbf{x}) = a_{24}(\mathbf{x}) \quad (\text{A.37})$$

$$a_{\text{nc},26}(\mathbf{x}) = a_{26}(\mathbf{x}) \quad (\text{A.38})$$

$$a_{\text{nc},42}(\mathbf{x}) = \frac{\sin(\theta)}{\rho_1(\theta)} \frac{1}{\dot{x}} (K_1 K_4 g) \quad (\text{A.39})$$

$$a_{\text{nc},44}(\mathbf{x}) = a_{44}(\mathbf{x}) \quad (\text{A.40})$$

$$a_{\text{nc},46}(\mathbf{x}) = a_{46}(\mathbf{x}) \quad (\text{A.41})$$

$$a_{\text{nc},66}(\mathbf{x}) = \frac{\sin(\theta)}{\rho_2(\theta)} \left( -2K_2 \cos(\theta) \dot{\theta} - K_4 \dot{x} \right) \quad (\text{A.42})$$

### A.4.3 Physically Meaningless SDC-Parametrization

The matrix entries of the physically meaningless example parametrization are listed in detail in the following:

$$a_{\text{tp},25}(\mathbf{x}) = \frac{\sin(\theta)}{\rho_1(\theta)} \frac{K_4}{\psi} \left( -K_4 g \cos(\theta) + K_3 \dot{\theta}^2 + (K_3 - K_2 \cos^2(\theta)) \dot{\psi}^2 \right) \quad (\text{A.43})$$

$$a_{\text{tp},45}(\mathbf{x}) = \frac{\sin(\theta)}{\rho_1(\theta)} \frac{1}{\psi} \left( K_1 K_4 g - K_4^2 \cos(\theta) \dot{\theta}^2 + (K_1 K_2 - K_4^2) \cos(\theta) \dot{\psi}^2 \right) \quad (\text{A.44})$$

$$a_{\text{tp},65}(\mathbf{x}) = \frac{\sin(\theta)}{\rho_2(\theta)} \frac{1}{\psi} \left( -2K_2 \cos(\theta) \dot{\theta} \dot{\psi} - K_4 \dot{x} \dot{\psi} \right). \quad (\text{A.45})$$

In order to avoid the singularity arising with  $\psi \rightarrow 0$  this model switched to the Kim2017-parametrization for yaw angles of smaller than  $10^{-12}$ .

### A.4.4 Kim2017 SDC-Parametrization

The matrix entries for the parametrization introduced in [26] are as follows:

$$a_{\text{Kim},23}(\mathbf{x}) = \frac{\sin(\theta)}{\rho_1(\theta)} \frac{K_4}{\theta} \left( -K_4 g \cos(\theta) + K_3 \dot{\theta}^2 + (K_3 - K_2 \cos^2(\theta)) \dot{\psi}^2 \right) \quad (\text{A.46})$$

$$a_{\text{Kim},43}(\mathbf{x}) = \frac{\sin(\theta)}{\rho_1(\theta)} \frac{1}{\theta} \left( K_1 K_4 g - K_4^2 \cos(\theta) \dot{\theta}^2 + (K_1 K_2 - K_4^2) \cos(\theta) \dot{\psi}^2 \right) \quad (\text{A.47})$$

$$a_{\text{Kim},63}(\mathbf{x}) = \frac{\sin(\theta)}{\rho_2(\theta)} \frac{1}{\theta} \left( -2K_2 \cos(\theta) \dot{\theta} \dot{\psi} - K_4 \dot{x} \dot{\psi} \right). \quad (\text{A.48})$$

Note that the inconsistency with the model derived in [25] that was discussed in detail in sec. 2 was corrected for this model, as well, such that it is not identical to the formulae in [26]. However, as the structure is the exact same, it was nevertheless denoted as the Kim2017-SDC-parametrization.

## A.5 Dynamics Linearized about Upright Equilibrium

The linearization of the TWIP's non-linear dynamics about its upright equilibrium point yields the following dynamics:

$$\begin{bmatrix} \dot{x} \\ \ddot{x} \\ \dot{\theta} \\ \ddot{\theta} \\ \dot{\psi} \\ \ddot{\psi} \end{bmatrix} = \begin{bmatrix} 0 & 1 & 0 & 0 & 0 & 0 \\ 0 & 0 & a_{\text{lin},23} & 0 & 0 & 0 \\ 0 & 0 & 0 & 1 & 0 & 0 \\ 0 & 0 & a_{\text{lin},43} & 0 & 0 & 0 \\ 0 & 0 & 0 & 0 & 0 & 1 \\ 0 & 0 & 0 & 0 & 0 & 0 \end{bmatrix} \begin{bmatrix} x \\ \dot{x} \\ \theta \\ \dot{\theta} \\ \psi \\ \dot{\psi} \end{bmatrix} + \begin{bmatrix} 0 & 0 \\ b_{\text{lin},2} & b_{\text{lin},2} \\ 0 & 0 \\ b_{\text{lin},4} & b_{\text{lin},4} \\ 0 & 0 \\ b_{\text{lin},6} & -b_{\text{lin},6} \end{bmatrix} \begin{bmatrix} \tau_l \\ \tau_r \end{bmatrix} \quad (\text{A.49})$$

where the constant matrix entries are defined as:

$$a_{\text{lin},23} = \frac{-K_4^2 g}{\mu_1} \quad (\text{A.50})$$

$$a_{\text{lin},43} = \frac{K_1 K_4 g}{\mu_1} \quad (\text{A.51})$$

$$b_{\text{lin},2} = \frac{K_3/r + K_4}{\mu_1} \quad (\text{A.52})$$

$$b_{\text{lin},4} = -\frac{K_4/r + K_1}{\mu_1} \quad (\text{A.53})$$

$$b_{\text{lin},6} = -\frac{d}{2r\mu_2}. \quad (\text{A.54})$$



# List of Theorems and Other Statements

3.1	Definition (Stability According to Lyapunov) . . . . .	18
3.2	Definition (Asymptotic Stability According to Lyapunov) . . . . .	19
3.3	Definition (Exponential Stability According to Lyapunov) . . . . .	19
3.4	Definition (Global Stability According to Lyapunov) . . . . .	19
3.5	Definition (Contraction Region) . . . . .	24
3.6	Definition (Exponential Convergence to a Single Trajectory) . . . . .	24
3.7	Definition (Global Exponential Convergence to a Single Trajectory) . . . . .	25
3.8	Definition (Contraction Metrics for Autonomous Systems) . . . . .	26
3.9	Definition (Contraction Metrics Assuring Exponential Convergence) . . . . .	26
3.10	Definition (Controllability of Dynamical Systems) . . . . .	29
4.1	Definition (Controllable SDC-Parametrization) . . . . .	36
4.2	Definition (Strongly Controllable SDC-Parametrization) . . . . .	36



# List of Algorithms

2.1 Reconstructing Pathak's Position Coordinates,  $x_0$  and  $y_0$ , from Travelled Path Length,  $x$ , and Yaw Angle,  $\psi$ . . . . . 6



# List of Figures

1.1	The TWIP Developed at the Chair of Automatic Control . . . . .	3
2.1	State-space Variables of the TWIP . . . . .	7
2.2	Overview of Parameters of the TWIP . . . . .	8
2.3	Simulation Results of Pathak- and Kim-Model in Their Original Form . .	9
2.4	Simulation Results of Pathak- and Kim-Model after Correction of Kim-Model . . . . .	11
2.5	Simulation Results of Pathak- and Kim-Model after Correction of Both Models . . . . .	14
3.1	Lyapunov's Different Notions of Stability for a Scalar System . . . . .	19
3.2	Lyapunov's Different Notions of Stability for a Two-dimensional System .	20
3.3	Geometrical Interpretation of Lyapunov's Direct Method for a Two-dimensional System . . . . .	22
3.4	Contracting Behaviour and Convergence to a Single Trajectory . . . . .	24
3.5	Generalization of Results through Introduction of Local Coordinates . . .	27
5.1	Simulation Results Comparing the Non-linear Model and the Chosen SDC-parametrization . . . . .	45
5.2	Comparative Controller Performance of Used-SDC-parametrization and an Alternate TP-SDC-parametrization - State Trajectories . . . . .	52
5.3	Comparative Controller Performance of Used-SDC-parametrization and an Alternate TP-SDC-parametrization - Input Trajectories . . . . .	54
5.4	Comparative Controller Performance for State-dependent and Constant Weighting Matrices - State Trajectories . . . . .	56
5.5	Comparative Controller Performance for State-dependent and Constant Weighting Matrices - Input Trajectories . . . . .	57
5.6	Comparative Controller Performance of SDRE-based and LQR-based Controllers - State Trajectories . . . . .	59
5.7	Comparative Controller Performance of SDRE-based and LQR-based Controllers - Input Trajectories . . . . .	60

---

5.8	Comparative Controller Performance of SDRE-based and LQR-based Controllers with Applied Step-disturbance - State Trajectories . . . . .	61
5.9	Comparative Controller Performance of SDRE-based and LQR-based Controllers with Applied Step-disturbance - Input Trajectories . . . . .	63
5.10	Performance of SDRE-based Controller Subject to Non-linear Friction Effects. . . . .	65
5.11	Diverging State Trajectories of the LQR-controlled System when Subject to Non-linear Friction Effects. . . . .	66

# List of Tables

- 2.1 Comparison of Symbols to Describe State-space Variables within Different Models . . . . . 7
- 2.2 Comparison of Variables Used to Describe Parameters within Different Models . . . . . 8
  
- 5.1 State-space Limits of Shape Variables . . . . . 46
- 5.2 Initial States Used within Comparative Simulations . . . . . 50
  
- A.1 Numerical Values of Parameters of the Used TWIP . . . . . 81





# References

- [1] F. Anhalt. *Zeitdiskreter Regler- und Führungsfilterentwurf für ein zweirädriges inverses Pendel*. Master's thesis, Technische Universität München, München, 2016.
- [2] E. M. Aylward, P. A. Parrilo, and J. E. Slotine. Stability and robustness analysis of nonlinear systems via contraction metrics and sos programming. *Automatica*, 44(8):2163–2170, 2008. ISSN 00051098. doi: 10.1016/j.automatica.2007.12.012.
- [3] A. Bogdanov. Dual-loop augmented state-dependent Riccati equation control for a helicopter model. In *AIAA Infotech@Aerospace 2010*, Reston, Virginia, 04202010. American Institute of Aeronautics and Astronautics. ISBN 978-1-60086-963-1. doi: 10.2514/6.2010-3542.
- [4] A. Bogdanov, E. Wan, and G. Harvey. SDRE flight control for X-cell and R-max autonomous helicopters. In *2004 43rd IEEE Conference on Decision and Control (CDC) (IEEE Cat. No.04CH37601)*, pages 1196–1203 Vol.2. IEEE, 17.12.2004 - 17.12.2004. ISBN 0-7803-8682-5. doi: 10.1109/CDC.2004.1430204.
- [5] A. Bracci, M. Innocenti, and L. Pollini. Estimation of the region of attraction for state-dependent Riccati equation controllers. *Journal of Guidance, Control, and Dynamics*, 29(6):1427–1430, 2006. ISSN 0731-5090. doi: 10.2514/1.22122.
- [6] R. P. M. Chan, K. A. Stol, and C. R. Halkyard. Review of modelling and control of two-wheeled robots. *Annual Reviews in Control*, 37(1):89–103, 2013. ISSN 13675788. doi: 10.1016/j.arcontrol.2013.03.004.
- [7] I. Chang and S. Chung. Exponential stability region estimates for the state-dependent Riccati equation controllers. In *Proceedings of the 48th IEEE Conference on Decision and Control (CDC) held jointly with 2009 28th Chinese Control Conference*, pages 1974–1979. IEEE, 2009. ISBN 978-1-4244-3871-6. doi: 10.1109/CDC.2009.5400575.
- [8] C. Chen. *Linear system theory and design*. The Oxford series in electrical and computer engineering. Oxford Univ. Press, New York, 3. ed., 3. print edition, 1999. ISBN 0-19-511777-8.
- [9] T. Çimen. State-dependent Riccati equation (SDRE) control: a survey. *IFAC Proceedings Volumes*, 41(2):3761–3775, 2008. ISSN 14746670. doi: 10.3182/20080706-5-KR-1001.00635.
- [10] J. R. Cloutier. State-dependent Riccati equation techniques: an overview. In *Proceedings of the 1997 American Control Conference (Cat. No.97CH36041)*, pages 932–936 vol.2. IEEE, 1997. ISBN 0-7803-3832-4. doi: 10.1109/ACC.1997.609663.

- 
- [11] J. R. Cloutier and D. T. Stansbery. The capabilities and art of state-dependent Riccati equation-based design. In *Proceedings of the 2002 American Control Conference (IEEE Cat. No.CH37301)*, pages 86–91. American Automatic Control Council, 2002. ISBN 0-7803-7298-0. doi: 10.1109/ACC.2002.1024785.
- [12] J. R. Cloutier, C. Dsouza, and C. P. Mracek. Nonlinear regulation and nonlinear  $H_\infty$  control via the state-dependent Riccati equation technique: part 1, theory. In *Proceedings of the International Conference on Nonlinear Problems in Aviation and Aerospace*, 1996.
- [13] J. R. Cloutier, C. Dsouza, and C. P. Mracek. Nonlinear regulation and nonlinear  $H_\infty$  control via the state-dependent Riccati equation technique: part 2, examples. In *Proceedings of the International Conference on Nonlinear Problems in Aviation and Aerospace*, 1996.
- [14] P. Dang and F. L. Lewis. Controller for swing-up and balance of single inverted pendulum using SDRE-based solution. In *31st Annual Conference of IEEE Industrial Electronics Society, 2005. IECON 2005*, page 6 pp. IEEE, 2005. ISBN 0-7803-9252-3. doi: 10.1109/IECON.2005.1568921.
- [15] S. Delgado Londono. *Total Energy Shaping for Underactuated Mechanical Systems: Dissipation and Nonholonomic Constraints*. Dissertation, Technische Universität München, München, 2016. URL <https://mediatum.ub.tum.de/doc/1296097/395699.pdf>.
- [16] E. B. Erdem. *Analysis and Real-Time Implementation of State-Dependent Riccati Equation Controlled Systems*. Dissertation, University of Illinois at Urbana-Champaign, 2001. URL <https://www.ideals.illinois.edu/handle/2142/83761>.
- [17] E. B. Erdem and A. G. Alleyne. Globally stabilizing second order nonlinear systems by SDRE control. In *Proceedings of the 1999 American Control Conference (Cat. No. 99CH36251)*, pages 2501–2505 vol.4. IEEE, 02.06.1999 - 04.06.1999. ISBN 0-7803-4990-3. doi: 10.1109/ACC.1999.786502.
- [18] E. B. Erdem and A. G. Alleyne. Estimation of stability regions of SDRE controlled systems using vector norms. In *Proceedings of the 2002 American Control Conference (IEEE Cat. No.CH37301)*, pages 80–85. American Automatic Control Council, 2002. ISBN 0-7803-7298-0. doi: 10.1109/ACC.2002.1024784.
- [19] E. B. Erdem and A. G. Alleyne. Design of a class of nonlinear controllers via state dependent Riccati equations. *IEEE Transactions on Control Systems Technology*, 12(1):133–137, 2004. ISSN 1063-6536. doi: 10.1109/TCST.2003.819588.
- [20] E. B. Erdem and A. G. Alleyne. Experimental real-time SDRE control of an underactuated robot. In *Proceedings of the 40th IEEE Conference on Decision and Control (Cat. No.01CH37228)*, pages 2986–2991. IEEE, 4-7 Dec. 2001. ISBN 0-7803-7061-9. doi: 10.1109/CDC.2001.980731.
- [21] Y. Huang and W. Lu. Nonlinear optimal control: alternatives to Hamilton-Jacobi equation. In *Proceedings of 35th IEEE Conference on Decision and Control*, pages 3942–3947. IEEE, 1996. ISBN 0-7803-3590-2. doi: 10.1109/CDC.1996.577297.

- [22] Z. Hussain and N. Z. Azlan. Kane's method for dynamic modeling. In *2016 IEEE International Conference on Automatic Control and Intelligent Systems (I2CACIS)*, pages 174–179. IEEE, 2016. ISBN 978-1-5090-4186-2. doi: 10.1109/I2CACIS.2016.7885310.
- [23] R. Kalman. Contribution to the theory of optimal control. *Boletín de la Sociedad Matemática Mexicana*, 5:102–119, 1960.
- [24] H. K. Khalil. *Nonlinear systems*. Prentice Hall, Upper Saddle River, NJ, 3. ed. edition, 2002. ISBN 0-13-067389-7.
- [25] S. Kim and S. Kwon. Dynamic modeling of a two-wheeled inverted pendulum balancing mobile robot. *International Journal of Control, Automation and Systems*, 13(4):926–933, 2015. ISSN 1598-6446. doi: 10.1007/s12555-014-0564-8.
- [26] S. Kim and S. Kwon. Nonlinear optimal control design for underactuated two-wheeled inverted pendulum mobile platform. *IEEE/ASME Transactions on Mechatronics*, 22(6):2803–2808, 2017. ISSN 1083-4435. doi: 10.1109/TMECH.2017.2767085.
- [27] E. V. Kumar and J. Jerome. Algebraic Riccati equation based q and r matrices selection algorithm for optimal lqr applied to tracking control of 3rd order magnetic levitation system. *Archives of Electrical Engineering*, 65(1):151–169, 2016. doi: 10.1515/aee-2016-0012.
- [28] E. V. Kumar, J. Jerome, and G. Raaja. State dependent Riccati equation based nonlinear controller design for ball and beam system. *Procedia Engineering*, 97:1896–1905, 2014. ISSN 18777058. doi: 10.1016/j.proeng.2014.12.343.
- [29] K. Leung and I. R. Manchester. Nonlinear stabilization via control contraction metrics: A pseudospectral approach for computing geodesics. In *2017 American Control Conference (ACC)*, pages 1284–1289. IEEE, 2017. ISBN 978-1-5090-5992-8. doi: 10.23919/ACC.2017.7963129.
- [30] L. Lin and M. Xin. Nonlinear control of two-wheeled robot based on novel analysis and design of SDRE scheme. *IEEE Transactions on Control Systems Technology*, 28(3):1140–1148, 2020. ISSN 1063-6536. doi: 10.1109/TCST.2019.2899802.
- [31] J. Löfberg. Yalmip : A toolbox for modeling and optimization in matlab. In *In Proceedings of the CACSD Conference*, Taipei, Taiwan, 2004.
- [32] W. Lohmiller. *Contraction Analysis of Nonlinear Systems*. Dissertation, Massachusetts Institute of Technology, Cambridge, 1999. URL <https://dspace.mit.edu/bitstream/handle/1721.1/9793/42916380-MIT.pdf?sequence=2&isAllowed=y>.
- [33] MOSEK ApS. The mosek optimization toolbox for matlab manual. version 9.0, 2019. URL <http://docs.mosek.com/9.0/toolbox/index.html>.
- [34] Ninebot Homepage. <http://www.ninebot.com/>. (visited on 15.09.2020).
- [35] R. Olfati-Saber. *Nonlinear Control of the Under-actuated Mechanical System with Application to Robotics and Aerospace Vehicles*. Dissertation, Massachusetts Institute of Technology, Cambridge, 2005. URL <https://dspace.mit.edu/handle/1721.1/8979>.

- [36] J. L. Oritz. *Dynamic Modeling Using Object-Oriented Programming*. Master's thesis, Texas Tech University, Lubbock, 1992. URL <https://ttu-ir.tdl.org/bitstream/handle/2346/59818/31295006957251.pdf?sequence=1>.
- [37] M. Papageorgiou, M. Leibold, and M. Buss. *Optimierung*. Springer Berlin Heidelberg, Berlin, Heidelberg, 2015. ISBN 978-3-662-46935-4. doi: 10.1007/978-3-662-46936-1.
- [38] K. Pathak, J. Franch, and S. K. Agrawal. Velocity and position control of a wheeled inverted pendulum by partial feedback linearization. *IEEE Transactions on Robotics*, 21(3):505–513, 2005. ISSN 1552-3098. doi: 10.1109/TRO.2004.840905.
- [39] J. D. Pearson. Approximation methods in optimal control i. sub-optimal control†. *Journal of Electronics and Control*, 13(5):453–469, 1962. ISSN 0368-1947. doi: 10.1080/00207216208937454.
- [40] P. Seiler. Stability region estimates for SDRE controlled systems using sum of squares optimization. In *Proceedings of the 2003 American Control Conference, 2003*, pages 1867–1872. IEEE, 4-6 June 2003. ISBN 0-7803-7896-2. doi: 10.1109/ACC.2003.1243345.
- [41] R. Sepulchre, M. Janković, and P. V. Kokotović. *Constructive Nonlinear Control*. Communications and Control Engineering. Springer, London, 1997. ISBN 978-1-4471-0967-9. doi: 10.1007/978-1-4471-0967-9.
- [42] J. E. Slotine and W. Li. *Applied nonlinear control*. Prentice Hall, Englewood Cliffs, NJ, 1991. ISBN 978-0130408907.
- [43] J. E. Slotine and W. Lohmiller. On contraction analysis for non-linear systems. *Automatica*, 34(6):683–696, 1998. ISSN 00051098. doi: 10.1016/S0005-1098(98)00019-3.
- [44] Toyota Motor Corporation. Toyota begins public trials of the winglet personal mobility robot in tokyo / toyota global news room. (visited on 15.09.2020). URL <https://global.toyota/en/detail/11463035>.
- [45] H. L. Trentelman, A. A. Stoorvogel, and M. Hautus. *Control Theory for Linear Systems*. Communications and Control Engineering. Springer, London and New York, 2001. ISBN 978-1-4471-0339-4. doi: 10.1007/978-1-4471-0339-4. URL <http://site.ebrary.com/lib/alltitles/docDetail.action?docID=10649424>.
- [46] J. G. VanAntwerp and R. D. Braatz. A tutorial on linear and bilinear matrix inequalities. *Journal of Process Control*, 10(4):363–385, 2000. ISSN 09591524. doi: 10.1016/S0959-1524(99)00056-6.
- [47] M. Vidyasagar. *Nonlinear systems analysis*. Prentice-Hall International editions. Prentice-Hall International, Englewood Cliffs, N.J., 2. ed. edition, 1993. ISBN 0-13-623463-1.
- [48] R. Weissauer. *Kompndium der reellen Analysis: Grundlagen und Methoden für Physiker*. Springer Spektrum, Berlin, 2020. ISBN 978-3-662-58773-7.
- [49] S. H. Žak. *Systems and Control*. The Oxford series in electrical and computer engineering. Oxford Univ. Press, New York, 2003. ISBN 0-19-515011-2. URL <http://www.loc.gov/catdir/enhancements/fy0613/2002066792-d.html>.